Ecosystems and Environment Research Programme
Faculty of Biological and Environmental Sciences
University of Helsinki
Finland

Methane processes in the coastal sediments and water column of the Baltic Sea

Jukka-Pekka Myllykangas

DOCTORAL DISSERTATION

To be presented for public discussion, with the permission of the Faculty of Biological and Environmental Sciences of the University of Helsinki, in Auditorium 2041, Biokeskus 2, 11th of June 2020 at 12 o'clock noon.

HELSINKI, 2020

Supervisors

Dr. Tom Jilbert, University of Helsinki, Finland

Dr. Susanna Hietanen, University of Helsinki, Finland

Advisory committee

Prof. Gregor Rehder, Leibniz Institute for Baltic Sea Research Warnemünde (IOW), Germany

Dr. Anne Ojala, University of Helsinki, Finland

Dr. Antti Rissanen, Tampere University, Finland

Pre-examiners

Dr. Laura Lapham, University of Maryland Center for Environmental Science, United States of America

Dr. Hannu Nykänen, University of Eastern Finland, Finland

Opponent

Dr. Jouni Lehtoranta, Finnish Environment Institute

Custos

Prof. Atte Korhola, University of Helsinki, Finland

ISBN 978-951-51-6186-4 (paperback)

ISBN 978-951-51-6187-1 (PDF)

Unigrafia

Helsinki 2020

"There is nothing like looking, if you want to find something. You certainly usually find something, if you look, but it is not always quite the something you were after."

- J.R.R. Tolkien, "The Hobbit, or There and Back Again"

Contents

List of original publications and the author's contribution **3**

Abbreviations **5**

1 Introduction **9**
- 1.1 Methane as a greenhouse gas 9
- 1.2 Methane sources 10
- 1.3 Methanotrophy 12
- 1.4 The Baltic Sea 15
- 1.5 This thesis 17

2 Materials and methods **21**
- 2.1 Study areas (Papers I-III) 21
- 2.2 Porewater methane sampling (Papers II-III) 22
- 2.3 Water column dissolved gas sampling (Papers I-II) 23
- 2.4 Gas chromatography (Papers I-III) 24
- 2.5 Other dissolved porewater constituents (Papers II-III) 24
- 2.6 Radiotracer incubation (Paper III) 25
- 2.7 Methane flux calculations and modelling of production and consumption in sediments (Paper II) 26

3 Results and discussion **29**
- 3.1 Main findings of the thesis 29
- 3.2 Sources of methane in the Baltic Sea 30
- 3.3 Sinks of methane in the Baltic Sea 34
- 3.4 The Baltic Sea as a source of atmospheric methane 39

4 The Future of Baltic Sea methane processes **43**

5 Conclusions **47**

Acknowledgements **48**

List of original publications and the author's contribution

This thesis consists of an introduction and three research articles, which will be cited according to their roman numerals presented here.

I. Myllykangas, J.-P., T. Jilbert, G. Jakobs, G. Rehder, J. Werner, and S. Hietanen. 2017. Effects of the 2014 major Baltic inflow on methane and nitrous oxide dynamics in the water column of the central Baltic Sea. Earth System Dynamics 8: 817–826. doi:10.5194/esd-8-817-2017

JPM performed the majority of shipboard sampling, all laboratory work and data analysis, and was primarily responsible for manuscript preparation.

II. Myllykangas J.-P., S. Hietanen, T. Jilbert. 2019. Legacy Effects of Eutrophication on Modern Methane Dynamics in a Boreal Estuary. Estuaries and Coasts 43: 189–206. doi: 10.1007/s12237-019-00677-0

JPM performed most field sampling, laboratory and data analysis and prepared the manuscript.

III. Myllykangas, J.-P, A. J. Rissanen, S. Hietanen, and T. Jilbert. 2020. Influence of electron acceptor availability and microbial community structure on sedimentary methane oxidation in a boreal estuary. Biogeochemistry 148: 291–309. doi: 10.1007/s10533-020-00660-z

JPM performed all field sampling, incubations and laboratory work, aside from microbial sample and data processing. JPM was primarily responsible for writing the manuscript.

Abbreviations

ANME	ANaerobic MEthane oxidizers
AOM	Anaerobic Oxidation of Methane
CH_4	Methane
CO_2	Carbon dioxide
EGB	Eastern Gotland Bay
H_2S	Hydrogen sulphide
MBI	Major Baltic Inflow
MOB	Methane oxidizing bacteria
MOX	Aerobic methane oxidation
SMTZ	Sulphate-methane transition zone
SO_4^{2-}	Sulphate
SRB	Sulphate reducing bacteria
WGB	Western Gotland Bay

Abstract

Methane is a powerful greenhouse gas that contributes significantly to global warming. In aquatic systems, microbes in anoxic sediments are the main methane producers. However, due to effective oxidative filters in the sediments and the water column, most of the methane produced does not end up in the atmosphere. This study explores methane dynamics in the Baltic Sea from the open sea, to estuaries and specific microbial processes. Major inflow cycles control methane dynamics in the open Baltic by bringing oxygen to the deep basins, where methane typically accumulates in large amounts during stagnation. The introduction of oxygen during a major inflow in 2014–2015 caused the disappearance of methane from the deep basins due to a combination of oxidation and displacement. However, the effects of the inflow were short-lived and methane started accumulating again in less than a year after the inflow.

The coastal areas were more dynamic, and the primary source of methane varied with distance offshore. Near the river mouth of the studied estuarine system, methane brought in by the river was the most important source, whereas further offshore sedimentary methanogenesis fuelled by a legacy of eutrophication was the primary source. Atmospheric fluxes of methane were highest near the river mouth and decreased seawards, while bathymetry was the main control of sedimentary fluxes. Seasonality had a strong effect on methane dynamics, with methane concentrations generally increasing towards winter. However, as in the open Baltic, displacement also played a role at times, removing large amounts of methane at a time.

While aerobic methane oxidation in the water column was the primary sink offshore, in the coastal areas, anaerobic oxidation of methane (AOM) was by far the most important sink. Offshore, sulphate mediated AOM is expected to be the most important type of AOM. However in this study, metal mediated AOM was an equally important sink in the sediments. Both rates of AOM, and microbial community abundances, were high below the main sulfidic zone in the sediment, pointing towards non-sulphate AOM pathways.

Overall, eutrophication has a large impact on methane dynamics in the Baltic Sea. The legacy of past eutrophication fuels methanogenesis in the coastal areas to this day, despite reductions in nutrient and organic matter input from land, leading to enhanced atmospheric flux of methane. In the future, climate change will likely exacerbate methane emissions from the Baltic Sea.

1 Introduction

1.1 Methane as a greenhouse gas

Methane (CH_4) is the most abundant organic gas in the atmosphere and an important greenhouse gas that contributes significantly to global warming (IPCC, 2014). While its atmospheric concentrations are much lower than those of carbon dioxide (CO_2), per gram it is capable of absorbing more infrared radiation and contributes to radiative forcing up to 34 times more over a 100 year period compared to CO_2 (Myhre *et al.*, 2013). The concentration of CH_4 in the atmosphere has more than doubled since pre-industrial times (Myhre *et al.*, 2013; Blasing, 2016). Terrestrial and aquatic primary producers consume and incorporate fully oxidized carbon in the form of CO_2 into biomass, while the final stages in breakdown of organic matter produce fully reduced CH_4 (Thauer, 1998). CH_4 is subsequently oxidized back into CO_2, either within the biosphere or in the atmosphere (Cicerone & Oremland, 1988). Hence, CH_4 is a key link in the global carbon cycle between the inorganic and organic carbon pools (Dean *et al.*, 2018). Wetlands and fresh water systems are among the most significant natural sources of CH_4, while anthropogenic sources, such as agriculture, fossil fuels and waste treatment, make up between 46–67% of global emissions (Kirschke *et al.*, 2013).

Globally, oceanic methane emissions to the atmosphere are negligible (Reeburgh, 2007). However, the origin of methane in the ocean surface is still largely unknown and large uncertainties exist (Bange *et al.*, 1994; Bange, 2006). Furthermore, estuaries and other coastal areas are among the

most productive aquatic systems in the world and thus considered hotspots for biogeochemical activity (Bianchi, 2007). Though they constitute a very small portion of the global ocean area, coasts contribute up to 75% of all oceanic CH_4 emissions (Bange, 2006; Hamdan & Wickland, 2016).

The main atmospheric sink of CH_4 is a photochemical reaction with hydroxyl radicals (Cicerone & Oremland, 1988), which both removes one of the main reactants involved in atmospheric pollutant removal (Myhre *et al.*, 2013), but also leads into formation of ozone, carbon dioxide and water vapour, all of which further contribute to radiative forcing in the atmosphere (Crutzen, 1974).

The biochemical pathways for both the production and consumption of methane are complex and mediated by a polyphyletic community of microbes, often working syntrophically with the wider microbial community (Valentine, 2002; McGlynn, 2017; Timmers *et al.*, 2017). Many of these pathways and the organisms involved remain poorly understood (Timmers *et al.*, 2017), and the situation is made even more complex because some of the pathways seem reversible (Zehnder & Brock, 1979; Ding *et al.*, 2016). The processes and microbial groups involved in the natural cycle of methane are discussed in detail in the following sections.

1.2 Methane sources

Organic matter is broken down in sediments by a succession of microbial processes utilizing different electron acceptors, each yielding less energy than the previous one (Schulz & Zabel, 2006) and operating at ever decreasing rates (Middelburg, 1989). Methanogenesis typically occurs when all other electron

acceptors have been depleted and is performed by a unique group of strictly anaerobic archaea collectively known as methanogens (Thauer, 1998). The depth of the main methanogenic zone in sediments varies from a few centimetres to several metres, depending on the local organic matter loading (Jørgensen *et al.*, 2001). The two primary metabolic pathways of methanogenesis are acetate fermentation and CO_2 reduction by hydrogenotrophic methanogens. Of these two, CO_2 reduction is more common in marine environments and acetate fermentation in freshwaters (Whiticar *et al.*, 1986). Methanogens share both acetate and hydrogen as substrates with sulphate reducing bacteria (SRB), and are commonly considered to be outcompeted by them (Iversen & Jørgensen, 1985). However, there is also some evidence that under certain conditions, methanogens are able to coexist with SRB by utilizing non-competitive substrates (Cicerone & Oremland, 1988; Maltby *et al.*, 2018).

Methanogenesis is much more prevalent in coastal areas than in the deep sea because of the low organic matter content of deep-sea sediments (Valentine, 2002). Furthermore, methanogenesis is also typically more active in freshwater sediments than in marine sediments (Capone & Kiene, 1988). It was recently estimated that approximately 3—18% of carbon buried into ocean sediments is converted into CH_4 globally (Wallmann *et al.*, 2012; Egger *et al.*, 2018). Previous studies in lakes have suggested that up 50% of carbon produced by primary production may end up in the water column as CH_4 (Fallon *et al.*, 1980). Under certain circumstances, methanogenesis can also produce sufficient quantities of CH_4 in the sediment pore waters to surpass the local hydrostatic pressure, leading to formation of bubbles con-

sisting of nearly pure CH_4 in the sediment (Chanton *et al.*, 1989; Borges & Abril, 2011). The role of ebullition in global CH_4 emissions has been recognized as potentially highly important (McGinnis *et al.*, 2006), but the high spatial and temporal variability of ebullitive processes makes them difficult to study (Flury *et al.*, 2015; Wik *et al.*, 2016).

Methanogenesis is a strictly anoxic process (Cicerone & Oremland, 1988; Thauer, 1998). It is therefore worrying that anoxic and hypoxic areas are spreading at increasing rates throughout the coastal oceans, due to human-induced eutrophication (Diaz & Rosenberg, 2008). Furthermore, methanogenesis is not only dependent on oxygen conditions, but also on the availability of organic carbon (Bange *et al.*, 2010).Thus, the interlinked effects of anoxia and increased carbon loading caused by eutrophication could lead to increased rates of methanogenesis in the oceans globally (Naqvi *et al.*, 2010; Borges *et al.*, 2016). Methanogenesis may be especially enhanced during transitions between oxic and anoxic conditions (Schmaljohann, 1996; Steinle *et al.*, 2015).

1.3 Methanotrophy

While methanogenesis produces vast amounts of CH_4 globally, most of it is re-oxidized before it can reach the atmosphere by several oxidative filters working across the spectrum from fully anoxic to oxic environments (Reeburgh, 2007; Knittel & Boetius, 2009). The first and most important filter in marine environments is the anaerobic oxidation of methane (AOM). It typically takes place in sediments at the depth were upwards diffusing CH_4 meets downwards diffusing sulphate (SO_4^{2-}). This zone is commonly referred

to as the sulphate-methane transition zone (SMTZ). It was originally thought that CH_4 oxidation was only possible with oxygen, due to methane's thermodynamic stability. However, it was later shown that CH_4 oxidation was also occurring in anoxic marine environments in conditions where sulphate was the only possible electron acceptor (Reeburgh, 1976). The stoichiometry of reaction is generally formulated:

$$CH_4 + SO_4^{2-} \rightarrow HS^- + HCO_3^- + H_2O \quad (1)$$

Sulphate-mediated AOM is the major sink of CH_4 in the oceans, though extreme variability in process rates exists (Abril & Borges, 2004; Knittel & Boetius, 2009). AOM is a nearly quantitative sink for CH_4 in the oceans, capable of removing over 90% of all CH_4 produced by methanogenesis (Knittel & Boetius, 2009; Egger *et al.*, 2018). In sediments, where diffusion is the primary transport mechanism, first order kinetics apply and AOM rates are highly dependent on CH_4 availability (Valentine, 2002).

Though AOM is primarily considered a sedimentary process, it has been shown to be also active in anoxic water columns (Durisch-Kaiser *et al.*, 2005). Due to its sulphate dependence, AOM was previously regarded as an exclusively marine process. However, it has been since shown to be active also in fresh waters (Eller *et al.*, 2005; Sivan *et al.*, 2011; Martinez-Cruz *et al.*, 2018). While lakes have limited supplies of sulphate, it is possible that AOM is mediated by other electron acceptors there (Rissanen *et al.*, 2017). Indeed, soon after AOM was originally discovered, Zehnder & Brock (1980) demonstrated that the addition of iron and manganese to both anoxic sediments and digested sewage sludge increased rates of AOM by an order of

magnitude. It has since been established, that at least nitrite (Ettwig et al. 2010), nitrate (Haroon et al. 2013), iron (Egger et al. 2015), manganese (Beal et al. 2009) and chromium (Lu et al. 2016) can potentially act as electron acceptors for AOM. However, alternative electron acceptors for AOM have mostly been studied in bioreactor experiments and studies regarding these reactions in nature are still lacking. Knowledge about the role of non-sulphate AOM occurring below the SMTZ is especially lacking.

AOM is most commonly associated with a polyphyletic group of anaerobic methanotrophic archaea collectively abbreviated as ANME (ANaerobic MEthanotrophs). ANME have been taxonomically divided into three primary groups: ANME-1, with subgroups a and b, ANME-2 with subgroups a, b, c and d (of which two of the latter are distinct from the former, and also each other) and ANME-3 (Timmers *et al.*, 2017). Outside ANME, a group of bacteria called *Candidatus* Methylomirablis (NC10 phyla) are capable of AOM (Ettwig *et al.*, 2016). It has been suggested that ANME are closely related to methanogens and that the main biochemical pathway of methane oxidation in ANME is the enzymatic reversal of methanogenesis (McGlynn, 2017; Timmers *et al.*, 2017). While ANME have been shown to form syntrophic consortia with several different microbial groups (Raghoebarsing *et al.*, 2006; McGlynn *et al.*, 2015; Timmers *et al.*, 2016), there have also been studies which suggest that certain ANME clades are also capable of AOM independently (Ettwig *et al.*, 2010, 2016).

The second oxidative filter against the atmospheric release of CH_4 is oxic methane oxidation (MOX). When CH_4 is exposed to oxic environments, it is oxidized into CO_2 via methanol by methane oxidizing bacteria (MOB). Two

of the most common groups of MOB involved in MOX are γ-proteobacteria and α-proteobacteria, known also as type I and type II methanotrophs, respectively (Hanson & Hanson, 1996). Though MOX is ostensibly an oxic process, Steinle *et al.* (2017) showed that it was actually most efficient in sub-micromolar oxygen conditions. Such conditions are common at sites of steep oxyclines, e.g. at the sediment-water interface or the pycnocline in a stratified water column (Fenchel *et al.*, 1995). Water column stratification dampens turbulent mixing and often the pycnocline hosts a significant community of methane oxidizers (Schmale *et al.*, 2012; Jakobs *et al.*, 2013), which makes it the main barrier preventing CH_4 escaping to the atmosphere in the open ocean (Gentz *et al.*, 2014). However, in coastal areas where the water column is relatively shallow and the diffusive distances are short, or the whole water mass is constantly turbulently mixed, CH_4 may escape into the atmosphere more readily (Humborg *et al.*, 2019).

1.4 The Baltic Sea

The Baltic Sea is the second largest brackish water body in the world, after the Black Sea. It is a semi-enclosed marginal sea of the Atlantic Ocean and receives strong freshwater inputs from dozens of rivers along its coast (HELCOM, 1996). Salt water from the North Sea enters the Baltic only through a narrow channel in the Danish straits, and mostly only during rare events called Major Baltic Inflows (MBI), which require a set of persistent and very specific meteorological and hydrological conditions (Schinke & Matthäus, 1998; Gräwe *et al.*, 2015). The imbalance of water inputs leads to strong stratification which, combined to the slow renewal of the deep water pool

(ca. 30 yr.), leads to a semi-permanent state of anoxia in the sub-halocline waters (Neumann *et al.*, 1996). This makes the Baltic Sea also the second largest anoxic water body in the world, again after the Black Sea. In the last century, hypoxia has spread also to the coastal areas of the Baltic Sea due to human induced eutrophication (Conley *et al.*, 2011; Carstensen *et al.*, 2014b; Jokinen *et al.*, 2018). Climate change is also expected to affect the Baltic Sea in several ways in the future. According to models, by 2100 average temperatures in the Baltic Sea area are expected to increase 2–4 °C, precipitation to increase by 30% and ice cover to decrease 50–80% (Andersson *et al.*, 2015). The combined and partially interlinked effects of eutrophication and climate change have the potential to greatly affect CH_4 dynamics in the Baltic Sea (**II**, Davidson *et al.* 2018; Humborg *et al.* 2019; Beaulieu *et al.* 2019).

There are several knowledge gaps regarding methane dynamics in the Baltic Sea. It has been established, that while CH_4 saturation varies spatially and temporally throughout the surface waters of the open Baltic, they are generally slightly supersaturated with CH_4, making it a net source of CH_4 to the atmosphere (Bange, 2006; Schmale *et al.*, 2010; Gülzow *et al.*, 2014). The role of water column oxidation occurring in the redoxclines of the deep Baltic Sea has been identified as an important sink of CH_4 (Schmale *et al.*, 2012; Jakobs *et al.*, 2013). However, prior to the inflow of late 2014 (Gräwe *et al.*, 2015), the effects of the oxygen brought in to the deep Baltic had been studied only with regards to N_2O (Walter *et al.*, 2006). The first studies the effects of MBIs on methane dynamics have only recently been published (**I**, Schmale *et al.* 2016).

Coastal areas of the Baltic Sea are even less studied in terms of methane

dynamics, and the results have been conflicting. Some studies have identified coastal areas in the Baltic as potential hot spots for CH_4 release (Heyer & Berger, 2000; Bange *et al.*, 2010), while others have not found significant CH_4 release (Treude *et al.*, 2005; Mogollón *et al.*, 2011). Especially lacking are studies about the coastal areas in the northern Baltic Sea. The eastern Gulf of Finland (Pimenov *et al.*, 2012) and the northern Bothnian Bay (Silvennoinen *et al.*, 2008) have been identified as potential sources of atmospheric methane, with rates of methanogenesis intensifying due to increased carbon loading caused by eutrophication. Humborg *et al.* (2019) recently showed that sea-air exchange rates of CH_4 in the coastal zone of the Northern Baltic are enhanced by heat waves and extreme weather events. The role of sediment AOM has been investigated in the deep Baltic (Egger *et al.*, 2017), but studies of coastal AOM and methanogenesis have mostly been limited to the southern Baltic (*e.g.* Treude *et al.* 2005; Dale *et al.* 2008; Maltby *et al.* 2018), with a few exceptions (Thang *et al.*, 2013; Bonaglia *et al.*, 2017).

1.5 This thesis

The primary goal of this thesis was to produce new scientific knowledge regarding the natural processes consuming and producing methane in the Baltic Sea, across multiple spatial and temporal scales, and especially in relation to eutrophication and climate change. Eutrophication in both coastal and open areas of the Baltic Sea will likely enhance methane production, which will in turn have feedback effects with climate change.

This thesis consists of three studies, each of which concentrates on different aspects of the Baltic Sea methane cycle (Fig. 1). In study **I**, changes

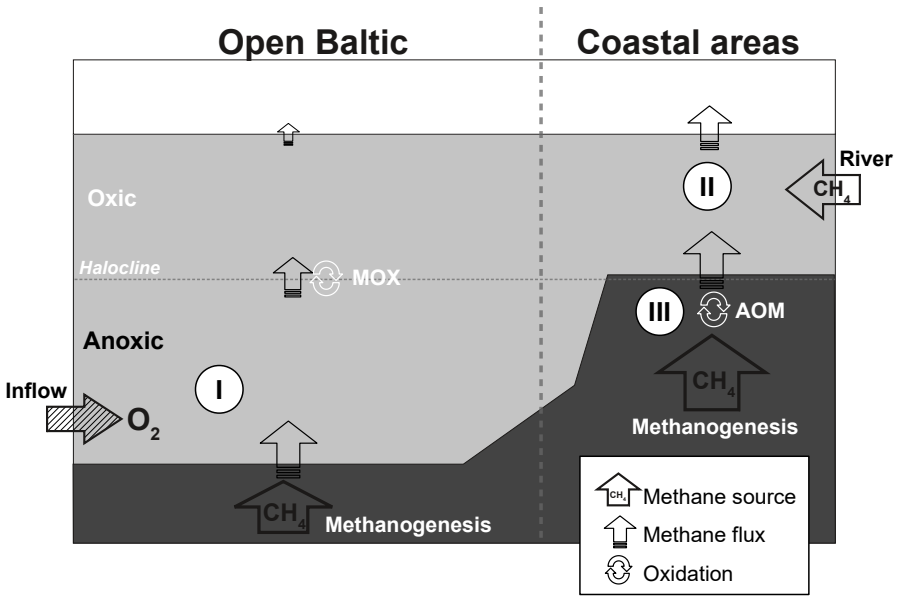

Figure 1: Schematic representation of the main Baltic Sea methane processes studied in this thesis. In the coastal areas, sedimentary methanogenesis and river input are the primary sources of CH_4 (**II**), while anaerobic oxidation of methane (AOM) in the sediments is the primary removal process (**III**). Sedimentary methanogenesis is also the primary source in the open Baltic, while aerobic methane oxidation (MOX) in the water column is the primary sink. Inflows bringing oxygen are the main removal mechanism for CH_4 in the deep water (**I**).

occurring in the deep Baltic, which is the largest reservoir of CH_4 in the Baltic Sea, were investigated in response to the oxygen introduced by MBIs. With study **II**, the balance of methane process across an estuarine gradient in the coastal Baltic Sea was studied. Finally, study **III** is wholly concentrated on the oxidative filters in the coastal sediments, and the microbial communities involved in the various stages of the methane cycle.

The thesis aimed to answer the following questions:

1. What are the main factors controlling the production and consumption of methane in the Baltic Sea?

2. How does the balance of methane processes vary spatially in coastal areas of the Baltic Sea?

3. How does seasonality affect methane dynamics on a local scale?

2 Materials and methods

2.1 Study areas (Papers I-III)

This thesis had two main study areas: one in the Central Baltic Sea (Fig. 2a, paper **I**) and another in the Pojo Bay estuary situated in the Gulf of Finland (Fig 2c, papers **II-III**).

The five sampling locations in the open Baltic are long time monitoring stations. Especially BY15 (also known as TF271 in literature) has been studied extensively over the years (e.g. Schmaljohann *et al.* 1998; Schmale *et al.* 2010; Jakobs *et al.* 2013), as it is located in the deepest part of the sub-basin. The two main basins studied in paper **I** were eastern Gotland basin (EGB: BY10, BY15, BY20) and western Gotland basin (WGB: BY32, BY38). Of these two, EGB is first exposed to the effects of the inflows from the south, from where the water masses circle around the island of Gotland counter-clockwise before propagating towards both the EGB and the Gulf of Finland (Meier, 2007).

The Pojo Bay estuary has also been studied extensively for over a century (Stipa, 1999). It is a narrow, fjord-like estuary with one primary river, river Mustionjoki (also known as Karjaanjoki), discharging into it. Until the 1980s, the estuary and its catchment were the site for moderate industrial activity and organic matter loading from the land was much higher, leading to periods of severe anoxia (Malve *et al.*, 2000; Jilbert *et al.*, 2018). Since then, land use changes and reductions in industry point sources have seen improvements in the condition of the estuary (Asmala *et al.*, 2012).

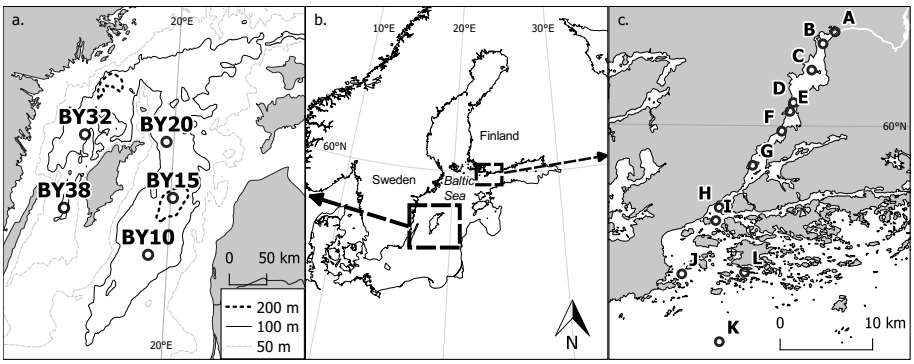

Figure 2: Map of the study areas. Panel a. contains the study sites of paper **I**, panel c. contains the study sites for papers **II** and **III** (only sites (A, C, D and J for paper **III**). Note the different scales in the panels.

The sampling sites in the open Baltic were selected because they are situated along the expected propagation route of the MBIs (Meier, 2007). Samples were collected from large research vessels (R/V *Aranda* and R/V *Salme*) on six separate cruises during 2015. Sampling sites in the Pojo Bay were selected because they run along the main channel of the estuary and span a salinity gradient from nearly fresh water in the river mouth to approximately salinity of eight in the open sea. In **III**, sites A, C and J were studied more closely, with site D included for microbial data. Pojo Bay sites were sampled from small boats in 2015–2017 and additionally once from a hovercraft during a winter sampling campaign in 2017.

2.2 Porewater methane sampling (Papers II-III)

Sediment samples were collected with a GEMAX™ twin gravity corer. Holes were pre-drilled vertically along the acrylic core tubes at 1.5 cm intervals. During sampling, the holes were covered with waterproof tape. Back on deck,

the tape was punctured and 10 mL of sediment was retrieved with a cut-off syringe. Sediment was immediately transferred into a 65 mL glass bottle pre-loaded with supersaturated NaCl, after which the bottle was topped up with NaCl solution and capped with a butyl-rubber septum and a screw cap (Egger *et al.*, 2015). At the home lab, a headspace of 10 mL N_2 was introduced into the samples by removing an equivalent amount of sediment slurry. Two subsamples of 1 mL were retrieved from the headspace after thorough shaking, transferred into two 10 mL pre-evacuated Exetainers™ (model 839W) and pressurised with 20 mL of N_2, prior to analysis with a gas chromatograph.

2.3 Water column dissolved gas sampling (Papers I-II)

Water column methane samples were retrieved either with a shipboard rosette system in Niskin bottles (**I**) or with a 5 L Limnos™ water sample retriever (**II**). In both cases, the dissolved gas concentration was measured using a headspace equilibration technique. In brief, 60 mL of water was retrieved from the sampling vessel with a 60 mL plastic syringe capped with a three-way stopcock. Water volume was brought down to 30 mL, after which a headspace of 31 mL N_2 was introduced and the syringes were left to room temperature to warm up for 30 minutes. Subsequently, the syringes were shaken vigorously for 3 minutes to ensure equilibration. The headspace was then transferred to a dry syringe via a three-way stopcock and from there to a 10 mL Exetainer™ (model 839W). Partial pressure of CH_4 in the vial was measured with a gas chromatograph. The original concentration of dissolved CH_4 was then calculated by applying Henry's law and Bunsen solubility

coefficients as given by Wiesenburg & Guinasso (1979).

The method is inaccurate at low gas concentrations due to air contamination in the Exetainers™ (Sturm *et al.*, 2015). For this reason, an analytical cut-off value was established, below which all values were set to that of the cut-off. The salinity dependent cut-off value was based on the mean concentration of the constituent gases in the pre-evacuated Exetainers and other sources of imprecision in the data (for details, see **I**: Supplement). This error primarily affected the surface concentrations in study **I**, but did not affect any of the main findings of the study. All concentrations in study **II** were well above the cut-off and therefore unaffected by this issue.

2.4 Gas chromatography (Papers I-III)

After transfer to the Exetainers™, both water column and porewater CH_4 samples were analysed with a gas chromatograph (Agilent Technologies 7890B). Four-point calibration of known CH_4 concentrations was used for both water column and sediment porewater samples, applying different concentration series for each. Standard series were analysed before and after each analytical series to monitor between-series drift. Single standards were also analysed after every ten samples to account for drift within each series.

2.5 Other dissolved porewater constituents (Papers II-III)

Additional porewater parameters were measured with Rhizons™ from a GEMAX™ core parallel to the porewater CH_4 core. The syringes for ΣH_2S (paper **II**) were preloaded with 1 mL of zinc acetate (10%) while syringes for SO_4^{2-}, Fe, Mn and P (papers **II** and **III**) were acidified with 1 M HNO_3 after sampling.

The ΣH_2S series was analysed spectrophotometrically (Cline, 1969; Reese *et al.*, 2011) while the rest of the porewater constituents were analysed with inductively coupled plasma optical emission spectrometry (ICP-OES) in a HNO_3 matrix and against known standard concentrations.

2.6 Radiotracer incubation (Paper III)

Methane oxidation rates were measured with sediment incubations. Four acrylic minicores (26 ID x 400 mm) were pushed into GEMAX™ cores at each study site. They were capped from both ends with rubber stoppers and stored upright fully immersed in bottom water collected from each site. At the home lab, $^{14}CH_4$ tracer was injected into the cores at vertical intervals of 1 cm and the cores were left to incubate for 24 h at *in situ* temperature. Incubation was stopped by sectioning the minicores at 2 cm intervals and transferring the sediment slices into 100 mL glass bottles containing NaOH, which also fixed all inorganic carbon in the sample as carbonates. Residual $^{14}CH_4$, not incorporated into CO_2 during the incubation, was measured by flushing the headspace of the glass bottles through a combustion oven at 850 °C, and trapping the $^{14}CO_2$ produced from combustion with an amine solution. Next, a scintillation cocktail was added and the activity of the residual aliquot was measured with a liquid scintillation counter. After the removal of residual $^{14}CH_4$, a scintillation vial containing an amine trapping solution was gently inserted into the sediment slurry in the glass vials. To evolve the ^{14}C carbonates into the headspace, 6 M HCl was added prior to capping of the bottles. To ensure that all gas was evolved, the samples were left under gentle magnetic stirring for 12 h, after which the scintillation

vials were removed and thoroughly cleaned from the outside. Subsequently, a scintillation cocktail was added and activity of the microbially produced $^{14}CO_2$ was measured with a liquid scintillation counter (Wallac 1415 LSC). Oxidation rates were calculated based on in situ, pre-incubation methane concentrations, measured from a parallel sediment core (see subsection 2.2), and the ratio between the microbially produced $^{14}CO_2$ and the residual $^{14}CH_4$ according to Treude *et al.* (2005).

2.7 Methane flux calculations and modelling of production and consumption in sediments (Paper II)

Fluxes of CH_4 from sediment to the water column were calculated from the concentration gradient between bottom water and surface sediment pore-water CH_4 concentrations using Fick's first law. The calculation took into account porosity (Boudreau, 1997) and sediment diffusivity of CH_4 (Berner, 1980; Iversen & Jørgensen, 1993).

Atmospheric flux of CH_4 was calculated from the concentration gradient between surface water and atmospheric CH_4 using a two-layer model of Liss & Slater (1974). The calculation uses a gas transfer velocity coefficient k, which was parametrized as a function of wind speed (Wanninkhof, 1992). In this study, an estuary based exponential formulation of wind speed and gas transfer was used (Raymond & Cole, 2001). Atmospheric CH_4 concentrations and wind speed data from monitoring stations of the Finnish Meteorological Institute were used in the calculations. Wind speed was estimated as a function of distance between two weather stations using linear interpolation.

The software PROFILE (Berg *et al.*, 1998) was used to model net con-

sumption and production of porewater CH_4 in vertical zones of the sediment column. The model is based on a simplified mass conservation equation of Boudreau (1997).

3 Results and discussion

3.1 Main findings of the thesis

The main aim of this thesis was to broaden and deepen the scientific knowledge regarding methane processes in the Baltic Sea. To that end, study **I** showed that the MBIs are capable of efficiently and rapidly removing almost all methane that had accumulated in the EGB during the previous period of stagnation. The removal of CH_4 was mostly through oxidation, though displacement also played a role. However, it would seem that the oxygen quantity of the MBI was insufficient to maintain oxic conditions in the deep Baltic for an extended period. Less than one year after the MBI of late 2014, CH_4 started rapidly accumulating in the bottom of EGB. The WGB was mostly unaffected by the MBI of 2014 during the period of observation.

Study **II** showed that the Pojo Bay estuary is a perpetual and significant net source of CH_4 into the atmosphere. While rivers are an important source of allochthonous CH_4 into the coastal Baltic Sea, autochthonous methanogenesis fuelled by a legacy of eutrophication and near-bottom hypoxia was still the main source of CH_4 in the Pojo Bay estuary, and primarily responsible for the atmospheric flux of CH_4. The atmospheric fluxes of CH_4 decreased with distance offshore and were mostly decoupled from local sedimentary fluxes, implying that seasonal hydrodynamics have an important role in water column transport of CH_4.

The sedimentary oxidative sinks of CH_4 in the Pojo Bay estuary were quantified in study **III**. Instead of a single (sulphate-mediated) filter against

atmospheric emissions of CH_4, three distinct processes were at work at different depths of the sediment. Evidence of MOX at the sediment-water interface was found, along with active sulphate-mediated AOM at the SMTZ. However, the highest rates of CH_4 oxidation, with largest abundances of microbes commonly associated with AOM, were found well below the SMTZ. Since sulphate was completely depleted at these depths, AOM was likely mediated by other electron acceptors, such as iron or manganese.

In the following sections, methane dynamics in the Baltic Sea are discussed in detail and the findings of this thesis are put into context of previous literature.

3.2 Sources of methane in the Baltic Sea

In the Baltic Sea, methanogenesis is generally more prevalent in shallower coastal regions, gradually decreasing towards the deeper basins, such as the Gotland Basin (Lein *et al.*, 1981; Heyer & Berger, 2000). In the deep basins of the Baltic Sea, methanogenesis typically occurs relatively deep (80–160 cm) in the Holocene sediments (Lein, 1983; Piker *et al.*, 1998; Schmaljohann *et al.*, 1998), though high spatial variability exists (Schmaljohann *et al.*, 1998; Ulyanova *et al.*, 2012; Brodecka *et al.*, 2013; Jilbert & Slomp, 2013). The results of this study concur with the previous literature. In the studied coastal transect, sediment methanogenesis was consistently a strong source of CH_4 into the water column (**II**). At shallow, well oxygenated coastal sites, or sites without strong sedimentation (e.g. transportation bottoms), methane fluxes from the sediment to the water column were generally low ($<$40 µmol m^{-2} d^{-1}). However, deeper sites with higher OM content, that also undergo

intermittent seasonal hypoxia, fluxes typically ranged between 200—6000 µmol m^{-2} d^{-1} (**II**: Fig. 2, Table 1), with an average of 1972 µmol m^{-2} d^{-1}. While typically sedimentary fluxes decrease offshore (Lein *et al.*, 1981; Heyer & Berger, 2000), the single highest sedimentary flux value of 9600 µmol m^{-2} d^{-1} of this study was found at site K (**II**: Fig. 3), which is the site furthest from the river mouth (Fig. 2c,). However, as the site remains quite close to the coast (<5 km), it cannot be considered a true offshore site.

The calculated sedimentary fluxes in this study are in general agreement with previous studies from coastal sites in the Baltic. Schmaljohann (1996) estimated sedimentary fluxes between 372–4848 µmol m^{-2} d^{-1} from the Kiel Harbour in the southern Baltic Sea, with one extreme value of 17808 µmol m^{-2} d^{-1}, which they attributed to seasonal anoxia. Sedimentary fluxes between 301–1014 µmol m^{-2} d^{-1} were reported from the Himmelfjärden Bay, Sweden (Thang *et al.*, 2013), and 100–2600 µmol m^{-2} d^{-1} by Sawicka & Brüchert (2017) from the same area. In comparison to the open Baltic, Ulyanova *et al.* (2012) reported an average flux of 140 µmol m^{-2} d^{-1} in the Gdansk deep and 330 µmol m^{-2} d^{-1} from the Gotland deep. During inflow conditions, sedimentary fluxes of <50 µmol m^{-2} d^{-1} have been reported (Piker *et al.*, 1998).

In this study, two sites (J and L) in the Pojo estuary were studied in more detail. Site J is situated in the main channel of the estuary, and consequently features more active hydrodynamics. In contrast, site L is sheltered by surrounding islands and typically exhibits stronger thermal stratification and seasonal hypoxia (Fig. 2c). No clear seasonal trend in sedimentary CH_4 fluxes was observed, with site L having slightly higher sedimentary fluxes during

winter and lower during summer, while site J exhibited an opposite trend (**II**: Table 1). In contrast, Sawicka & Brüchert (2017) reported generally higher sedimentary fluxes during summer. Mogollón *et al.* (2011) also found direct relationship between methanogenesis and seasonal temperature changes, but did not find significant diffusive flux into the water column at any point of the study, due to active AOM. Schmaljohann (1996) and Borges *et al.* (2018) found seasonal patterns in methanogenesis mostly related to phytoplankton blooms, with elevated rates occurring after the settling of the blooms.

Modelled rates of sedimentary methane production (methanogenesis) varied between 5–20 nmol cm^{-3} d^{-1} at the sites, with generally higher maximum values found from site J (**II**: Fig. 6). However, while the more oxic site J (Fig. 2c) had a relatively compressed zone of methanogenesis below the SMTZ, the seasonally hypoxic site L featured a much broader zone of active methanogenesis throughout the SMTZ. Deeper in the sediment column, methanotrophy became more dominant and porewater CH_4 concentrations decreased with depth at both sites. This is likely a legacy effect of past eutrophication (**II**), which has increased OM loading in the system in the last 40 years, causing enhanced methanogenesis in the surface sediments (Jilbert *et al.*, 2018). In the open Baltic, rates of methanogenesis are generally lower, especially in the surface sediments, with values between 0.3–2.8 nmol cm^{-3} d^{-1} reported from the Gotland deep (Piker *et al.*, 1998). However, at other Baltic coastal sites, rates of up to 37 nmol cm^{-3} d^{-1} have been reported (Treude *et al.*, 2005).

Schmaljohann *et al.* (1998) estimated that the area of highest methane and sulphide concentrations (ca. 35 km^2) in the bottom of the Gotland basin

was producing 1435–1939 mol CH_4 d^{-1}, which according to their estimate was enough to supply the majority of the CH_4 pool in the deep water of the Gotland deep. In comparison, the Mustionjoki River introduced between 215–1369 mol d^{-1} of CH_4 in to the Pojo Bay (Table 1). Hence, though the river is just a single point source, it introduced a large amount of dissolved CH_4, which contributed significantly to atmospheric fluxes of CH_4 near the river mouth (**II**: Fig. 3). Other rivers have also been identified as potentially strong sources of CH_4 into the Baltic Sea. For example, Abril & Iversen (2002) estimated that in Randers Fjord, Denmark, the river brought on average 1093 mol d^{-1} of CH_4 into the estuary and Silvennoinen *et al.* (2008) showed that the Temmesjoki River in the Northern Baltic Sea was consistently a strong source of atmospheric CH_4 and introduced 491 mol d^{-1} to the adjacent estuary.

Table 1: Calculated ranges of daily riverine inputs of CH_4 from the river Mustionjoki. Discharge values are from SYKE hydrological monitoring data.

Date	CH_4 concentration in river water (nmol L^{-1})	Daily mean discharge (m^3 s^{-1})	Total river input (mol d^{-1})
2015-06-15	454	11.5	449
2016-06-07	660	7	397
2017-03-14	199	20.6	354
2017-06-06	281	8.8	215
2017-08-15	1666	9.5	1369

In further comparison to the deep Baltic, study **II** showed that 5234 mol d^{-1} of CH_4 was released from the inner bay sediments of Pojo Bay alone (area ca. 9.2 km^2). Abril & Iversen (2002) reported a slightly more modest value

of 1580 mol d^{-1} from Randers Fjord, which is still comparable the deep water sediment fluxes reported by Schmaljohann *et al.* (1998). Overall, it can be concluded that both rivers and sediments are significant sources of CH_4 into the coastal water column of the Baltic Sea (**II**). Furthermore, eutrophication and the ensuing coastal hypoxia (Conley *et al.*, 2011; Carstensen *et al.*, 2014b; Jokinen *et al.*, 2018) have the potential to expand the importance of coastal areas as sources of CH_4 even further.

3.3 Sinks of methane in the Baltic Sea

The two primary sinks of CH_4 against atmospheric emission in the Baltic Sea are AOM in the sediments (**III**; Treude *et al.* 2005; Thang *et al.* 2013; Egger *et al.* 2015) and MOX in the water column (**I**; Schmale *et al.* 2012; Jakobs *et al.* 2013). Both play a role in both coastal and open sea settings, but broadly speaking MOX is more prevalent in the open Baltic and AOM in the coastal areas. The importance of MOX increases further in the open Baltic Sea when inflows bring oxygen below the halocline, (**I**; Schmale *et al.* 2016).

Methane concentrations in the EGB in the open Baltic changed dramatically in response to the MBI of 2015 (**I**). Oxic water reached the bottom of the EGB (Fig. 2a, site BY15) early in March, which pushed the old bottom water both northwards and upwards. However, though oxygen was introduced and CH_4 concentrations decreased near the bottom, a midwater layer rich in methane ($>$ 200 nM) and containing H_2S (ca. 18 µM) could still be seen early in March at 100–200 m depth (Fig. 3).

Though oxygen concentrations remained low ($<$ 60 µM), all H_2S and most

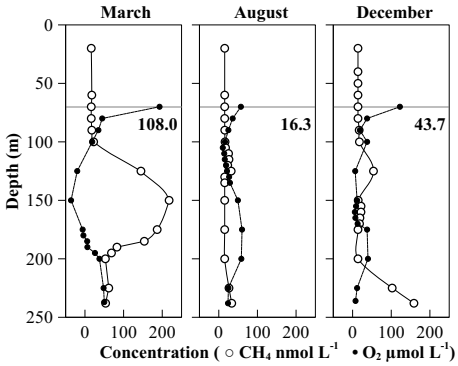

Figure 3: Methane and oxygen concentrations at BY15 in the central EGB from March to December 2015. The grey line indicates the approximate depth of the halocline (70 m) and the figure underneath indicates the volume weighted average concentration of CH_4 below that depth (nmol L^{-1}). The presence of H_2S is expressed in negative oxygen equivalents. Note the different units of the two parameters.

of the CH_4 was removed from below the halocline by August. From March 2015 to August 2015, the inflow decreased the volume weighted average concentration of CH_4 below 70 m depth from 108 to 16.3 nM (-0.65 nM d^{-1}). Oxidation accounted for 79% of the CH_4 removal (**I**: Fig. 3). However, soon thereafter oxygen concentrations began declining again and by December 2015, the volume weighted average concentration of CH_4 had increased back to 43.7 nM, with the bottom water concentration having increased back to 158.7 nM (0.22 nM d^{-1}). Though the MBI of late 2014 was the third largest ever recorded (Mohrholz, 2018) and brought large amounts of oxygen in the deep Baltic, conditions soon became anoxic again (Neumann *et al.*, 2017). This is typically followed with high sedimentary fluxes of CH_4 (Piker *et al.*, 1998). The persistence of oxic conditions in the deep Baltic after MBIs depends on the hydrodynamics of the individual MBIs, e.g. whether the main

inflow is followed by smaller inflows (Neumann *et al.*, 2017). Furthermore, legacy of eutrophication caused by land-based nutrient discharge, which leads to a high oxygen demand in deep-basin sediments, also plays a role (Vahtera *et al.*, 2007; Carstensen *et al.*, 2014a). Consequently, it appears that the oxygen content of recent inflows has been insufficient to maintain oxic and CH_4-free conditions in the deep Baltic for extended periods.

Not only were the effects of the MBI of 2014 limited in time, but also in spatial coverage. BY20, which is the site immediately north of BY15, near the northern rim of the EGB (Fig. 2a), never exhibited a clear pattern of CH_4 removal during the year following the inflow. Instead, CH_4 concentrations were highly dynamic throughout the year, likely due to complex spatial displacement effects between the old CH_4-rich water masses and CH_4-free inflow water (**I**: Fig. 2). The inflow also never seemed to reach the WGB during 2015 (**I**: Fig. 2). Instead, water column concentrations of CH_4 remained between 400–700 nM below the halocline, which are similar to CH_4 concentrations at the EGB during stagnation periods (Schmale *et al.*, 2010; Jakobs *et al.*, 2014).

Water column oxidation is important also in the coastal areas of the Baltic Sea. Steinle *et al.* (2017) estimated that in the Eckernförde Bay in the southern Baltic Sea, 2.4–19 times more CH_4 was oxidized in the water column than was emitted to the atmosphere. Schmaljohann (1996) estimated that MOX accounted for 28% of oxygen uptake in the Kiel harbour. This is congruent with the findings of this thesis; in Pojo Bay sediment fluxes were mostly decoupled from atmospheric fluxes (**II**), which was likely due to a combination of water column MOX and local hydrodynamics. Evidence of

MOX occurring at the sediment surface was also found, likely enhanced by bioturbation (**II**: Fig. 6; **III**: Fig. 3). Type I MOB were also present in large numbers above the SMTZ at the studied sites (**III**: Fig. 4).

While MOX had an important role in the water column and surface sediments in this study, AOM formed the primary sink against atmospheric emissions of CH_4 in the Pojo Bay estuary (**III**). Rates of AOM varied both horizontally across sites and vertically within sites. AOM activity near the SMTZ became more pronounced and vertically compressed offshore. Near the river mouth at site A, mean AOM rates near the SMTZ were relatively low at only 1.55–2.08 nmol cm^{-3} d^{-1}, from which they increased to 15.08–19.46 nmol cm^{-3} d^{-1}, and finally to 32.09 nmol cm^{-3} d^{-1} (**III**: Fig. 3). These rates are slightly higher, but still broadly comparable to AOM rates from other Baltic Sea sites. Thang *et al.* (2013) reported AOM rates of 1–16 nmol cm^{-3} d^{-1} from the Himmerfjärden estuary in Sweden and Treude *et al.* (2005) reported rates between 1–14 nmol cm^{-3} d^{-1} from the Eckernförde Bay in Germany.

All three sites of this study also featured distinct AOM activity well below the SMTZ, with the highest rate found from site J at 31 cm depth (13.89 nmol cm^{-3} d^{-1}). At these depths SO_4^{2-} was completely depleted, which implies that AOM below the SMTZ at the sites was mediated by alternative electron acceptors, such as iron or manganese (Beal *et al.*, 2009; Egger *et al.*, 2015). ANME-2a/b were the most dominant group of AOM clades at both site A and C (**III**: Fig. 4), which is typical for shallow coastal SMTZ systems (Treude *et al.*, 2005; Knittel *et al.*, 2018). ANME-2d was also present, especially near the river mouth. Both groups of ANME have been shown to be more flexible

in their use of electron acceptors compared to the ANME-1 (Timmers *et al.*, 2017), which were nearly non-existent in this study (**III**: Fig. 4). As with the AOM rates, the highest relative abundances of ANME were found well below the main SMTZ (**III**: Fig. 4).

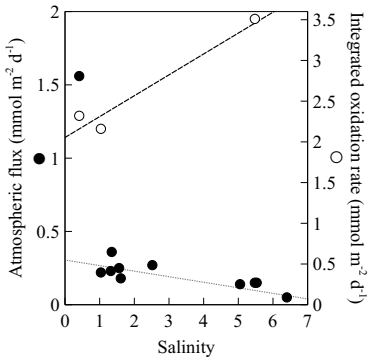

Figure 4: Atmospheric flux of CH_4 in June 2016 (black dots) and integrated sediment CH_4 oxidation rates in August 2017 (white dots) along the surface salinity gradient of the Pojo Bay estuary. Note the different scales in the y-axes.

The total depth-integrated oxidation rates (0–31 cm) of AOM increased offshore, from 2.32 to 3.51 mmol m^{-2} d^{-1} (Fig. 4; **III**: Table 1). This is likely a reflection of increased substrate availability, as AOM is dependent on the availability of both CH_4 and SO_4^{2-} (Valentine, 2002; Treude *et al.*, 2005), both of which increased offshore in the studied transect (**III**: Fig. 2). However, the highest below-SMTZ integrated rates were also found from the most offshore site J (**III**: Table 1). This was somewhat surprising, considering that sites near the river mouth featured much higher concentrations of iron and manganese (**III**: Fig. 2). It is possible that since both iron and manganese mediated AOM are up to 10 times more favourable energetically compared to sulphate (Beal *et al.*, 2009), smaller quantities of them are required as

substrates. Thus, it is conceivable that AOM rates are primarily limited by the availability CH_4 and not electron acceptors throughout the whole study transect.

While fully quantifying the role of iron-AOM was beyond the scope of this study, it still reinforces the findings of previous works that implicate the importance of iron-AOM in the Baltic Sea (e.g., Egger *et al.* 2015). The conditions in the Baltic Sea, i.e. low salinity, which causes relatively low SO_4^{2-} availability, combined to high availability of CH_4 and rapid accumulation of Fe oxides in sediments, create ideal conditions for iron-AOM (Rooze *et al.*, 2016). Not only has iron mediated AOM the potential to reduce CH_4 emissions from the Baltic sediments, it has been identified as a key component in iron biogeochemistry in the Baltic Sea (Egger *et al.*, 2015, 2017), and by extension e.g. phosphorus biogeochemistry (Jilbert & Slomp, 2013). Other electron acceptors of AOM may have similar cascading effects in the wider sediment biogeochemistry. Hence, more study of non-sulphate AOM is required, especially in natural settings.

3.4 The Baltic Sea as a source of atmospheric methane

Though oxic conditions were not maintained in the deep Baltic for long after the inflow and CH_4 started accumulating again, the surface waters of the open Baltic are usually only slightly supersaturated with CH_4 even during periods of stagnation (Bange *et al.*, 1994; Schmale *et al.*, 2010; Gülzow *et al.*, 2013). Hence, the open Baltic is only a marginal source of CH_4 into the atmosphere during stagnation and likely even less so during inflows, as the inflow of 2014 did not seem to cause any large changes in CH_4 concentrations

above the halocline in the year following the inflow (**I**).

However, shallow coastal areas have been identified as sites of extremely large and potentially underestimated sources of CH_4 emissions to the atmosphere (Borges *et al.*, 2016), with atmospheric fluxes up to three orders of magnitudes higher than in the open ocean (Heyer & Berger, 2000; Borges *et al.*, 2018). This was replicated also in this study. Atmospheric emissions were consistently highest near the river mouth in the Pojo Bay (**II**), and decreased seawards. This trend continues all the way to the Gulf of Finland (Fig. 5).

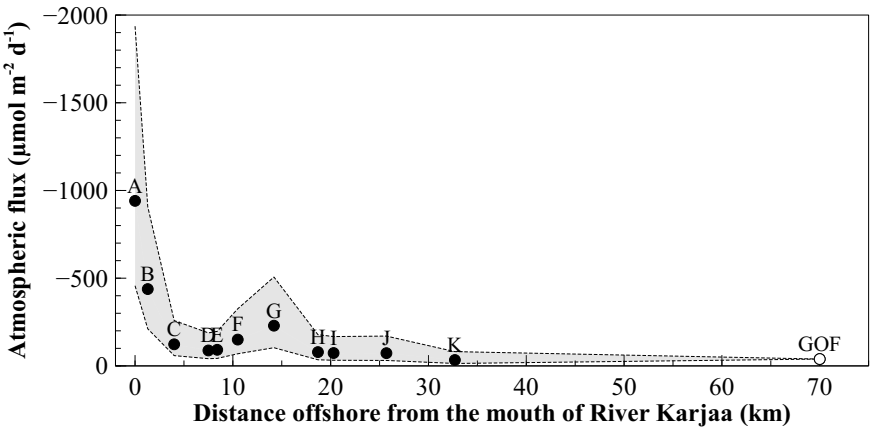

Figure 5: Average atmospheric fluxes of methane in Pojo Bay in 2015. The value GOF is a reference value of atmospheric flux in the open Gulf of Finland from Gülzow *et al.* (2013). The grey area represents the range of fluxes based on monthly wind averages (does not apply to GOF value).

Fluxes to the atmosphere from the whole Pojo Bay across all sampling sites ranged between 34–4340 µmol m^{-2} d^{-1}, with an average of 354 µmol m^{-2} d^{-1}. The single highest atmospheric flux of the whole study, 4340 µmol m^{-2} d^{-1}, was from site A in August 2017. The potential of rivers as sources of at-

mospheric CH_4 has been recognized previously (Upstill-Goddard *et al.*, 2000; Stanley *et al.*, 2016). Silvennoinen *et al.* (2008) measured atmospheric fluxes of up to 4112 µmol m^{-2} d^{-1} upstream in the Temmesjoki River, situated approximately 500 km North from Pojo Bay, and 1184 µmol m^{-2} d^{-1} where the river runs in to the Bothnian Bay. Similarly to this study, Silvennoinen *et al.* also measured the highest atmospheric fluxes of CH_4 during winter. Gutiérrez-Loza *et al.* (2019) reported winter fluxes of 1132–1624 µmol m^{-2} d^{-1} and summer fluxes of 1115–1287 µmol m^{-2} d^{-1} from the east coast of the Gotland Island. Conversely, Heyer & Berger (2000) reported highest fluxes during summer in coastal Southern Baltic Sea, similar to Bange *et al.* (1994) for the central and southern open Baltic. Gülzow *et al.* (2013) also report highest overall atmospheric fluxes from the Baltic Sea during winter. However, they suggest that the effects of seasonality are not uniform in the Baltic Sea. Permanently stratified basins such EGB and WGB are less affected by seasonality, while in shallow coastal areas, CH_4 accumulates below the pycnocline during summer stratification and is released during winter when the water column is mixed. Evidence of this phenomenon was observed also in the seasonally studied sites of this study (**II**). However, as coastal areas are highly heterogeneous and dynamic, large local variability in these seasonal patterns can be expected, which was also shown in the seasonally studied sites of this study (**II**).

Heyer & Berger (2000) used floating chambers to measure surface fluxes of 156–363 mmol m^{-2} d^{-1} from a shallow coastal area located in the Southern Baltic Sea. While these are outlier values, and the fluxes they measured were most likely ebullitive and thus not directly comparable to the calculated

fluxes of this study, it still shows that the coastal areas of the Baltic Sea have the potential for extremely high atmospheric emissions of methane. Ebullition was not measured directly in this study, but circumstantial evidence of it was observed, such as visually extremely gassy sediment cores and extreme outlier concentrations in water column CH_4 measurements, likely caused by trapped gas bubbles. Furthermore, in a recent study, Humborg *et al.* (2019) detected strong ebullitive activity in the Pojo Bay area using acoustic methods. While ebullition is certainly occurring also in the deep Baltic, the deeper water column means that there is more time for the gas bubbles to dissolve (Martens & Val Klump, 1980; McGinnis *et al.*, 2006; Gentz *et al.*, 2014). In shallow coastal areas, travel times through the water column are much shorter and ebullitive atmospheric CH_4 flux much more likely. Furthermore, coastal areas are much more susceptible to wind-driven advective mixing, which can cause greatly enhanced diffusive atmospheric fluxes (Gelesh *et al.*, 2016; Humborg *et al.*, 2019), especially since gas transfer across is directly related to wind speed Wanninkhof (2014).

Lakes and other freshwater systems are typically considered a more important source of atmospheric CH_4 than seas (Kirschke *et al.*, 2013). However, Juutinen *et al.* (2009) reported an average flux of 134 µmol m^{-2} d^{-1} from 177 Finnish lakes and Bastviken *et al.* (2004) reported a similar figure of 112 µmol m^{-2} d^{-1} from 8 Swedish lakes. Globally, the average flux of CH_4 from lakes has been estimated to be 2048 µmol m^{-2} d^{-1}, of which over half is ascribed to ebullition (Bastviken *et al.*, 2004). While comparison between different studies and environments is difficult due to different methodologies and various scaling issues, it is still apparent that the atmospheric flux values

of this study are comparable to lacustrine values, and potentially even exceed them.

In conclusion, the coastal Baltic Sea is potentially a strong source of atmospheric CH_4. Globally the CH_4 dynamics and fluxes from coastal areas remain poorly quantified (Kirschke *et al.*, 2013; Humborg *et al.*, 2019), even though they have been long considered potential hotspots for CH_4 emissions (Reeburgh, 1969). Hence, this study joins several other recent studies, which suggest that the role of coastal areas may have been underestimated in the global CH_4 budgets (Thornton *et al.*, 2016; Borges *et al.*, 2018; Gutiérrez-Loza *et al.*, 2019; Humborg *et al.*, 2019).

4 The Future of Baltic Sea methane processes

Human induced eutrophication has caused the spread of hypoxia at an unprecedented rate throughout the coastal oceans (Diaz & Rosenberg, 1995, 2008). Eutrophication has significantly contributed to propagation of hypoxic and anoxic areas also in the Baltic Sea during the last century (Conley *et al.*, 2011; Carstensen *et al.*, 2014a; Jokinen *et al.*, 2018). Eutrophication increases the availability of organic matter, which is one of the key drivers of methanogenesis (Middelburg *et al.*, 1996; Heyer & Berger, 2000; Naqvi *et al.*, 2010; Borges & Abril, 2011) and there is compelling evidence that eutrophication is directly linked to CH_4 concentrations in aquatic systems (Borges *et al.*, 2018).

Effects of climate change are expected to be strongest in the boreal and arctic areas (Soja *et al.*, 2007; IPCC, 2014). In the Baltic Sea region, annual

average temperatures are expected to increase by 2–4 °C during this century (Andersson *et al.*, 2015). As with most microbial processes, methanogenesis is also temperature dependent (Conrad, 2009; Yvon-Durocher *et al.*, 2014) and temperature has been identified as an extremely important component in CH_4 dynamics (Mogollón *et al.*, 2011; DelSontro *et al.*, 2016; Sawicka & Brüchert, 2017; Borges *et al.*, 2018). It has also been suggested that enhanced mineralization rates caused by higher temperatures were the reason why oxygen was depleted so rapidly after the MBI of 2014 (Neumann *et al.*, 2017). Climate change is also expected to decrease the duration and extent of ice-cover during winters (Andersson *et al.*, 2015), which will likely affect the propagation of CH_4-rich fresh water from river sources (Schneider *et al.*, 2014) and increase CH_4 emissions in the ice-free areas (Silvennoinen *et al.*, 2008; Wik *et al.*, 2016).

However, while the relationship between eutrophication and atmospheric emissions of CH_4 is mostly straightforward, the relationship between increasing ambient temperatures and CH_4 emissions is slightly less so. Firstly, while rates of methanogenesis are increased in higher temperatures, so are the rates of methanotrophy (Zehnder & Brock, 1980; Naqvi *et al.*, 2010; Fuchs *et al.*, 2016), which might offset the increases in methanogenesis. Secondly, climate change is also predicted to increase precipitation in the Baltic Sea region by up to 30% (Andersson *et al.*, 2015). This, combined to increases in temperature, will likely lead to stronger stratification especially in the open Baltic, which in turn might enhance water column methanotrophy (Fenchel *et al.*, 1995; Bastviken *et al.*, 2004; Schmale *et al.*, 2012), and decrease the likelihood of advective mixing occurring due to storms (Gelesh *et al.*, 2016; Humborg

et al., 2019).

Nevertheless, taken together, the combined effects of higher temperature and organic matter availability have been strongly linked to enhanced aquatic methane fluxes to the atmosphere (Borges *et al.*, 2016, 2018; Sawicka & Brüchert, 2017; Humborg *et al.*, 2019). Moreover, most studies seem to suggest that ebullitive fluxes are affected the most by the combined effects of climate change and eutrophication (Heyer & Berger, 2000; Bastviken *et al.*, 2004; Davidson *et al.*, 2018; Humborg *et al.*, 2019). Increased ebullitive fluxes in the deep open Baltic might be effectively mitigated by bubble dissolution and subsequent oxidation (Martens & Val Klump, 1980; McGinnis *et al.*, 2006; Gentz *et al.*, 2014). However, in shallow coastal areas, ebullition enhanced by the combined effects of ongoing climate change, along with past and present eutrophication (**II**), can bypass the oxidative filters both in the sediment and in the water column. Hence, total CH_4 emissions from the Baltic Sea can be expected to increase in the future (Heyer & Berger, 2000; Borges *et al.*, 2016; Humborg *et al.*, 2019).

5 Conclusions

- Methane dynamics in the Baltic Sea are complex, and spatially and temporally variable.
- The whole Baltic Sea is a perpetual net source of CH_4, though magnitude of atmospheric fluxes varies with distance offshore.
- Sedimentary methanogenesis is an important source of CH_4 throughout the Baltic, but in the coastal areas, it is supplemented by river inputs. Methanogenesis is largely fuelled by past eutrophication, while river CH_4 is a signal of present-day eutrophication in river catchments
- Methane content of the open Baltic is largely governed by the MBIs, which introduce oxygen into the deep stagnant basins and remove CH_4 via MOX
- Sulphate-mediated AOM is the most important sink of CH_4 in the coastal sediments of the Baltic Sea. However, iron and manganese are likely also important electron acceptors for AOM in the coastal areas below the SMTZ
- Coastal areas in the Baltic Sea are susceptible to intermittent ebullitive fluxes of CH_4 during summer and enhanced diffusive fluxes during winter.
- The combined effects of eutrophication and climate change can be expected to increase ebullitive fluxes of CH_4 to the atmosphere in the coastal areas of the Baltic Sea in the future

Acknowledgements

This thesis was funded by the Academy of Finland. Further financial support was provided by the Onni Talas Foundation, Walter and Andrée de Nottbeck foundation and the University of Helsinki. My thanks to all of them for enabling this work in the first place.

I wish to extend my deepest gratitude to my supervisors Tom and Susanna for giving me this chance, even though I did not really have a background in aquatic biogeochemistry previously. Many thanks also to my advisory committee, Gregor, Anne and Antti, who offered lots of great input and ideas during our meetings. My sincere gratitude also to my co-authors Gregor, Gunnar, Jan and Antti.

I'm very grateful to the Swedish Meteorological and Hydrological Institute (SMHI), the Finnish Environment Institute (SYKE) and the Tallin University of Technology for allowing us to hitch a ride on their research cruises. Many thanks also to the captains and crews of R/V *Aranda* and R/V *Salme* of those cruises. The Tvärminne Zoological Station was an excellent base of operations for our coastal research, so thank you to the staff of the station. I'm also indebted to Kaj-Roger Hurme from the Instrument Centre, whose help, hospitality and expertise in radionuclides was crucial for the completion of this thesis. Special thanks also to Esa Tulisalo for his support with the gas chromatography work and Tina Treude for helping with the design of the incubation experiments.

I wish to thank all my colleagues at Viikki for the company and many discussions at coffee and lunch breaks. Thanks also to all my fellow PhD students for the peer pressure/support group. Warm thanks also to all the ABRU people, past and present. Fishy thanks to Joni for for reintroducing me to the fine art of angling, and for all the fishing trips we've gone to.

Thank you also to all my dear friends for the many reprieves you gave me from the academic life, and for being the charming bunch of rogues that you are. Thank you also to my parents for gently pushing me to try and make something of myself, and for politely nodding to my many stories from the world of mud. Finally, I wish to thank my beloved Laura, for your invaluable support and for being the best possible companion in life I could hope for. You and our lovely daughter make me want to become the best version of myself every day.

References

Abril, G. & Borges, A. V. (2004). Carbon Dioxide and Methane Emissions from Estuaries. In *Greenhouse Gas Emissions – Fluxes and Processes*, pp. 187–207. Berlin/Heidelberg: Springer-Verlag. doi:10.1007/3-540-26643-7_7.

Abril, G. & Iversen, N. (2002). Methane dynamics in a shallow non-tidal estuary (Randers Fjord, Denmark). *Marine Ecology Progress Series* **230**, 171–181. doi:10.3354/meps230171.

Andersson, A., Ripszam, M., Rowe, O., Wikner, J., Haglund, P., Eilola, K., Legrand, C., Figueroa, D., Paczkowska, J., Lindehoff, E., Tysklind, M. & Elmgren, R. (2015). Projected future climate change and Baltic Sea ecosystem management. *AMBIO* **44**, 345–356. doi:10.1007/s13280-015-0654-8.

Asmala, E., Stedmon, C. A. & Thomas, D. N. (2012). Linking CDOM spectral absorption to dissolved organic carbon concentrations and loadings in boreal estuaries. *Estuarine, Coastal and Shelf Science* **111**, 107–117. doi:10.1016/j.ecss.2012.06.015.

Bange, H. W. (2006). Nitrous oxide and methane in European coastal waters. *Estuarine, Coastal and Shelf Science* **70**, 361–374. doi:10.1016/j.ecss.2006.05.042.

Bange, H. W., Bartell, U. H., Rapsomanikis, S. & Andreae, M. O. (1994). Methane in the Baltic and North Seas and a reassessment of the marine emissions of methane. *Global Biogeochemical Cycles* **8**, 465–480.

Bange, H. W., Bergmann, K., Hansen, H. P., Kock, A., Koppe, R., Malien, F. & Ostrau, C. (2010). Dissolved methane during hypoxic events at the Boknis Eck time series station (Eckernförde Bay, SW Baltic Sea). *Biogeosciences* **7**, 1279–1284. doi:10.5194/bg-7-1279-2010.

Bastviken, D., Cole, J. J., Pace, M. L. & Tranvik, L. J. (2004). Methane emissions from lakes: Dependence of lake characteristics, two regional assessments, and a global estimate. *Global Biogeochemical Cycles* **18**, n/a–n/a. doi:10.1029/2004GB002238.

Beal, E. J., House, C. H. & Orphan, V. J. (2009). Manganese- and iron-dependent marine methane oxidation. *Science* **325**, 184–187. doi:10.1126/science.1169984.

Beaulieu, J. J., DelSontro, T. & Downing, J. A. (2019). Eutrophication will increase methane emissions from lakes and impoundments during the 21st century. *Nature Communications* **10**, 1375. doi:10.1038/s41467-019-09100-5.

Berg, P., Risgaard-Petersen, N. & Rysgaard, S. (1998). Interpretation of measured concentration profiles in sediment pore water. *Limnology and Oceanography* **43**, 1500–1510. doi:10.4319/lo.1998.43.7.1500.

Berner, R. A. (1980). *Early Diagenesis: A Theoretical Approach*. 241 pp., Princeton University Press, 1980.

Bianchi, T. S. (2007). *Biogeochemistry of Estuaries*. 720 pp., New York: Oxford University Press, Inc.

Blasing, T. (2016). Recent Greenhouse Gas Concentrations. doi:10.3334/CDIAC/atg.032.

Bonaglia, S., Brüchert, V., Callac, N., Vicenzi, A., Chi Fru, E. & Nascimento, F. J. (2017). Methane fluxes from coastal sediments are enhanced by macrofauna. *Scientific Reports* **7**, 1–10. doi:10.1038/s41598-017-13263-w.

Borges, A. V. & Abril, G. (2011). Carbon dioxide and methane dynamics in estuaries. In *Treatise on Estuarine and Coastal Science*, vol. 5, pp. 119–161. Elsevier. doi:10.1016/B978-0-12-374711-2.00504-0.

Borges, A. V., Champenois, W., Gypens, N., Delille, B. & Harlay, J. (2016). Massive marine methane emissions from near-shore shallow coastal areas. *Scientific Reports* **6**, 27908. doi:10.1038/srep27908.

Borges, A. V., Speeckaert, G., Champenois, W., Scranton, M. I. & Gypens, N. (2018). Productivity and Temperature as Drivers of Seasonal and Spatial Variations of Dissolved Methane in the Southern Bight of the North Sea. *Ecosystems* **21**, 583–599. doi:10.1007/s10021-017-0171-7.

Boudreau, B. P. (1997). *Diagenetic Models and Their Implementation*. 414 pp., Berlin, Heidelberg: Springer Berlin Heidelberg. doi:10.1007/978-3-642-60421-8.

Brodecka, A., Majewski, P., Bolałek, J. & Klusek, Z. (2013). Geochemical and acoustic evidence for the occurrence of methane in sediments of the Polish sector of the southern Baltic Sea. *Oceanologia* **55**, 951–978. doi:10.5697/oc.55-4.951.

Capone, D. G. & Kiene, R. P. (1988). Comparison of microbial dynamics in marine and freshwater sediments: Contrasts in anaerobic carbon catabolism. *Limnology and Oceanography* **33**, 725–749. doi:10.4319/lo.1988.33.4part2.0725.

Carstensen, J., Andersen, J. H., Gustafsson, B. G. & Conley, D. J. (2014a). Deoxygenation of the Baltic Sea during the last century. *Proceedings of the National Academy of Sciences* **111**, 5628–5633. doi:10.1073/pnas.1323156111.

Carstensen, J., Conley, D. J., Bonsdorff, E., Gustafssson, B. G., Hietanen, S., Janas, U., Jilbert, T., Maximov, A., Norkko, A., Norkko, J., Reed, D. C., Slomp, C. P., Timmermann, K. & Voss, M. (2014b). Hypoxia in the Baltic Sea: Biogeochemical cycles, benthic fauna, and management. *Ambio* **43**, 26–36. doi:10.1007/s13280-013-0474-7.

Chanton, J. P., Martens, C. S. & Kelley, C. A. (1989). Gas transport from methane-saturated, tidal freshwater and wetland sediments. *Limnology and Oceanography* **34**, 807–819. doi:10.4319/lo.1989.34.5.0807.

Cicerone, R. J. & Oremland, R. S. (1988). Biogeochemical aspects of atmospheric methane. *Global Biogeochemical Cycles* **2**, 299–327. doi:10.1029/GB002i004p00299.

Cline, J. D. (1969). Spectrophotometric determination of hydrogen sulfide in natural waters. *Limnology and Oceanography* **14**, 454–458. doi:10.4319/lo.1969.14.3.0454.

Conley, D. J., Carstensen, J., Aigars, J., Axe, P., Bonsdorff, E., Eremina, T., Haahti, B.-M., Humborg, C., Jonsson, P., Kotta, J., Lännegren, C., Larsson, U., Maximov, A., Medina, M. R., Lysiak-Pastuszak, E., Remeikaite-Nikiene, N., Walve, J., Wilhelms, S. & Zillén, L. (2011). Hypoxia is increasing in the coastal zone of the Baltic Sea. *Environmental Science & Technology* **45**, 6777–6783. doi:10.1021/es201212r.

Conrad, R. (2009). The global methane cycle: Recent advances in understanding the microbial processes involved. *Environmental Microbiology Reports* **1**, 285–292. doi:10.1111/j.1758-2229.2009.00038.x.

Crutzen, P. (1974). Estimates pf possible variations in total ozone due to natural causes and human activities. *Ambio* **3**, 201–210.

Dale, A. W., Aguilera, D. R., Regnier, P., Fossing, H., Knab, N. J. & Jørgensen, B. B. (2008). Seasonal dynamics of the depth and rate of anaerobic oxidation of methane in Aarhus Bay (Denmark) sediments. *Journal of Marine Research* **66**, 127–155. doi:10.1357/002224008784815775.

Davidson, T. A., Audet, J., Jeppesen, E., Landkildehus, F., Lauridsen, T. L., Søndergaard, M. & Syväranta, J. (2018). Synergy between nutrients and warming enhances methane ebullition from experimental lakes. *Nature Climate Change* **8**, 156–160. doi:10.1038/s41558-017-0063-z.

Dean, J. F., Middelburg, J. J., Röckmann, T., Aerts, R., Blauw, L. G., Egger, M., Jetten, M. S. M., de Jong, A. E. E., Meisel, O. H., Rasigraf, O., Slomp, C. P., in't Zandt, M. H., Dolman, A. J. & in 't Zandt, M. H. (2018). Methane feedbacks to the global climate system in a warmer world. *Reviews of Geophysics* **56**, 207–250. doi:10.1002/2017RG000559.

DelSontro, T., Boutet, L., St-Pierre, A., del Giorgio, P. A. & Prairie, Y. T. (2016). Methane ebullition and diffusion from northern ponds and lakes regulated by the interaction between temperature and system productivity. *Limnology and Oceanography* **61**, S62–S77. doi:10.1002/lno.10335.

Diaz, R. & Rosenberg, R. (1995). Marine benthic hypoxia: A review of its ecological effects and the behavioural responses of benthic macrofauna. *Oceanography and Marine Biology: An Annual Review* **33**, 245–303. doi:10.1021/je700185m.

Diaz, R. J. & Rosenberg, R. (2008). Spreading dead zones and consequences for marine ecosystems. *Science* **321**, 926–929. doi:10.1126/science.1156401.

Ding, J., Fu, L., Ding, Z. W., Lu, Y.-Z., Cheng, S. H. & Zeng, R. J. (2016). Experimental evaluation of the metabolic reversibility of ANME-2d between anaerobic methane oxidation and methanogenesis. *Applied Microbiology and Biotechnology* **100**, 6481–6490. doi:10.1007/s00253-016-7475-y.

Durisch-Kaiser, E., Klauser, L., Wehrli, B. & Schubert, C. (2005). Evidence of Intense Archaeal and Bacterial Methanotrophic Activity in the Black Sea Water Column. *Applied and Environmental Microbiology* **71**, 8099–8106. doi:10.1128/AEM.71.12.8099-8106.2005.

Egger, M., Rasigraf, O., Sapart, C. J., Jilbert, T., Jetten, M. S., Röckmann, T., van der Veen, C., Bândă, N., Kartal, B., Ettwig, K. F. & Slomp, C. P. (2015). Iron-mediated anaerobic oxidation of methane in brackish coastal sediments. *Environmental Science & Technology* **49**, 277–283. doi:10.1021/es503663z.

Egger, M., Hagens, M., Sapart, C. J., Dijkstra, N., van Helmond, N. A., Mogollón, J. M., Risgaard-Petersen, N., van der Veen, C., Kasten, S., Riedinger, N., Böttcher, M. E., Röckmann, T., Jørgensen, B. B. B., Slomp, C. P., van Helmond, N. A. & van der Veen, C. (2017). Iron oxide reduction in methane-rich deep Baltic Sea sediments. *Geochimica et Cosmochimica Acta* **207**, 256–276. doi:10.1016/j.gca.2017.03.019.

Egger, M., Riedinger, N., Mogollón, J. M. & Jørgensen, B. B. (2018). Global diffusive fluxes of methane in marine sediments. *Nature Geoscience* **11**, 421–425. doi:10.1038/s41561-018-0122-8.

Eller, G., Kanel, L. & Krüger, M. (2005). Cooccurrence of Aerobic and Anaerobic Methane Oxidation in the Water Column of Lake Plu see. *Applied and Environmental Microbiology* **71**, 8925–8928. doi:10.1128/AEM.71.12.8925-8928.2005.

Ettwig, K. F., Butler, M. K., Le Paslier, D., Pelletier, E., Mangenot, S., Kuypers, M. M. M., Schreiber, F., Dutilh, B. E., Zedelius, J., de Beer, D., Gloerich, J., Wessels, H. J. C. T., van Alen, T., Luesken, F. A., Wu, M. L., van de Pas-Schoonen, K. T., Op den Camp, H. J. M., Janssen-Megens, E. M., Francoijs, K.-J., Stunnenberg, H., Weissenbach, J., Jetten, M. S. & Strous, M. (2010). Nitrite-driven anaerobic methane oxidation

by oxygenic bacteria. *Nature* **464**, 543–548. doi:10.1038/nature08883.

Ettwig, K. F., Zhu, B., Speth, D., Keltjens, J. T., Jetten, M. S. M. & Kartal, B. (2016). Archaea catalyze iron-dependent anaerobic oxidation of methane. *Proceedings of the National Academy of Sciences* **113**, 12792–12796. doi:10.1073/pnas.1609534113.

Fallon, R. D., Harrits, S., Hanson, R. S. & Brock, T. D. (1980). The role of methane in internal carbon cycling in Lake Mendota during summer stratification. *Limnology and Oceanography* **25**, 357–360. doi:10.4319/lo.1980.25.2.0357.

Fenchel, T., Bernard, C., Esteban, G., Finlay, B. J., Hansen, P. J. & Iversen, N. (1995). Microbial diversity and activity in a Danish Fjord with anoxic deep water. *Ophelia* **43**, 45–100. doi:10.1080/00785326.1995.10430576.

Flury, S., Glud, R. N., Premke, K. & McGinnis, D. F. (2015). Effect of sediment gas voids and ebullition on benthic solute exchange. *Environmental Science and Technology* **49**, 10413–10420. doi:10.1021/acs.est.5b01967.

Fuchs, A., Lyautey, E., Montuelle, B. & Casper, P. (2016). Effects of increasing temperatures on methane concentrations and methanogenesis during experimental incubation of sediments from oligotrophic and mesotrophic lakes. *Journal of Geophysical Research: Biogeosciences* **121**, 1394–1406. doi:10.1002/2016JG003328.

Gelesh, L., Marshall, K., Boicourt, W. & Lapham, L. (2016). Methane concentrations increase in bottom waters during summertime anoxia in the highly eutrophic estuary, Chesapeake Bay, U.S.A. *Limnology and Oceanography* **61**, S253–S266. doi:10.1002/lno.10272.

Gentz, T., Damm, E., Schneider von Deimling, J., Mau, S., McGinnis, D. F. & Schlüter, M. (2014). A water column study of methane around gas flares located at the West Spitsbergen continental margin. *Continental Shelf Research* **72**, 107–118. doi:10.1016/j.csr.2013.07.013.

Gräwe, U., Naumann, M., Mohrholz, V. & Burchard, H. (2015). Anatomizing one of the largest saltwater inflows into the Baltic Sea in December 2014. *Journal of Geophysical Research: Oceans* **120**, 7676–7697. doi:10.1002/2015JC011269.

Gülzow, W., Rehder, G., Deimling, J. S. V., Seifert, T., Tóth, Z. & Schneider Von Deimling, J. (2013). One year of continuous measurements constraining methane emissions from the Baltic Sea to the atmosphere using a ship of opportunity. *Biogeosciences* **10**, 81–99. doi:10.5194/bg-10-81-2013.

Gülzow, W., Gräwe, U., Kedzior, S., Schmale, O. & Rehder, G. (2014). Seasonal variation of methane in the water column of Arkona and Bornholm Basin, western Baltic Sea. *Jour-*

nal of Marine Systems **139**, 332–347. doi:10.1016/j.jmarsys.2014.07.013.

Gutiérrez-Loza, L., Wallin, M. B., Sahlée, E., Nilsson, E., Bange, H. W., Kock, A. & Rutgersson, A. (2019). Measurement of Air-Sea Methane Fluxes in the Baltic Sea Using the Eddy Covariance Method. *Frontiers in Earth Science* **7**, 1–13. doi:10.3389/feart.2019.00093.

Hamdan, L. J. & Wickland, K. P. (2016). Methane emissions from oceans, coasts, and freshwater habitats: New perspectives and feedbacks on climate. *Limnology and Oceanography* **61**, S3–S12. doi:10.1002/lno.10449.

Hanson, R. S. & Hanson, T. E. (1996). Methanotrophic bacteria. *Microbiological reviews* **60**, 439–71.

HELCOM (1996). Chapter 4.4.1, Hydrography. In *Third periodic assessment of the state of the marine environment of the Baltic Sea 1989–1993, Baltic Sea Environment Proceedings no. 64b*, chap. 4.4.1, p. 75.

Heyer, J. & Berger, U. (2000). Methane Emission from the Coastal Area in the Southern Baltic Sea. *Estuarine, Coastal and Shelf Science* **51**, 13–30. doi:10.1006/ecss.2000.0616.

Humborg, C., Geibel, M. C., Sun, X., McCrackin, M., Mörth, C.-M., Stranne, C., Jakobsson, M., Gustafsson, B., Sokolov, A., Norkko, A. & Norkko, J. (2019). High Emissions of Carbon Dioxide and Methane From the Coastal Baltic Sea at the End of a Summer Heat Wave. *Frontiers in Marine Science* **6**, 1–14. doi:10.3389/fmars.2019.00493.

IPCC, ed. (2014). *Climate Change 2013 - The Physical Science Basis*. 1535 pp., Cambridge: Cambridge University Press. doi:10.1017/CBO9781107415324.

Iversen, N. & Jørgensen, B. (1985). Anaerobic methane oxidation rates at the sulphate-methane transition in marine sediments from Kattegat and Skagerrak (Denmark). *Limnology and Oceanography* **30**, 944–955.

Iversen, N. & Jørgensen, B. (1993). Diffusion coefficients of sulfate and methane in marine sediments: Influence of porosity. *Geochimica et Cosmochimica Acta* **57**, 571–578. doi:10.1016/0016-7037(93)90368-7.

Jakobs, G., Rehder, G., Jost, G., Kießlich, K., Labrenz, M. & Schmale, O. (2013). Comparative studies of pelagic microbial methane oxidation within the redox zones of the Gotland Deep and Landsort Deep (central Baltic Sea). *Biogeosciences* **10**, 7863–7875. doi:10.5194/bg-10-7863-2013.

Jakobs, G., Holtermann, P., Berndmeyer, C., Rehder, G., Blumenberg, M., Jost, G., Nausch, G. & Schmale, O. (2014). Seasonal and spatial methane dynamics in the water column of the central Baltic Sea (Gotland Sea). *Continental Shelf Research*

91, 12–25. doi:10.1016/j.csr.2014.07.005.

Jilbert, T. & Slomp, C. P. (2013). Iron and manganese shuttles control the formation of authigenic phosphorus minerals in the euxinic basins of the Baltic Sea. *Geochimica et Cosmochimica Acta* **107**, 155–169. doi:10.1016/j.gca.2013.01.005.

Jilbert, T., Asmala, E., Schröder, C., Tiihonen, R., Myllykangas, J., Virtasalo, J. J., Kotilainen, A., Peltola, P., Ekholm, P. & Hietanen, S. (2018). Impacts of flocculation on the distribution and diagenesis of iron in boreal estuarine sediments. *Biogeosciences* **15**, 1243–1271. doi:10.5194/bg-15-1243-2018.

Jokinen, S. A., Virtasalo, J. J., Jilbert, T., Kaiser, J., Dellwig, O., Arz, H. W., Hänninen, J., Arppe, L., Collander, M. & Saarinen, T. (2018). A 1500-year multiproxy record of coastal hypoxia from the northern Baltic Sea indicates unprecedented deoxygenation over the 20th century. *Biogeosciences* **15**, 3975–4001. doi:10.5194/bg-15-3975-2018.

Jørgensen, B. B., Weber, A. & Zopfi, J. (2001). Sulfate reduction and anaerobic methane oxidation in Black Sea sediments. *Deep Sea Research Part I: Oceanographic Research Papers* **48**, 2097–2120. doi:10.1016/S0967-0637(01)00007-3.

Joye, S. B., Boetius, A., Orcutt, B. N., Montoya, J. P., Schulz, H. N., Erickson, M. J. & Lugo, S. K. (2004). The anaerobic oxidation of methane and sulfate reduction in sediments from Gulf of Mexico cold seeps. *Chemical Geology* **205**, 219–238. doi:10.1016/j.chemgeo.2003.12.019.

Juutinen, S., Rantakari, M., Kortelainen, P., Huttunen, J. T., Larmola, T., Alm, J., Silvola, J. & Martikainen, P. J. (2009). Methane dynamics in different boreal lake types. *Biogeosciences* **6**, 209–223. doi:10.5194/bg-6-209-2009.

Kirschke, S., Bousquet, P., Ciais, P., Saunois, M., Canadell, J. G., Dlugokencky, E. J., Bergamaschi, P., Bergmann, D., Blake, D. R., Bruhwiler, L., Cameron-Smith, P., Castaldi, S., Chevallier, F., Feng, L., Fraser, A., Heimann, M., Hodson, E. L., Houweling, S., Josse, B., Fraser, P. J., Krummel, P. B., Lamarque, J.-F., Langenfelds, R. L., Le Quéré, C., Naik, V., O'doherty, S., Palmer, P. I., Pison, I., Plummer, D., Poulter, B., Prinn, R. G., Rigby, M., Ringeval, B., Santini, M., Schmidt, M., Shindell, D. T., Simpson, I. J., Spahni, R., Steele, L. P., Strode, S. A., Sudo, K., Szopa, S., Van Der Werf, G. R., Voulgarakis, A., Van Weele, M., Weiss, R. F., Williams, J. E. & Zeng, G. (2013). Three decades of global methane sources and sinks. *Nature Geoscience* **6**, 813–823. doi:10.1038/ngeo1955.

Knittel, K. & Boetius, A. (2009). Anaerobic Oxidation of Methane: Progress

with an Unknown Process. *Annual Review of Microbiology* **63**, 311–334. doi:10.1146/annurev.micro.61.080706.093130.

Knittel, K., Wegener, G. & Boetius, A. (2018). Anaerobic Methane Oxidizers. In *Microbial Communities Utilizing Hydrocarbons and Lipids: Members, Metagenomics and Ecophysiology*, January, pp. 1–21. Cham: Springer International Publishing. doi:10.1007/978-3-319-60063-5_7-1.

Lein, A. Y. (1983). Biogeochemistry of the Anaerobic Diagenesis of Recent Baltic Sea Sediments. *Ecological Bulletins* pp. 441–461.

Lein, A. Y., Namsaraev, B. B., Trotsyuk, V. Y. & Ivanov, M. V. (1981). Bacterial methanogenesis in holocene sediments of the Baltic sea. *Geomicrobiology Journal* **2**, 299–315. doi:10.1080/01490458109377770.

Liss, P. S. & Slater, P. G. (1974). Flux of gases across the air-sea interface. *Nature* **247**, 181–184. doi:10.1038/247181a0.

Maltby, J., Steinle, L., Löscher, C. R., Bange, H. W., Fischer, M. A., Schmidt, M. & Treude, T. (2018). Microbial methanogenesis in the sulfate-reducing zone of sediments in the Eckernförde Bay, SW Baltic Sea. *Biogeosciences* **15**, 137–157. doi:10.5194/bg-15-137-2018.

Malve, O., Virtanen, M., Villa, L., Karonen, M., Aakerla, H., Heiskanen, A. S., Lappalainen, K. M. & Holmberg, R. (2000). Artificial oxygenation experiment in hypolimnion of Pojo Bay estuary in 1995 and 1996: Factors regulating estuary circulation and oxygen and salt balances. Tech. rep., Finnish Environment Institute, Helsinki (Finland).

Martens, C. S. & Val Klump, J. (1980). Biogeochemical cycling in an organic-rich coastal marine basin—I. Methane sediment-water exchange processes. *Geochimica et Cosmochimica Acta* **44**, 471–490. doi:10.1016/0016-7037(80)90045-9.

Martinez-Cruz, K., Sepulveda-Jauregui, A., Casper, P., Anthony, K. W., Smemo, K. A. & Thalasso, F. (2018). Ubiquitous and significant anaerobic oxidation of methane in freshwater lake sediments. *Water Research* **144**, 332–340. doi:10.1016/j.watres.2018.07.053.

McGinnis, D. F., Greinert, J., Artemov, Y., Beaubien, S. E. & Wüest, A. (2006). Fate of rising methane bubbles in stratified waters: How much methane reaches the atmosphere? *Journal of Geophysical Research* **111**, C09007. doi:10.1029/2005JC003183.

McGlynn, S. E. (2017). Energy Metabolism during Anaerobic Methane Oxidation in ANME Archaea. *Microbes and environments* **32**, 5–13. doi:10.1264/jsme2.ME16166.

McGlynn, S. E., Chadwick, G. L., Kempes, C. P. & Orphan, V. J. (2015). Single cell activity reveals direct electron transfer in methanotrophic consortia. *Nature* **526**, 531–535. doi:10.1038/nature15512.

Meier, H. E. M. (2007). Modeling the pathways and ages of inflowing salt- and freshwater in the Baltic Sea. *Estuarine, Coastal and Shelf Science* **74**, 717–734. doi:10.1016/j.ecss.2007.05.019.

Middelburg, J. J. (1989). A simple rate model for organic matter decomposition in marine sediments. *Geochimica et Cosmochimica Acta* **53**, 1577–1581. doi:10.1016/0016-7037(89)90239-1.

Middelburg, J. J., Klaver, G., Nieuwenhuize, J., Wielemaker, A., De Haas, W., Vlug, T. & Van Der Nat, J. F. (1996). Organic matter mineralization in intertidal sediments along an estuarine gradient. *Marine Ecology Progress Series* **132**, 157–168. doi:10.3354/meps132157.

Mogollón, J. M., Dale, A. W., L'Heureux, I. & Regnier, P. (2011). Impact of seasonal temperature and pressure changes on methane gas production, dissolution, and transport in unfractured sediments. *Journal of Geophysical Research* **116**, G03031. doi:10.1029/2010JG001592.

Mohrholz, V. (2018). Major Baltic Inflow Statistics – Revised. *Frontiers in Marine Science* **5**, 1–16. doi:10.3389/fmars.2018.00384.

Myhre, G., Shindell, D. T., Bréon, F.-M., Collins, W., Fuglestvedt, J., Huang, J., Koch, D., Lamarque, J.-F., Lee, D., Mendoza, B., Nakajima, T., Robock, A., Stephens, G., Takemura, T. & Zhang, H. (2013). Anthropogenic and Natural Radiative Forcing. In *Climate Change 2013: The Physical Science Basis. Contribution of Working Group I to the Fifth Assessment Report of the Intergovernmental Panel on Climate Change*, pp. 659–740. Cambridge, United Kingdom and New York, NY, USA.: Cambridge University Press. doi:10.1017/CBO9781107415324.018.

Naqvi, S. W. A., Bange, H. W., Farías, L., Monteiro, P. M. S., Scranton, M. I. & Zhang, J. (2010). Marine hypoxia/anoxia as a source of CH_4 and N_2O. *Biogeosciences* **7**, 2159–2190. doi:10.5194/bg-7-2159-2010.

Neumann, T., Christiansen, C., Clasen, S., Emeis, K. C. & Kunzendorf, H. (1996). Geochemical records of saltwater inflows into the deep basins of the Baltic Sea. *Continental Shelf Research* **17**, 95–115. doi:10.1016/0278-4343(96)00023-4.

Neumann, T., Radtke, H. & Seifert, T. (2017). On the importance of Major Baltic Inflows for oxygenation of the central Baltic Sea. *Journal of Geophysical Research: Oceans* **122**, 1090–1101. doi:10.1002/2016JC012525.

Piker, L., Schmaljohann, R. & Imhoff, J. F. (1998). Dissimilatory sulfate reduction and methane production in

Gotland Deep sediments (Baltic Sea) during a transition period from oxic to anoxic bottom water (1993-1996). *Aquatic Microbial Ecology* **14**, 183–193. doi:10.3354/ame014183.

Pimenov, N. V., Kanapatskii, T. a., Sigalevich, P. a., Rusanov, I. I., Veslopolova, E. F., Grigor'ev, a. G. & Zhamoida, V. a. (2012). Sulfate reduction, methanogenesis, and methane oxidation in the Holocene sediments of the Vyborg Bay, Baltic Sea. *Microbiology* **81**, 79–89. doi:10.1134/S0026261712010122.

Raghoebarsing, A. A., Pol, A., van de Pas-Schoonen, K. T., Smolders, A. J. P., Ettwig, K. F., Rijpstra, W. I. C., Schouten, S., Damsté, J. S. S., Op den Camp, H. J. M., Jetten, M. S. M. & Strous, M. (2006). A microbial consortium couples anaerobic methane oxidation to denitrification. *Nature* **440**, 918–921. doi:10.1038/nature04617.

Raymond, P. A. & Cole, J. J. (2001). Gas exchange in rivers and estuaries : Choosing a gas transfer velocity. *Estuaries* **24**, 312–317.

Reeburgh, W. S. (1969). Observations of gases in Chesapeake Bay sediments. *Limnology and Oceanography* **14**, 368–375. doi:10.4319/lo.1969.14.3.0368.

Reeburgh, W. S. (1976). Methane consumption in Cariaco Trench waters and sediments. *Earth and Planetary Science Letters* **28**, 337–344. doi:10.1016/0012-821X(76)90195-3.

Reeburgh, W. S. (2007). Oceanic Methane Biogeochemistry. *Chemical Reviews* **107**, 486–513. doi:10.1021/cr050362v.

Reese, B. K., Finneran, D. W., Mills, H. J., Zhu, M.-X. & Morse, J. W. (2011). Examination and refinement of the determination of aqueous hydrogen sulfide by the methylene blue method. *Aquatic Geochemistry* **17**, 567–582. doi:10.1007/s10498-011-9128-1.

Rissanen, A. J., Karvinen, A., Nykänen, H., Peura, S., Tiirola, M., Mäki, A. & Kankaala, P. (2017). Effects of alternative electron acceptors on the activity and community structure of methane-producing and consuming microbes in the sediments of two shallow boreal lakes. *FEMS Microbiology Ecology* **93**, 1–16. doi:10.1093/femsec/fix078.

Rooze, J., Egger, M., Tsandev, I. & Slomp, C. P. (2016). Iron-dependent anaerobic oxidation of methane in coastal surface sediments: Potential controls and impact. *Limnology and Oceanography* **61**, S267–S282. doi:10.1002/lno.10275.

Sawicka, J. E. & Brüchert, V. (2017). Annual variability and regulation of methane and sulfate fluxes in Baltic Sea estuarine sediments. *Biogeosciences* **14**, 325–339. doi:10.5194/bg-14-325-2017.

Schinke, H. & Matthäus, W. (1998). On the causes of major Baltic inflows - An analysis of long time series. *Continental Shelf Research* **18**, 67–97. doi: 10.1016/S0278-4343(97)00071-X.

Schmale, O., Schneider v. Deimling, J., Gülzow, W., Nausch, G., Waniek, J. J. & Rehder, G. (2010). Distribution of methane in the water column of the Baltic Sea. *Geophysical Research Letters* **37**, 1–5. doi: 10.1029/2010GL043115.

Schmale, O., Blumenberg, M., Kießlich, K., Jakobs, G., Berndmeyer, C., Labrenz, M., Thiel, V. & Rehder, G. (2012). Aerobic methanotrophy within the pelagic redox-zone of the Gotland Deep (central Baltic Sea). *Biogeosciences* **9**, 4969–4977. doi: 10.5194/bg-9-4969-2012.

Schmale, O., Krause, S., Holtermann, P., Power Guerra, N. C. & Umlauf, L. (2016). Dense bottom gravity currents and their impact on pelagic methanotrophy at oxic/anoxic transition zones. *Geophysical Research Letters* **43**, 5225–5232. doi:10.1002/ 2016GL069032.

Schmaljohann, R. (1996). Methane dynamics in the sediment and water column of Kiel Harbour (Baltic Sea). *Marine Ecology Progress Series* **131**, 263–273. doi:10.3354/meps131263.

Schmaljohann, R., Piker, L. & Imhoff, J. (1998). The distribution of methane and hydrogen sulfide in basin sediments of the central and southern Baltic Sea. *Meyniana* **50**, 191–211.

Schneider, B., Gülzow, W., Sadkowiak, B. & Rehder, G. (2014). Detecting sinks and sources of CO2 and CH4 by ferrybox-based measurements in the Baltic Sea: Three case studies. *Journal of Marine Systems* **140**, 13–25. doi:10.1016/j.jmarsys.2014.03.014.

Schulz, H. D. & Zabel, M., eds. (2006). *Marine Geochemistry*. 574 pp., Berlin/Heidelberg: Springer-Verlag, 2 ed. doi:10.1007/3-540-32144-6.

Silvennoinen, H., Liikanen, A., Rintala, J. & Martikainen, P. J. (2008). Greenhouse gas fluxes from the eutrophic Temmesjoki River and its Estuary in the Liminganlahti Bay (the Baltic Sea). *Biogeochemistry* **90**, 193–208. doi:10.1007/s10533-008-9244-1.

Sivan, O., Adler, M., Pearson, A., Gelman, F., Bar-Or, I., John, S. G. & Eckert, W. (2011). Geochemical evidence for iron-mediated anaerobic oxidation of methane. *Limnology and Oceanography* **56**, 1536–1544. doi: 10.4319/lo.2011.56.4.1536.

Soja, A. J., Tchebakova, N. M., French, N. H., Flannigan, M. D., Shugart, H. H., Stocks, B. J., Sukhinin, A. I., Parfenova, E., Chapin, F. S. & Stackhouse, P. W. (2007). Climate-induced boreal forest change: Predictions versus current observations. *Global and Planetary Change* **56**, 274–296. doi: 10.1016/j.gloplacha.2006.07.028.

Stanley, E. H., Casson, N. J., Christel, S. T., Crawford, J. T., Loken, L. C. & Oliver, S. K. (2016). The ecology of methane in streams and rivers: Patterns, controls, and global significance. *Ecological Monographs* **86**, 146–171. doi:10.1890/15-1027.

Steinle, L., Graves, C. A., Treude, T., Ferré, B., Biastoch, A., Bussmann, I., Berndt, C., Krastel, S., James, R. H., Behrens, E., Böning, C. W., Greinert, J., Sapart, C.-J., Scheinert, M., Sommer, S., Lehmann, M. F. & Niemann, H. (2015). Water column methanotrophy controlled by a rapid oceanographic switch. *Nature Geoscience* **8**, 378–382. doi:10.1038/ngeo2420.

Steinle, L., Maltby, J., Treude, T., Kock, A., Bange, H. W., Engbersen, N., Zopfi, J., Lehmann, M. F. & Niemann, H. (2017). Effects of low oxygen concentrations on aerobic methane oxidation in seasonally hypoxic coastal waters. *Biogeosciences* **14**, 1631–1645. doi:10.5194/bg-14-1631-2017.

Stipa, T. (1999). Water exchange and mixing in a semi-enclosed coastal basin (Pohja Bay). *Boreal Environment Research* **4**, 307–317.

Sturm, K., Keller-Lehmann, B., Werner, U., Raj Sharma, K., Grinham, A. R. & Yuan, Z. (2015). Sampling considerations and assessment of Exetainer usage for measuring dissolved and gaseous methane and nitrous oxide in aquatic systems. *Limnology and Oceanography: Methods* **13**, 375–390. doi:10.1002/lom3.10031.

Thang, N. M., Brüchert, V., Formolo, M., Wegener, G., Ginters, L., Jørgensen, B. B. B. & Ferdelman, T. G. (2013). The Impact of Sediment and Carbon Fluxes on the Biogeochemistry of Methane and Sulfur in Littoral Baltic Sea Sediments (Himmerfjärden, Sweden). *Estuaries and Coasts* **36**, 98–115. doi:10.1007/s12237-012-9557-0.

Thauer, R. K. (1998). Biochemistry of methanogensis: a tribute to Marjory Stephenson. *Microbiology* **144**, 2377–2407.

Thornton, B. F., Geibel, M. C., Crill, P. M., Humborg, C. & Mörth, C.-M. (2016). Methane fluxes from the sea to the atmosphere across the Siberian shelf seas. *Geophysical Research Letters* **43**, 5869–5877. doi:10.1002/2016GL068977.

Timmers, P. H. A., Suarez-Zuluaga, D. A., Van Rossem, M., Diender, M., Stams, A. J. M., M Plugge, C. & Plugge, C. M. (2016). Anaerobic oxidation of methane associated with sulfate reduction in a natural freshwater gas source. *ISME Journal* **10**, 1400–1412. doi:10.1038/ismej.2015.213.

Timmers, P. H. A., Welte, C. U., Koehorst, J. J., Plugge, C. M., Jetten, M. S. & Stams, A. J. M. (2017). Reverse Methanogenesis and Respiration in Methanotrophic Archaea. *Ar-*

chaea **2017**, 1–22. doi:10.1155/2017/1654237.

Treude, T., Krüger, M., Boetius, A. & Jørgensen, B. (2005). Environmental control on anaerobic oxidation of methane in the gassy sediments of Eckernfoerde Bay(German Baltic). *Limnology and Oceanography* **50**, 1771–1786.

Ulyanova, M., Sivkov, V. V., Kanapatskij, T., Sigalevich, P. & Pimenov, N. (2012). Methane fluxes in the southeastern Baltic Sea. *Geo-Marine Letters* **32**, 535–544. doi:10.1007/s00367-012-0304-0.

Upstill-Goddard, R. C., Barnes, J., Frost, T., Punshon, S. & Owens, N. J. P. (2000). Methane in the southern North Sea: Low-salinity inputs, estuarine removal, and atmospheric flux. *Global Biogeochemical Cycles* **14**, 1205–1217. doi:10.1029/1999GB001236.

Vahtera, E., Conley, D. J., Gustafsson, B. G., Kuosa, H., Pitkänen, H., Savchuk, O. P., Tamminen, T., Viitasalo, M., Voss, M., Wasmund, N. & Wulff, F. (2007). Internal ecosystem feedbacks enhance nitrogen-fixing cyanobacteria blooms and complicate management in the Baltic Sea. *Ambio* **36**, 186–194. doi:10.1579/0044-7447(2007)36[186:IEFENC]2.0.CO;2.

Valentine, D. L. (2002). Biogeochemistry and microbial ecology of methane oxidation in anoxic environments: A review. *Antonie van Leeuwenhoek, International Journal of General and Molecular Microbiology* **81**, 271–282. doi:10.1023/A:1020587206351.

Wallmann, K., Pinero, E., Burwicz, E., Haeckel, M., Hensen, C., Dale, A. & Ruepke, L. (2012). The Global Inventory of Methane Hydrate in Marine Sediments: A Theoretical Approach. *Energies* **5**, 2449–2498. doi:10.3390/en5072449.

Walter, S., Breitenbach, U., Bange, H. W., Nausch, G. & Wallace, D. W. (2006). Distribution of N2O in the Baltic Sea during transition from anoxic to oxic conditions. *Biogeosciences* **3**, 557–570. doi:10.5194/bg-3-557-2006.

Wanninkhof, R. H. (1992). Relationship between wind speed and gas exchange. *Journal of Geophysical Research* **97**, 7373–7382. doi:10.1029/92JC00188.

Wanninkhof, R. H. (2014). Relationship between wind speed and gas exchange over the ocean revisited. *Limnology and Oceanography: Methods* **12**, 351–362. doi:10.4319/lom.2014.12.351.

Whiticar, M. J., Faber, E. & Schoell, M. (1986). Biogenic methane formation in marine and freshwater environments: CO2 reduction vs. acetate fermentation—Isotope evidence. *Geochimica et Cosmochim-*

ica Acta **50**, 693–709. doi:10.1016/0016-7037(86)90346-7.

Wiesenburg, D. A. & Guinasso, N. L. (1979). Equilibrium solubilities of methane, carbon monoxide, and hydrogen in water and sea water. *Journal of Chemical & Engineering Data* **24**, 356–360. doi:10.1021/je60083a006.

Wik, M., Thornton, B. F., Bastviken, D., Uhlbäck, J. & Crill, P. M. (2016). Biased sampling of methane release from northern lakes: A problem for extrapolation. *Geophysical Research Letters* **43**, 1256–1262. doi:10.1002/2015GL066501.

Yvon-Durocher, G., Allen, A. P., Bastviken, D., Conrad, R., Gudasz, C., St-Pierre, A., Thanh-Duc, N. & del Giorgio, P. A. (2014). Methane fluxes show consistent temperature dependence across microbial to ecosystem scales. *Nature* **507**, 488–491. doi:10.1038/nature13164.

Zehnder, A. J. & Brock, T. D. (1980). Anaerobic methane oxidation : Occurrence and ecology. *Applied and Environmental Microbiology* **39**, 194–204.

Zehnder, A. J. B. & Brock, T. D. (1979). Methane formation and methane oxidation by methanogenic bacteria. *Journal of Bacteriology* **137**, 420–432.

Paper I

Jukka-Pekka Myllykangas, Tom Jilbert, Gunnar Jakobs, Gregor Rehder, Jan Werner, and Susanna Hietanen

Effects of the 2014 major Baltic inflow on methane and nitrous oxide dynamics in the water column of the central Baltic Sea

In *Earth System Dynamics*,
Volume 8, issue 3, 2017, pages 817–826.

Earth Syst. Dynam., 8, 817–826, 2017
https://doi.org/10.5194/esd-8-817-2017

Earth System Dynamics
Open Access
EGU

Effects of the 2014 major Baltic inflow on methane and nitrous oxide dynamics in the water column of the central Baltic Sea

Jukka-Pekka Myllykangas[1], Tom Jilbert[1], Gunnar Jakobs[1,2], Gregor Rehder[3], Jan Werner[3], and Susanna Hietanen[1]

[1]Department of Environmental Sciences, University of Helsinki, P.O. Box 65, 00014 University of Helsinki, Helsinki, Finland
[2]Technical University of Denmark, Frederiksborgvej 399, 4000 Roskilde, Denmark
[3]Leibniz Institute for Baltic Sea Research Warnemünde (IOW), Seestraße 15, 18119 Rostock, Germany

Correspondence to: Jukka-Pekka Myllykangas (jukka-pekka.myllykangas@helsinki.fi)

Received: 10 February 2017 – Discussion started: 19 April 2017
Revised: 17 July 2017 – Accepted: 1 August 2017 – Published: 14 September 2017

Abstract. In late 2014, a large, oxygen-rich salt water inflow entered the Baltic Sea and caused considerable changes in deep water oxygen concentrations. We studied the effects of the inflow on the concentration patterns of two greenhouse gases, methane and nitrous oxide, during the following year (2015) in the water column of the Gotland Basin. In the eastern basin, methane which had previously accumulated in the deep waters was largely removed during the year. Here, volume-weighted mean concentration below 70 m decreased from 108 nM in March to 16.3 nM over a period of 141 days (0.65 nM d^{-1}), predominantly due to oxidation (up to 79 %) following turbulent mixing with the oxygen-rich inflow. In contrast nitrous oxide, which was previously absent from deep waters, accumulated in deep waters due to enhanced nitrification following the inflow. Volume-weighted mean concentration of nitrous oxide below 70 m increased from 11.8 nM in March to 24.4 nM in 141 days (0.09 nM d^{-1}). A transient extreme accumulation of nitrous oxide (877 nM) was observed in the deep waters of the Eastern Gotland Basin towards the end of 2015, when deep waters turned anoxic again, sedimentary denitrification was induced and methane was reintroduced to the bottom waters. The Western Gotland Basin gas biogeochemistry was not affected by the inflow.

1 Introduction

The Baltic Sea is a shallow, semi-enclosed brackish water body. It receives large fresh water inputs from the rivers along its coast, but also exchanges saline water with the North Sea through the narrow Danish straits, principally via the Darss Sill and the Drogden Sill (Fig. 1). This leads to a semi-permanent stratification between relatively fresh surface waters and denser, more saline deep waters. Although intermediate-depth water masses in the southern areas of the Baltic Sea are ventilated frequently, deep waters of the central Baltic are renewed only during major Baltic inflow (MBI) events, during which large amounts of saline oxygen-rich water enter the Baltic through the Danish straits over a short period of time (Schinke and Matthäus, 1998). These events require a specific sequence of weather conditions, occur exclusively in winter and have been occurring approximately once a decade in the recent past (Gräwe et al., 2015).

Due to the semi-permanent stratification, waters below the halocline of the Baltic Sea are typically anoxic (Carstensen et al., 2014) and contain large inventories of reduced compounds produced by microbial and abiotic reactions in the absence of oxygen (Neumann et al., 1997). Many biogeochemical processes are also active in the hypoxic boundary layers close to the halocline (Yakushev et al., 2007; Dellwig et al., 2010). When oxygen is introduced by MBIs, large quantities of the previously accumulated reduced compounds in the deep waters are subsequently oxidized

(Reissmann et al., 2009) and new redox fronts develop between new and old water masses (Schmale et al., 2016). As such, MBIs have a strong influence on many biogeochemical processes in the Baltic Sea.

In this study we focus on two gases that are strongly influenced by the spatial distribution of hypoxia and anoxia in the Baltic Sea: methane (CH_4) (Schmale et al., 2012) and nitrous oxide (N_2O) (Hietanen et al., 2012). Both are important greenhouse gases, which also have effects on atmospheric chemistry (Crutzen, 1974; Cicerone and Oremland, 1988). Ambient oxygen concentrations regulate the microbial processes involved in the production and consumption of CH_4 and N_2O. CH_4 is produced in sediments in vast quantities by a unique group of archaea called methanogens (Balch et al., 1979). Methanogenesis is the lowest energy-yield pathway of the anaerobic decay of organic matter, which typically occurs when all other electron acceptors have been depleted (Thauer, 1998). The primary methanogenesis pathway in marine sediments is CO_2 reduction by hydrogenotrophic methanogens, while fermentative acetotrophic methanogenesis is the dominant pathway in freshwater sediments (Whiticar et al., 1986). Typically, most of the produced CH_4 is consumed in anaerobic and aerobic processes in both sediments and the water column before it can escape to the atmosphere (Reeburgh, 2007; Knittel and Boetius, 2009). N_2O is produced by prokaryotes through both oxidative and reductive pathways: as a side product in nitrification (oxidation of ammonium, NH_4^+, to nitrate, NO_3^-), and as an intermediate product in denitrification (reduction of NO_3^- to elemental nitrogen gas, N_2) under suboxic conditions (Anderson and Levine, 1986; Goreau et al., 1980; Bakker et al., 2014). The main biological pathways of N_2O production are highly dependent on the oxygen conditions and the availability of organic matter, nitrite (NO_2^-) and nitrate (Ward, 2013; Murray et al., 2015). In seas, nitrification has been considered the primary pathway of N_2O production (Freing et al., 2012), but recent studies have suggested that the role of incomplete denitrification in the oceanic oxygen minimum zones might have been previously underestimated (Babbin et al., 2015; Ji et al., 2015). Furthermore, it has been shown that archaeal nitrification dominates oceanic N_2O production and that this is much more sensitive to oxygen concentrations than bacterial nitrication (Löscher et al., 2012; Freing et al., 2012). N_2O is consumed exclusively under anoxic conditions during denitrification (Goreau et al., 1980; Wrage et al., 2001; Bakker et al., 2014). The highest accumulations of N_2O in marine waters are typically associated with spatial and temporal redox gradients, such as the margins of oceanic oxygen minimum zones (Naqvi et al., 2010) and dynamic systems including estuaries (Brase et al., 2017).

In the Baltic Sea, surface water concentrations of both gases typically exceed equilibrium with the sea-level atmosphere, indicating supersaturation and an efflux of CH_4 and N_2O from surface waters (Bange, 2006; Gülzow et al., 2013). However, the sub-halocline profiles of the two gases differ markedly. Deep waters are typically strongly enriched in CH_4 below the halocline during stagnation periods (Bange et al., 2010; Jakobs et al., 2013), while N_2O is usually absent (Brettar and Rheinheimer, 1991). Increased anthropogenic nutrient loading during the last century has been linked to the enhanced production of both gases in the Baltic Sea (Bange, 2006). In the global CH_4 budget, the flux from the oceans to the atmosphere is estimated at approximately 2 % of total CH_4 emissions (Judd et al., 2002; Reeburgh, 2007), but estimates as high as 10 % have also been presented (Cicerone and Oremland, 1988). Shallow coastal areas and estuaries are an important component, potentially contributing up to 75 % of the total oceanic CH_4 flux (Bange et al., 1994). In the case of N_2O, the oceans are a much more important source in the global atmospheric budget, contributing up to 25 % of emissions (Nevison et al., 2003). However, there are large uncertainties in the role of coastal zones and estuaries. Previous studies have reported ranges from 11 to 60 % of the total N_2O flux from the marine environment (Bange et al., 1996; Seitzinger and Kroeze, 1998). In a more recent study, Naqvi et al. (2010) report a more conservative estimate of 16–33 %, though concede that large uncertainties still exist.

In late December of 2014 a large MBI occurred, during which 198 km^3 of water, containing 4 Gt of salt and 2.04×10^6 t of oxygen, entered the Baltic through the Darss sill (Fig. 1). The inflow was the third largest MBI observed since 1880 (Gräwe et al., 2015; Mohrholz et al., 2015) and caused large changes in the dissolved oxygen concentrations throughout the southern and central Baltic Sea (Mohrholz et al., 2015). The inflow strongly impacted the vertical distribution of CH_4 in the Gotland Basin (Schmale et al., 2016), which is the largest sub-basin of the Baltic Sea. Both advective processes (displacement and dilution of old CH_4-rich deep waters by the CH_4-poor inflow water) and aerobic oxidation of CH_4 (stimulated by mixing at the contact between these water masses) contributed to a decline in [CH_4] during 2015.

Here we present a broader investigation of the spatial and temporal evolution of both CH_4 and N_2O concentrations following the inflow, along a transect of sites in both the Eastern and Western Gotland Basin. We discuss the roles of advection and microbial processing in the observed distributions, and the timescales of change in biogeochemical processes in response to the perturbation caused by the MBI.

2 Materials and methods

Samples were collected on six cruises that took place between March and December 2015 on R/V *Aranda* and R/V *Salme*. Sampling covered the whole Gotland Basin, with three stations in the Eastern Gotland Basin (EGB: BY10, BY15 and BY20) and two stations in the western basin

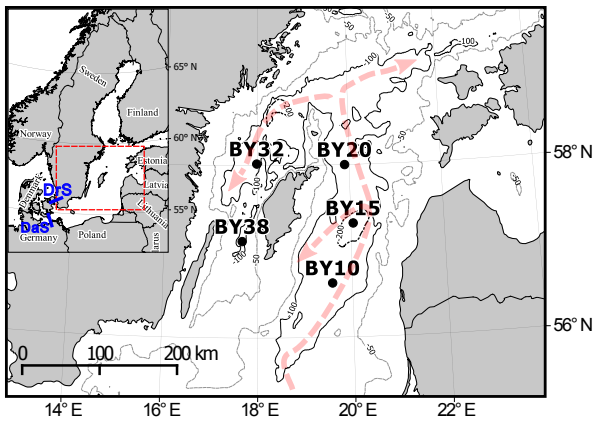

Figure 1. Map of the study area showing the five sampling locations in the central Baltic Sea. The red arrows show the prevailing sub-halocline circulation of the central Baltic Sea, redrawn from Meier (2007). The sub-halocline circulation approximates the expected route of major Baltic inflows (MBIs) along the transect of study locations. The inset shows the connection of the Baltic Sea to the North Sea via the Danish Straits (DaS: Darss Sill; DrS: Drogden Sill). The numbers along the depth contours represent depth in metres.

(WGB: BY32 and BY38) (Fig. 1). The coordinates, sampling times and depths of all stations are listed in Table S4 in the Supplement. All five stations have been monitored for several decades for basic hydrographic parameters and have been used in numerous previous studies.

Water samples were collected with rosette water samplers with 12 Niskin bottles and salinity, temperature and oxygen data were generated with attached CTD probes (bottle sizes 1.7 and 5 L, CTD probes Sea-Bird SBE 19+ and Sea-Bird SBE 911+, for R/V *Salme* and R/V *Aranda*, respectively). Supplementary nutrient, oxygen and hydrogen sulfide (H_2S) monitoring data were provided by the Finnish Environment Institute (SYKE), Swedish Meteorological and Hydrological Institute (SMHI) and Tallinn University of Technology (TTU).

Dissolved gas samples were collected in triplicate by filling 60 mL plastic syringes directly from the Niskin bottles with a 10 cm rubber tube that was flushed with sample water and from which visible bubbles were squeezed out prior to sampling. The water volume in the syringe was reduced to 30 mL, a three-way stopcock was attached to the syringe, and 31 mL of 5.0 purity N_2 gas was injected via the stopcock to create a headspace. Syringes were left at 20 °C for 30 min and then vigorously shaken for 3 min. At least 25 mL of the headspace was transferred into a dry syringe through a stopcock and then injected into a pre-evacuated 12 mL gastight glass vial with a 4 mm butyl rubber stopper (LabCo Exetainer™ model 839W). Care was taken to always keep the syringes closed with a stopcock.

The gas samples were analysed within 5 months from sampling using an Agilent Technologies 7890B gas chromatograph with a flame ionization detector (FID) for CH_4 and an electron capture detector (ECD) for N_2O, a 2.4 m Hayesep Q column with 1/8″ connection, 80/100 mesh range and a 1.0 mL sample loop. Carrier gases were nitrogen and helium at 21 mL min^{-1} flow rates, for N_2O and CH_4 respectively. The oven temperature was 60 °C, and detection temperatures for FID and ECD were 250 and 300 °C respectively. The samples were injected using a Gilson GX-271 auto sampler. Raw peak area data were converted to mole fraction (ppm) using linear calibration with standards. For CH_4, a three-point calibration was used (0.46, 5 and 47 ppm), consisting of a standard gas mixture (AGA Gas AB, Lidingö, Sweden) with 5 ppm ± 2 % CH_4, which was diluted 1 : 10 with 5.0 purity N_2 to create the low standard. For the high standard, a 1000 ppm ± 2 % CH_4 gas mixture (Air Products PLC, Surrey, UK) was diluted 1 : 20 with 5.0 N_2. For N_2O, a two-point calibration (0.10 and 1.1 ppm) was used, consisting of a standard gas mixture (AGA Gas AB, Lidingö, Sweden) with 1.1 ppm ± 5 % N_2O, which was then diluted 1 : 10 with 5.0 N_2. Standard series were analysed prior to each analysis sequence (length of sequence was 40–120 samples) and fitted linearly for each sequence separately to correct for between-series drift. Standards containing 5 ppm CH_4 and 1.1 ppm N_2O were analysed after every 10 samples to monitor within-series drift (observed to be negligible).

Total in situ dissolved gas concentrations (C_{tot}) in mol L^{-1} were calculated from measured wet mole fraction values in the headspace gas considering the ideal gas law and Henry's Law:

$$C_{tot} = \frac{\frac{P_{HS} \times V_{HS}}{R \times T} + F \times P_{HS} \times V_{Aq}}{V_{Aq}}, \quad (1)$$

where P_{HS} is the partial pressure of the gas in the headspace (atm), V_{HS} and V_{Aq} the syringe headspace and water volume respectively (L), R is the gas constant (0.08206 L atm K^{-1} mol^{-1}), T the temperature during equilibration in Kelvin (293 K), and F is a salinity- and temperature-dependent equilibrium solubility coefficient of a given gas in mol L^{-1} atm^{-1}, as defined in Wiesenburg and Guinasso (1979) for CH_4 and in Weiss and Price (1980) for N_2O (in situ salinity and 293 K were used in the calculations).

The calculation can be simplified by assuming that the total pressure in the syringe during equilibration is 1 atm, from which follows that $P_{HS} = P_{atm} \times X_{HS}$, where P_{atm} is the true atmospheric pressure during sampling in atm. Thus, the total original concentration of dissolved gas in the fluid sample can be calculated by summing the contributions from the headspace (C_{HS}) and the dissolved phase (C_{Aq}):

$$C_{tot} = \underbrace{\frac{(X_{HS} \times P_{atm} \times V_{HS})}{(R \times T \times V_{aq})}}_{C_{HS}} + \underbrace{F \times X_{HS} \times P_{atm}}_{C_{Aq}}, \quad (2)$$

where X_{HS} is the mole fraction of the gas measured from the syringe headspace in ppmv.

Pre-evacuated Exetainers contain small amounts of air, which contaminates the gas samples, standards and blanks (Sturm et al., 2015). Because the concentration of CH_4 and N_2O in air is variable, the contamination also introduced imprecision to sample data. We calculated cut-off concentrations for both gases, below which measured values were considered indistinguishable from those of blank pre-evacuated Exetainers (see Fig. S1 in the Supplement). The determination of the cut-off value took into account both the mean contamination of blank samples and various sources of imprecision in sample data. The cut-off concentrations are approximately equivalent to 9–19 and 4–6 nM for CH_4 and N_2O, respectively (exact values are salinity dependent). Precision, which includes errors introduced during transfer of gas samples between syringes and the variation in sample volumes in relation to the residual air in the Exetainers, of all reported data above the cut-off is $< 5\,\%$ relative standard deviation (RSD), as determined by triplicate analysis of all samples. In terms of accuracy, the residual air in the Exetainers caused an average underestimation of 0.9 % in CH_4 samples (full range for all reported samples −2.6 to 11.4 %) and a 1.1 % overestimation in N_2O samples (full range −2.7 to 10.1 %). Diffusive exchange through the plastic of the syringes was found to be negligible ($< 1\,\%$). The errors inherent to the method do not affect any of the main results or conclusions presented here. For a detailed description of the error and the establishment of the cut-off, we refer the reader to the Supplement.

3 Results

All stations exhibited strong salinity stratification on all sampling occasions, with clear differences between the surface and bottom water salinities (Fig. 2a). The halocline was typically at 60–80 m depth. We observed a net increase in the bottom water salinities at BY15, BY20, BY32 and BY38 from March to December. Absolute bottom water salinities decreased along the expected route of the inflow (Figs. 1, 2a).

As expected, the earliest major impact of the inflow on deep water oxygen was observed at the southernmost station BY10, where oxygen was detected already in March (up to 84 µM in the bottom water, Fig. 2b). At this site, the oxygenated zone in the bottom water expanded upwards until June, with concentrations between 90 and 120 µM. However, $[O_2]$ started to decrease considerably in August and remained low thereafter, dropping to 5 µM in December. No H_2S was detected at any time at BY10. $[CH_4]$ remained low throughout, with the highest value of 97 nM measured in April at 125 m depth (Fig. 2c). $[N_2O]$ was between 6 and 22 nM, with the lowest concentration found in June at 100 m depth, and the highest in December in the deepest 144 m sample (Fig. 2d).

At the deepest station, BY15, in the central EGB, oxygen was also detected in the bottom water in March, although the concentration was lower than at BY10 (50 µM, Fig. 2b). In the early part of the year, BY15 had a completely anoxic midwater layer from 100 to 175 m (Fig. 2b), which contained up to 21 µM H_2S in April. The anoxic layer diminished over time, and had completely disappeared by August, as the oxic zone in the deep waters expanded vertically over this period. The highest bottom water $[O_2]$ of 177 µM was measured in April (Fig. 2b). $[CH_4]$ was relatively low throughout, except for the anoxic layer, where concentrations of up to 217 nM were measured in March. By December, bottom water $[O_2]$ had decreased to below 10 µM and $[CH_4]$ of up to 158 nM were measured in the bottom water. Also, slightly elevated $[CH_4]$ and $[N_2O]$ were detected in October and December at 90–125 m (Fig. 2c). Minimal amounts of N_2O were found within the anoxic midwater layer of BY15, but concentrations of 18–20 nM could be detected around its upper and lower boundaries (Fig. 2d). In October however, very high $[N_2O]$ (877 nM) was measured at 225 m. The extreme concentrations had decreased by December, but still remained relatively high (41 nM at 225 and 236 m) compared to previous months (Fig. 2d).

At the northernmost station of the EGB, BY20, $[O_2]$ was very low or zero below 70–80 m (Fig. 2b) and H_2S was found in the bottom water on all sampling occasions, with concentrations up to 33 µM in August. Bottom water was devoid of N_2O and $[CH_4]$ remained high (299–525 nM) (Fig. 2c), except in October when bottom water $[CH_4]$ decreased to 91 nM and $[N_2O]$ increased to 151 nM (Fig. 2d). Concentrations of both gases had returned to typical values by December. In August, a transient midwater $[N_2O]$ maximum of 36 nM was found at 100 m depth and in October and December $[CH_4]$ of up to 230 nM were observed at 90 m depth.

In the WGB at BY32 and BY38, no oxygen was detected below the halocline at any time (Fig. 2b), and H_2S was present in all bottom water samples. Bottom water $[CH_4]$ displayed large variation between 308 and 726 nM (Fig. 2c), and $[N_2O]$ was consistently below the cut-off value, indicating values close to zero (Fig. 2d). At both stations, a strong shoaling of the halocline could be observed over the course of the year (Fig. 2a), with the CH_4-enriched deep water mass expanding from 125 to 80 m at BY32, and from 90 to 70 m at BY38.

4 Discussion

4.1 Spatial impacts of the MBI

Major Baltic inflows usually progress northwards through the EGB, encircle the island of Gotland counterclockwise, and finally move southwards through the WGB (Meier, 2007; Lessin et al., 2014). However, the MBI of 2014 had not reached the WGB by the end of 2015. Although bottom water salinities increased in the WGB during 2015 (Fig. 2a),

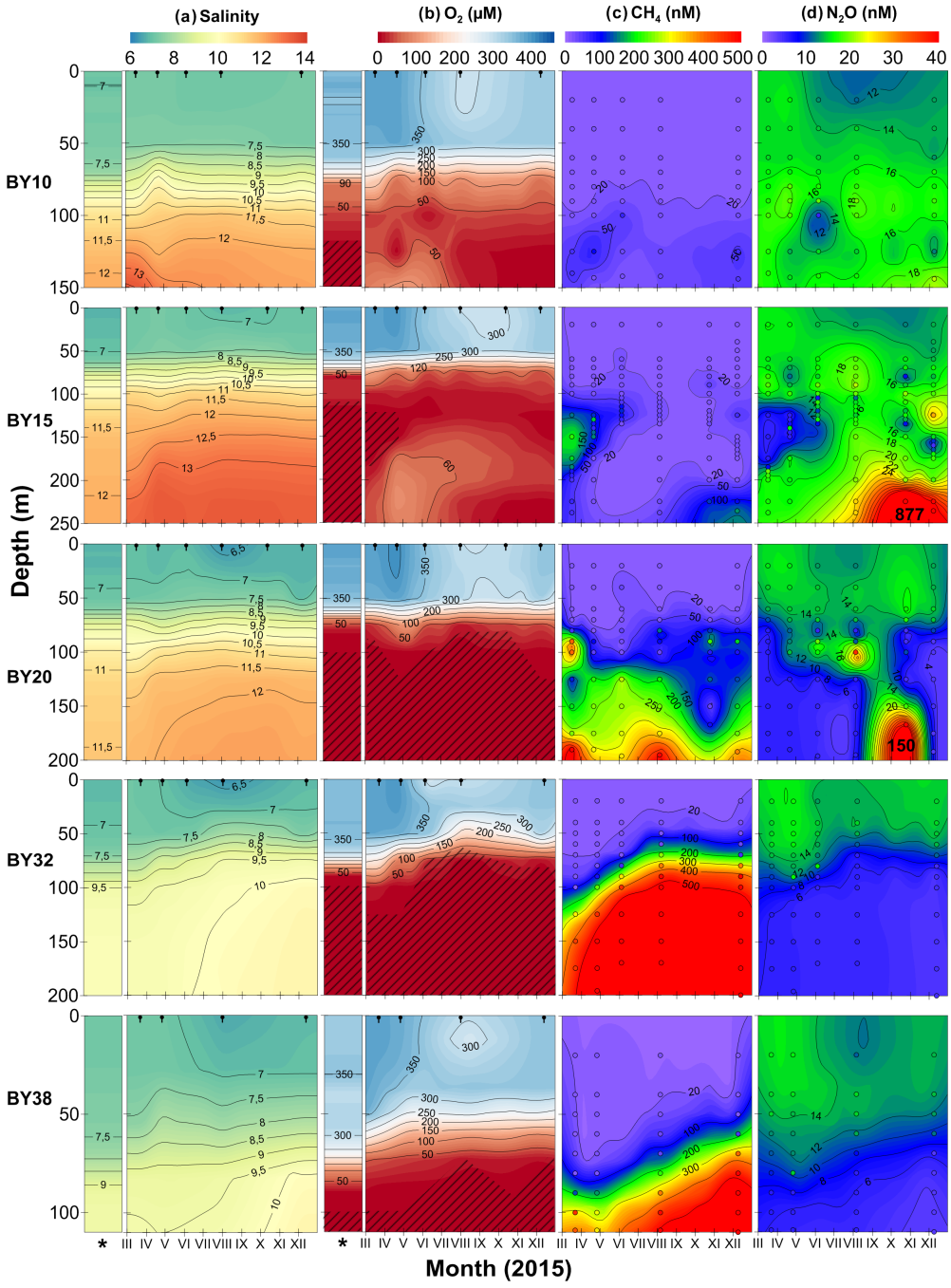

Figure 2. Bilinearly interpolated profiles of **(a)** CTD salinity, **(b)** CTD oxygen (µM, shading denotes presence of H_2S), **(c)** [CH_4] (nM) and **(d)** [N_2O] (nM) from all sampling stations at all sampling times of the survey. The *x* axis covers the period 17 March to 13 December 2015. Black notches in **(a, b)** indicate sampling dates, while the narrower bars marked with an asterisk represent conditions in June 2014, prior to the MBI. Circles in columns **(c, d)** represent gas sampling depths and times, while infill colour is the non-interpolated original concentration. Note that all CH_4 and N_2O data below the cut-off were set to cut-off prior to interpolation (see Supplement S1 for details).

the increase was continuous throughout the year and not accompanied by changes in oxygen conditions. The changes observed in the salinity of the WGB early in the year were therefore likely unrelated to the inflow. Based on 16 years of monitoring data (shown in Fig. S3 in the Supplement), the WGB experiences annual to multi-annual cycles of shoaling and deepening of the halocline, which are related to downward erosion of the halocline by winter storms (Reissmann et al., 2009). The resulting changes in salinity and oxygen conditions in the 60–100 m depth interval dictate the distribution of CH_4 (Jakobs et al., 2014) and N_2O in the WGB. [CH_4] is higher below the halocline, while [N_2O] is higher above it (Fig. 2c, d).

In the EGB, in contrast, large impacts of the 2014 MBI could be observed throughout 2015. Already by March, oxic water and noticeable changes in salinity were detected in the deepest part of the Eastern Gotland Basin (site BY15). These initial signals were a combination of new inflowing water and water pushed out of the Bornholm Basin ahead of the inflow (Schmale et al., 2016), as also occurred during the MBI of 2003 (Feistel et al., 2003). Over the following months, a distinct mass of saline, oxic inflow water accumulated in the EGB. At BY10 and BY15, oxygen was present below the halocline for much of 2015. However, [O_2] declined again towards the end of the year (Fig. 2b). Such a decline was also observed following the 2003 MBI (Walter et al., 2006), and indicates that the capacity of MBIs to ventilate the Baltic is short-lived. Introduced oxygen is expected to be consumed simultaneously by a range of electron donors, including hydrogen sulfide (H_2S), ammonium, reduced forms of manganese and iron, and CH_4, which are all present in the stagnant deep waters. Both the physical effects of the inflow (displacement of water masses) and the subsequent evolution of redox conditions throughout 2015 had strong impacts on the distribution of CH_4 and N_2O at the EGB sites (BY10, BY15 and BY20).

4.2 CH_4 dynamics in the EGB

Upon arrival of an MBI into the EGB, the former bottom water mass is typically displaced vertically upwards and northwards (Reissmann et al., 2009). This displacement of CH_4-rich stagnant deep water by CH_4-poor inflow water may deplete the inventory of CH_4 in the water column of the EGB. However, due to turbulent mixing at the contact between the inflow and older water masses (Schmale et al., 2016), oxidation of CH_4 may also be expected to accelerate the depletion of CH_4. In 2015, we observed the gradual erosion of a mid-water [CH_4] maximum between March and August, followed by a re-accumulation of CH_4 in both mid- and deep water towards the end of the year (Fig. 2). To estimate the relative effects of displacement and oxidation on the CH_4 inventory during the studied period, we compared the CH_4 inventory with that of phosphate (PO_4^{3-}) at BY15 (Fig. 3). Changes in deep water [PO_4^{3-}] in the EGB following an MBI have

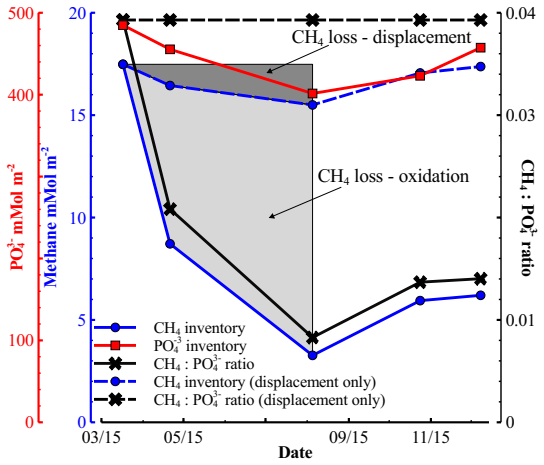

Figure 3. Evolution of the inventories of CH_4 (solid blue line with dots) and PO_4^{3-} (solid red line with squares) below 70 m at BY15, and the molar inventory ratio $CH_4 : PO_4^{3-}$ over the year 2015 (solid black line with crosses). Results from all measured depths at all sampling times were included in the integration, with the exception data from June, which was omitted due to the loss of deep water CH_4 samples. Pictured also is the hypothetical evolution of the CH_4 inventory (dashed blue line with dots) if the $CH_4 : PO_4^{3-}$ ratio (dashed black line with crosses) had remained constant during the year – i.e. the effect of water mass displacement was equal for CH_4 and PO_4^{3-}. The lighter grey area represents the estimated loss of CH_4 due to oxidation and the darker grey represents the loss due to displacement. Note the different scales of the *y* axes.

been shown to be predominantly controlled by displacement (Schneider, 2011), due to the fact that a stagnant PO_4^{3-}-rich bottom water mass is displaced by a PO_4^{3-}-poor inflow, and comparatively little PO_4^{3-} is sequestered into sediments over the following months despite the expansion of oxic conditions. The logic of the apparent slow response in the redox-sensitivity of PO_4^{3-} is that PO_4^{3-} sequestration requires the presence of solid-phase iron oxyhydroxides, which are not available in the open water column where the majority of the PO_4^{3-} is located. Accordingly, Schneider (2011) estimated that two-thirds of the decline in deep water [PO_4^{3-}] in the EGB following the MBI of 2003 could be attributed to displacement.

In the hypothetical scenario in which the decline in both CH_4 and PO_4^{3-} inventories from March to August 2015 was controlled by displacement only, the molar ratio of $PO_4^{3-} : CH_4$ would be expected to remain constant. Instead, we observe that the inventory ratio of $PO_4^{3-} : CH_4$ declined rapidly during this period, implying a far stronger impact of oxidation on CH_4 than on PO_4^{3-}. Indeed, the CH_4 inventory was depleted from ~ 18 to ~ 3 mMol m^{-2} over this interval, while the PO_4^{3-} inventory declined only slightly, from ~ 480 to ~ 400 mMol m^{-2} (Fig. 3). These results provide strong ev-

idence for significant aerobic oxidation of CH_4 in the water column as a consequence of the MBI, which concurs with a recent study in which in situ oxidation rates were measured (Schmale et al., 2016).

When expressed as volume-weighted averages (below 70 m), the observed decline in [CH_4] over March to August 2015 was from 108 nM in March to 16.3 nM in August. This is a period of 141 days, giving a total rate of loss of 0.65 nM d^{-1}, of which 0.51 nM d^{-1} (79 %) is potentially due to oxidation, based on the results shown in Fig. 3. Schmale et al. (2016) reported CH_4 oxidation rates of up to 0.9 nM d^{-1} and elevated cell counts for methane-oxidizing bacteria at central EGB in March 2015. Such oxidation rates are 2–10 times higher compared to stagnation conditions (Jakobs et al., 2014). The introduction of a second, deeper redoxcline and active turbulent mixing processes clearly accelerate CH_4 oxidation following an MBI by enhancing the volume of water in which CH_4 and O_2 come into contact. It should be noted, however, that the Schmale et al. (2016) study focused specifically on high turbulence transition zones and thus reports localized maximum estimates of CH_4 oxidation rates. In contrast, our study provides a first-order estimate of the bulk oxidation rate the sub-halocline water column at site BY15.

4.3 N_2O dynamics in the EGB

Under stagnation conditions, the deep anoxic waters of the EGB are almost entirely devoid of N_2O (Brettar and Rheinheimer, 1991), but the hypoxic margins are hotspots for N_2O production, similar to oceanic oxygen minimum zones (Babbin et al., 2015; Löscher et al., 2012). The accumulation of N_2O over time after an MBI is related to the formation of large hypoxic water masses. N_2O production is highest under nearly anoxic conditions, where oxygen concentrations restrain both nitrification (too little oxygen) and denitrification (too much oxygen). Both processes produce N_2O, with a higher N_2O yield in oxygen stress (Goreau et al., 1980; Patureau et al., 1994; Ji et al., 2015). In addition, when nitrifying microbes become oxygen limited, they too start to reduce NO_2^- to N_2O (Poth and Focht, 1985; Wilson et al., 2014).

For the most part, the N_2O concentrations measured in the oxic waters of this study were between 10 and 20 nM, which is well in agreement with previous studies (Bange, 2006; Walter et al., 2006). The volume-weighted average [N_2O] below 70 m depth at BY15 increased from 11.8 to 24.4 nM from March to August (141 d), giving a net increase rate of 0.09 nM d^{-1}. Walter et al. (2006) reported a similar increase rate of 0.105 nM d^{-1} from the whole water column below 70 m in the EGB, over a period of 167 days after the 2003 MBI, which they ascribed largely to nitrification. We observed a decline in [NH_4^+] in the mid-water layer at BY15 over the period March to August 2015 (Fig. 4). The decline in [NH_4^+] resembled the loss of CH_4 over the same period,

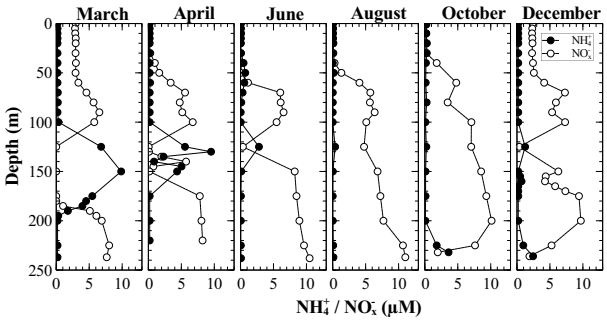

Figure 4. Ammonium (NH_4^+, filled circles, solid line) and combined nitrite–nitrate (NO_x^-, open circles, dotted line) concentrations (µM) at BY15 over the whole sampling period.

and was coupled to increasing [NO_2^-] and [NO_3^-] (Fig. 4). These observations strongly suggest that oxidation of NH_4^+ (i.e. nitrification) following the MBI was the main pathway of N_2O production during the first half of 2015.

One of the most interesting observations in this study was the extremely high [N_2O] (877 nM) measured at 225 m at BY15 in October, which is to our knowledge the second highest value ever reported from the Baltic Sea (Rönner, 1983, reported 1523 nM at BY38 bottom water in the WGB), and several times higher than the concentrations typically found from the Baltic (Brettar and Rheinheimer, 1991; Bange et al., 1996; Bange, 2006; Walter et al., 2006). The oxygen concentration at the depth of the extreme [N_2O] in this study was below 1 µM, which is comparable to values previously observed in settings of high N_2O production elsewhere in the ocean (Naqvi et al., 2010; Babbin et al., 2015). The large drop in the [NO_2^-] and [NO_3^-] below 200 m at BY15 from October onwards (Fig. 4) suggests that the rate of benthic denitrification increased towards the end of 2015. Simultaneously increasing [NH_4^+] indicate a slowing down of rates of nitrification and possibly enhanced DNRA (Jäntti and Hietanen, 2012). Hence, the transitional conditions between nitrification and denitrification regimes towards the end of 2015 appear to have favoured an extreme, short-lived accumulation of N_2O in the deep waters of the EGB. This may be seen as a delayed, but important consequence of the MBI on nitrogen cycling in the Baltic.

4.4 Processes at the northern limit of the MBI

As MBIs progress northwards, the density differences between the old and new water masses are weakened and the interactions become more complex and difficult to predict (Eilola et al., 2014). Inflowing water masses detach into intrusive layers (Baines, 2001) which may interact chaotically under turbulent flow. Site BY20 is situated near the northern margin of the EGB and represents the northernmost limit of the observable effects of the 2014 MBI. In this zone, various

physical factors, e.g. turbulent mixing and shearing, internal waves, and boundary waves breaking against the sloping seabed (Reissmann et al., 2009; Eilola et al., 2014; Schmale et al., 2016) likely created a complex and temporally variable vertical zonation of redox conditions during 2015. Despite the persistence of H_2S at BY20 throughout the year, the CH_4 and N_2O distributions are highly variable (Fig. 2), suggesting an impact of oxidation and reduction processes related to the inflow. For example, a large enrichment of N_2O was observed in the near bottom water of BY20 in October, similar to that observed at BY15, and the CH_4 and N_2O distributions generally anti-correlate as observed throughout our data from all stations. We interpret the observed patterns at BY20 as evidence for a dynamic water column at this site, with mobile interleaved layers which may carry a displaced signal of redox processes occurring further south (e.g. CH_4 oxidation, nitrification).

5 Conclusions

The major Baltic inflow of 2014 caused considerable changes in oxygen conditions of the Eastern Gotland Basin, which had extensive effects on the CH_4 and N_2O dynamics of the basin. CH_4 mostly disappeared from the eastern basin during the first half of 2015, mainly due to oxidation following turbulent mixing between old and new water masses. However, CH_4 began to accumulate again by the end of the year, as deep water conditions reverted to anoxia. Enhanced N_2O production was evident throughout the Eastern Gotland Basin during 2015, attributed primarily to nitrification as a consequence of the MBI. Extreme values of N_2O near the seafloor in late 2015 were likely caused by a combination of nitrification and denitrification under transitional conditions. The northern limit of the effect of the MBI on CH_4 and N_2O dynamics appears to have been the northern part of the Eastern Gotland Basin, and even here direct oxygenation of the deep waters was not observed. The Western Gotland Basin CH_4 and N_2O biogeochemistry was not influenced by the inflow at any point during the study period.

Data availability. Data are available at https://doi.pangaea.de/10.1594/PANGAEA.880534 (Myllykangas et al., 2017).

The Supplement related to this article is available online at https://doi.org/10.5194/esd-8-817-2017-supplement.

Competing interests. The authors declare that they have no conflict of interest.

Special issue statement. This article is part of the special issue "Multiple drivers for Earth system changes in the Baltic Sea region". It is a result of the 1st Baltic Earth Conference, Nida, Lithuania, 13–17 June 2016. However, these particular data were not presented at the conference.

Acknowledgements. We acknowledge the two anonymous reviewers and thank them for their input. This research was funded by the Academy of Finland projects 139267, 272964 and 267112. The research leading to these results has also received funding from the European Union Seventh Framework Programme (FP7/2007-2013) under grant agreement no. 312762. We would like to extend our thanks to SYKE, SMHI and Tallinn University of Technology for the supplementary data and for allowing us on board their cruises, as well as to the crews and captains of R/V *Aranda* and R/V *Salme*.

Edited by: Andrey Gritsun
Reviewed by: two anonymous referees

References

Anderson, I. C. and Levine, J. S.: Relative rates of nitric oxide and nitrous oxide production by nitrifiers, denitrifiers, and nitrate respirers, Appl. Environ. Microbiol., 51, 938–45, 1986.

Babbin, A. R., Bianchi, D., Jayakumar, A., and Ward, B. B.: Rapid nitrous oxide cycling in the suboxic ocean, Science, 348, 1127–1129, https://doi.org/10.1126/science.aaa8380, 2015.

Baines, P. G.: Mixing in flows down gentle slopes into stratified environments, J. Fluid Mech., 443, 237–270, https://doi.org/10.1017/S0022112001005250, 2001.

Bakker, D. C., Bange, H. W., Gruber, N., Johannassen, T., Upstill-Goddard, R. C., Borges, A. V., Delille, B., Loscher, C. R., Naqvi, W. A., Omar, A. M., and Santana-Casiano, M.: Air-Sea Interactions of Natural Long-Lived Greenhouse Gases (CO_2, N_2O, CH_4) in a Changing Climate, in: Ocean-Atmosphere Interactions of Gases and Particles, edited by: Liss, P. S. and Johnson, M. T., 55–112, Springer Berlin Heidelberg, Berlin, Heidelberg, https://doi.org/10.1007/978-3-642-25643-1, 2014.

Balch, W. E., Fox, G. E., Magrum, L. J., Woese, C. R., and Wolfe, R. S.: Methanogens: reevaluation of a unique biological group, Microbiol. Rev., 43, 260–96, 1979.

Bange, H. W.: Nitrous oxide and methane in European coastal waters, Estuarine, Coastal Shelf Sci., 70, 361–374, https://doi.org/10.1016/j.ecss.2006.05.042, 2006.

Bange, H. W., Bartell, U. H., Rapsomanikis, S., and Andreae, M. O.: Methane in the Baltic and North Seas and a reassessment of the marine emissions of methane, Global Biogeochem. Cy., 8, 465–480, https://doi.org/10.1029/94GB02181, 1994.

Bange, H. W., Rapsomanikis, S., and Andreae, M. O.: Nitrous oxide in coastal waters, Global Biogeochem. Cy., 10, 197–207, https://doi.org/10.1029/95GB03834, 1996.

Bange, H. W., Bergmann, K., Hansen, H. P., Kock, A., Koppe, R., Malien, F., and Ostrau, C.: Dissolved methane during hypoxic events at the Boknis Eck time series station (Eckernförde Bay, SW Baltic Sea), Biogeosciences, 7, 1279–1284, https://doi.org/10.5194/bg-7-1279-2010, 2010.

Brase, L., Bange, H. W., Lendt, R., Sanders, T., and Dähnke, K.: High Resolution Measurements of Nitrous Oxide (N_2O) in the Elbe Estuary, Frontiers in Marine Science, 4, 1–11, https://doi.org/10.3389/fmars.2017.00162, 2017.

Brettar, I. and Rheinheimer, G.: Denitrification in the Central Baltic: evidence for H2S-oxidation as motor of denitrification at the oxic-anoxic interface, Mar. Ecol.-Prog. Ser., 77, 157–169, https://doi.org/10.3354/meps077157, 1991.

Carstensen, J., Conley, D. J., Bonsdorff, E., Gustafsson, B. G., Hietanen, S., Janas, U., Jilbert, T., Maximov, A., Norkko, A., Norkko, J., Reed, D. C., Slomp, C. P., Timmermann, K., and Voss, M.: Hypoxia in the Baltic Sea: Biogeochemical Cycles, Benthic Fauna, and Management, Ambio, 43, 26–36, https://doi.org/10.1007/s13280-013-0474-7, 2014.

Cicerone, R. J. and Oremland, R. S.: Biogeochemical aspects of atmospheric methane, Global Biogeochem. Cy., 2, 299–327, https://doi.org/10.1029/GB002i004p00299, 1988.

Crutzen, P. J.: Estimates of Possible Variations in Total Ozone Due to Natural Causes and Human Activities, Ambio, 3, 201–210, 1974.

Dellwig, O., Leipe, T., März, C., Glockzin, M., Pollehne, F., Schnetger, B., Yakushev, E. V., Böttcher, M. E., and Brumsack, H.-J.: A new particulate Mn–Fe–P-shuttle at the redoxcline of anoxic basins, Geochim. Cosmochim. Ac., 74, 7100–7115, https://doi.org/10.1016/j.gca.2010.09.017, 2010.

Eilola, K., Almroth-Rosell, E., and Meier, H. E. M.: Impact of saltwater inflows on phosphorus cycling and eutrophication in the Baltic Sea: a 3D model study, Tellus A, 66, 1–17, https://doi.org/10.3402/tellusa.v66.23985, 2014.

Feistel, R., Nausch, G., Matthäus, W., and Hagen, E.: Temporal and spatial evolution of the Baltic deep water renewal in spring 2003, Oceanologia, 45, 623–642, 2003.

Freing, A., Wallace, D. W. R., and Bange, H. W.: Global oceanic production of nitrous oxide, Philos. T. R. Soc. B, 367, 1245–1255, https://doi.org/10.1098/rstb.2011.0360, 2012.

Goreau, T. J., Kaplan, W. A., Wofsy, S. C., Mcelroy, M. B., Valois, F. W., and Watson, S. W.: Production of nitrite and nitrous oxide by nitrifying bacteria at reduced concentrations of oxygen, Appl. Environ. Microbiol., 40, 526–532, 1980.

Gräwe, U., Naumann, M., Mohrholz, V., and Burchard, H.: Anatomizing one of the largest saltwater inflows into the Baltic Sea in December 2014, J. Geophys. Res.-Oceans, 120, 7676–7697, https://doi.org/10.1002/2015JC011269, 2015.

Gülzow, W., Rehder, G., Schneider v. Deimling, J., Seifert, T., and Tóth, Z.: One year of continuous measurements constraining methane emissions from the Baltic Sea to the atmosphere using a ship of opportunity, Biogeosciences, 10, 81–99, https://doi.org/10.5194/bg-10-81-2013, 2013.

Hietanen, S., Jäntti, H., Buizert, C., Jürgens, K., Labrenz, M., and Voss, M.: Hypoxia and nitrogen processing in the Baltic Sea water column, Limnol. Oceanogr., 57, 325–337, https://doi.org/10.4319/lo.2012.57.1.0325, 2012.

Jakobs, G., Rehder, G., Jost, G., Kießlich, K., Labrenz, M., and Schmale, O.: Comparative studies of pelagic microbial methane oxidation within the redox zones of the Gotland Deep and Landsort Deep (central Baltic Sea), Biogeosciences, 10, 7863–7875, https://doi.org/10.5194/bg-10-7863-2013, 2013.

Jakobs, G., Holtermann, P., Berndmeyer, C., Rehder, G., Blumenberg, M., Jost, G., Nausch, G., and Schmale, O.: Seasonal and spatial methane dynamics in the water column of the central Baltic Sea (Gotland Sea), Cont. Shelf Res., 91, 12–25, https://doi.org/10.1016/j.csr.2014.07.005, 2014.

Jäntti, H. and Hietanen, S.: The Effects of Hypoxia on Sediment Nitrogen Cycling in the Baltic Sea, Ambio, 41, 161–169, https://doi.org/10.1007/s13280-011-0233-6, 2012.

Ji, Q., Babbin, A. R., Jayakumar, A., Oleynik, S., and Ward, B. B.: Nitrous oxide production by nitrification and denitrification in the Eastern Tropical South Pacific oxygen minimum zone, Geophys. Res. Lett., 42, 10755–10764, https://doi.org/10.1002/2015GL066853, 2015.

Judd, A. G., Hovland, M., Dimitrov, L. I., Garcia Gil, S., and Jukes, V.: The geological methane budget at Continental Margins and its influence on climate change, Geofluids, 2, 109–126, https://doi.org/10.1046/j.1468-8123.2002.00027.x, 2002.

Knittel, K. and Boetius, A.: Anaerobic oxidation of methane: progress with an unknown process., Annu. Rev. Microbiol., 63, 311–334, https://doi.org/10.1146/annurev.micro.61.080706.093130, 2009.

Lessin, G., Raudsepp, U., and Stips, A.: Modelling the influence of major baltic inflows on near-bottom conditions at the entrance of the Gulf of Finland, PLoS ONE, 9, e112881, https://doi.org/10.1371/journal.pone.0112881, 2014.

Löscher, C. R., Kock, A., Könneke, M., LaRoche, J., Bange, H. W., and Schmitz, R. A.: Production of oceanic nitrous oxide by ammonia-oxidizing archaea, Biogeosciences, 9, 2419–2429, https://doi.org/10.5194/bg-9-2419-2012, 2012.

Meier, H.: Modeling the pathways and ages of inflowing salt- and freshwater in the Baltic Sea, Estuarine, Coast. Shelf Sci., 74, 610–627, https://doi.org/10.1016/j.ecss.2007.05.019, 2007.

Mohrholz, V., Naumann, M., Nausch, G., Krüger, S., and Gräwe, U.: Fresh oxygen for the Baltic Sea – An exceptional saline inflow after a decade of stagnation, J. Marine Syst., 148, 152–166, https://doi.org/10.1016/j.jmarsys.2015.03.005, 2015.

Murray, R. H., Erler, D. V., and Eyre, B. D.: Nitrous oxide fluxes in estuarine environments: response to global change, Glob. Change Biol., 21, 3219–3245, https://doi.org/10.1111/gcb.12923, 2015.

Myllykangas, J.-P., Jilbert, T., Jakobs, G., Rehder, G., Werner, J., and Hietanen, S.: Methane and nitrous oxide concentration profiles, CTD and nutrient data from the Central Baltic Sea between March and December 2015, following the major Baltic Inflow of 2014, PANGAEA, https://doi.org/10.1594/PANGAEA.880534, 2017.

Naqvi, S. W. A., Bange, H. W., Farías, L., Monteiro, P. M. S., Scranton, M. I., and Zhang, J.: Marine hypoxia/anoxia as a source of CH_4 and N_2O, Biogeosciences, 7, 2159–2190, https://doi.org/10.5194/bg-7-2159-2010, 2010.

Neumann, T., Christiansen, C., Clasen, S., Emeis, K.-C., and Kunzendorf, H.: Geochemical records of salt-water inflows into the deep basins of the Baltic Sea, Cont. Shelf Res., 17, 95–115, https://doi.org/10.1016/0278-4343(96)00023-4, 1997.

Nevison, C., Butler, J. H., and Elkins, J. W.: Global distribution of N_2O and the ΔN_2O-AOU yield in the subsurface ocean, Global Biogeochem. Cy., 17, 1119, https://doi.org/10.1029/2003GB002068, 2003.

Patureau, D., Davison, J., Bernet, N., and Moletta, R.: Denitrification under various aeration conditions in Comamonas

sp., strain SGLY2, FEMS Microbiol. Ecol., 14, 71–78, https://doi.org/10.1111/j.1574-6941.1994.tb00092.x, 1994.

Poth, M. and Focht, D. D.: N Kinetic Analysis of N(2)O Production by Nitrosomonas europaea: an Examination of Nitrifier Denitrification, Appl. Environ. Microbiol., 49, 1134–1141, 1985.

Reeburgh, W. S.: Oceanic methane biogeochemistry, Chem. Rev., 107, 486–513, https://doi.org/10.1021/cr050362v, 2007.

Reissmann, J. H., Burchard, H., Feistel, R., Hagen, E., Lass, H. U., Mohrholz, V., Nausch, G., Umlauf, L., and Wieczorek, G.: Vertical mixing in the Baltic Sea and consequences for eutrophication – A review, Prog. Oceanogr., 82, 47–80, https://doi.org/10.1016/j.pocean.2007.10.004, 2009.

Rönner, U.: Distribution, production and consumption of nitrous oxide in the Baltic Sea, Geochim. Cosmochim. Ac., 47, 2179–2188, https://doi.org/10.1016/0016-7037(83)90041-8, 1983.

Schinke, H. and Matthäus, W.: On the causes of major Baltic inflows – an analysis of long time series, Cont. Shelf Res., 18, 67–97, https://doi.org/10.1016/S0278-4343(97)00071-X, 1998.

Schmale, O., Blumenberg, M., Kießlich, K., Jakobs, G., Berndmeyer, C., Labrenz, M., Thiel, V., and Rehder, G.: Aerobic methanotrophy within the pelagic redox-zone of the Gotland Deep (central Baltic Sea), Biogeosciences, 9, 4969–4977, https://doi.org/10.5194/bg-9-4969-2012, 2012.

Schmale, O., Krause, S., Holtermann, P., Power Guerra, N. C., and Umlauf, L.: Dense bottom gravity currents and their impact on pelagic methanotrophy at oxic/anoxic transition zones, Geophys. Res. Lett., 43, 5225–5232, https://doi.org/10.1002/2016GL069032, 2016.

Schneider, B.: PO_4 release at the sediment surface under anoxic conditions: a contribution to the eutrophication of the Baltic Sea?, Oceanologia, 53, 415–429, https://doi.org/10.5697/oc.53-1-TI.415, 2011.

Seitzinger, S. P. and Kroeze, C.: Global distribution of nitrous oxide production and N inputs in freshwater and coastal marine ecosystems, Global Biogeochem. Cy., 12, 93–113, https://doi.org/10.1029/97GB03657, 1998.

Sturm, K., Keller-Lehmann, B., Werner, U., Raj Sharma, K., Grinham, A. R., and Yuan, Z.: Sampling considerations and assessment of Exetainer usage for measuring dissolved and gaseous methane and nitrous oxide in aquatic systems, Limnol. Oceanogr.-Meth., 13, 375–390, https://doi.org/10.1002/lom3.10031, 2015.

Thauer, R. K.: Biochemistry of methanogenesis: a tribute to Marjory Stephenson:1998 Marjory Stephenson Prize Lecture, Microbiology, 144, 2377–2406, https://doi.org/10.1099/00221287-144-9-2377, 1998.

Walter, S., Breitenbach, U., Bange, H. W., Nausch, G., and Wallace, D. W. R.: Distribution of N_2O in the Baltic Sea during transition from anoxic to oxic conditions, Biogeosciences, 3, 557–570, https://doi.org/10.5194/bg-3-557-2006, 2006.

Ward, B.: Nitrification, in: Reference Module in Earth Systems and Environmental Sciences, 1–8, Elsevier, https://doi.org/10.1016/B978-0-12-409548-9.00697-7, 2013.

Weiss, R. and Price, B.: Nitrous oxide solubility in water and seawater, Mar. Chem., 8, 347–359, https://doi.org/10.1016/0304-4203(80)90024-9, 1980.

Whiticar, M., Faber, E., and Schoell, M.: Biogenic methane formation in marine and freshwater environments: CO_2 reduction vs. acetate fermentation – Isotope evidence, Geochim. Cosmochim. Ac., 50, 693–709, https://doi.org/10.1016/0016-7037(86)90346-7, 1986.

Wiesenburg, D. A. and Guinasso, N. L.: Equilibrium solubilities of methane, carbon monoxide, and hydrogen in water and sea water, J. Chem. Eng. Data, 24, 356–360, https://doi.org/10.1021/je60083a006, 1979.

Wilson, S. T., del Valle, D. A., Segura-Noguera, M., and Karl, D. M.: A role for nitrite in the production of nitrous oxide in the lower euphotic zone of the oligotrophic North Pacific Ocean, Deep-Sea Res. Pt. I, 85, 47–55, https://doi.org/10.1016/j.dsr.2013.11.008, 2014.

Wrage, N., Velthof, G., van Beusichem, M., and Oenema, O.: Role of nitrifier denitrification in the production of nitrous oxide, Soil Biol. Biochem., 33, 1723–1732, https://doi.org/10.1016/S0038-0717(01)00096-7, 2001.

Yakushev, E., Pollehne, F., Jost, G., Kuznetsov, I., Schneider, B., and Umlauf, L.: Analysis of the water column oxic/anoxic interface in the Black and Baltic seas with a numerical model, Mar. Chem., 107, 388–410, https://doi.org/10.1016/j.marchem.2007.06.003, 2007.

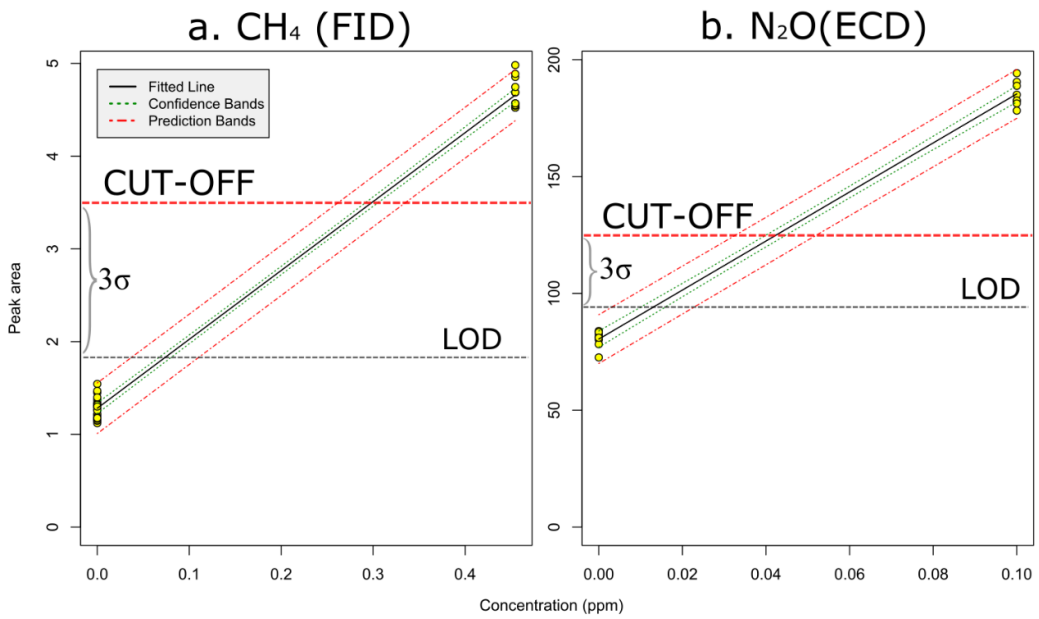

Figure S1. Establishment of cut-off concentrations of CH_4 (left) and N_2O (right), below which measured sample values are regarded as indistinguishable from those of blank pre-evacuated Exetainers. Yellow points represent measured peak areas of CH_4 and N_2O from blank pre-evacuated Exetainers (i.e. Exetainers from the supplier, subsequently filled with N_2, nominal CH_4 and N_2O concentrations = 0 ppm) and measured peak areas of the lowest standards for each gas, also stored in pre-evacuated Exetainers (CH_4 and N_2O concentrations 0.45 ppm and 0.1 ppm, respectively). A total of NN replicate blanks and NN replicate low standards were measured. The linear fits (peak area vs. ppm) derived from the blanks and the low standards are shown for both gases, with the corresponding 95% confidence and prediction bands. Note that these fits are linear across the full range of standards (not shown). Limit of detection (LOD) was determined according to Armbruster and Pry (2008) ($mean_{blank}$ + 1.645 * SD_{blank}) + 1.645 * $SD_{low\ standard}$. To determine the cut-off, a conservative additional margin was added to the LOD to account for the imprecision of real sample data (in contrast to standard measurements), in which multiple transfers of water and gas between Niskin bottles, syringes and pre-evacuated Exetainers introduce error between replicates. The mean standard deviation in peak area determined from all triplicate samples (n=N) was multiplied by 3 and added to LOD to estimate cut-offs of 3.49 and 125.82 peak area units for CH_4 and N_2O, respectively (3σ in the figure). Mean standard deviation of samples was calculated as the square root of mean variances of all sample triplicates: $\sqrt{\frac{\sum \sigma^2_{sample}}{n_{samples}}}$.

Note the different y-axis scales of the panels, which are due to the different detectors used for the GC measurement of each gas (FID vs. ECD).

Reference:

Armbruster, D. A. and Pry, T.: Limit of blank, limit of detection and limit of quantitation., Clin. Biochem. Rev., 29 Suppl 1(August), S49-52

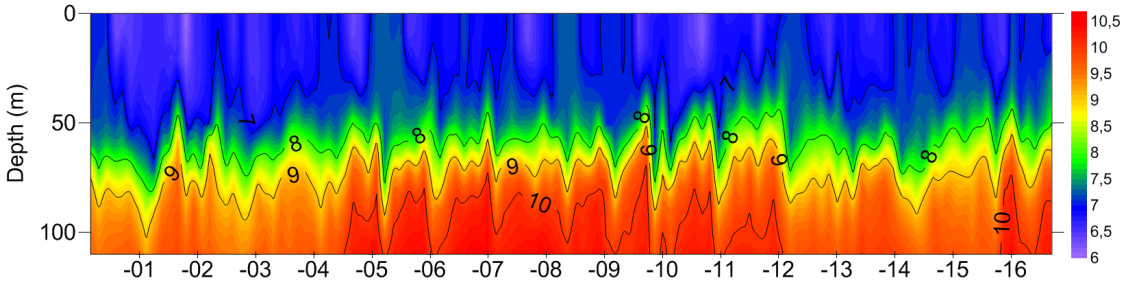

Figure S2. Water column salinity at western Gotland Basin station BY38 from 2000 to 2016, based on CTD salinity data retrieved from the SMHI Shark database (http://www.smhi.se/klimatdata/oceanografi/havsmiljodata/marina-miljoovervakningsdata). Note the annual to multi-annual oscillations in halocline depth.

Table S1. Sampling dates and depths of gas samples, along with exact sampling station coordinates in decimal minutes (WGS 84).

Sampling Date	Site	Coordinates (D M.m) Long.	Lat.	Ship / org.	Max depth (m)	Sampling depths (m) 20	40	50	60	70	80	90	100	105	109	110	115	120	125	130	135	140	142	143	144	145	150	155	160	165	167	170	175	185	190	192	195	196	200	225	236	237	238
17.3.2015	BY20	57 59.89 N	019 52.73 E	Aranda / SMHI	195	x	x		x	x	x	x	x						x								x						x		x								
17.3.2015	BY15	57 18.73 N	020 04.57 E	Aranda / SMHI	239	x			x	x	x	x	x						x								x						x	x	x		x		x	x		x	
17.3.2015	BY10	56 38.02 N	019 35.09 E	Aranda / SMHI	145	x	x		x	x	x	x	x						x																								
22.3.2015	BY32	58 01.01 N	017 59.07 E	Aranda / SMHI	202	x	x	x	x	x	x	x	x						x								x						x										
22.3.2015	BY38	57 07.03 N	017 40.12 E	Aranda / SMHI	110	x	x	x	x	x	x	x	x		x																												
21.4.2015	BY20	57 59.89 N	019 52.74 E	Aranda / SMHI	195	x	x		x	x	x	x	x						x								x						x		x								
21.4.2015	BY15	57 18.89 N	019 56.03 E	Aranda / SMHI	225	x			x	x	x	x	x						x	x	x	x				x	x						x						x	x			
21.4.2015	BY10	56 38.02 N	019 35.09 E	Aranda / SMHI	144	x	x		x	x	x	x	x						x					x																			
26.4.2015	BY32	58 01.01 N	017 59.07 E	Aranda / SMHI	201	x	x	x	x	x	x	x	x						x								x						x					x					
26.4.2015	BY38	57 07.03 N	017 40.12 E	Aranda / SMHI	110	x	x	x	x	x	x	x	x		x																												
4.6.2015	BY32	57 59.99 N	017 59.81 E	Aranda / SYKE	171	x	x	x	x	x	x	x	x						x								x					x											
5.6.2015	BY20	58 00.00 N	019 53.81 E	Aranda / SYKE	193	x	x		x	x	x	x	x						x								x						x					x					
5.6.2015	BY15	57 19.20 N	020 03.00 E	Aranda / SYKE	239	x			x	x	x	x	x	x		x	x	x	x	x	x	x					x						x						x	x		x†	
6.6.2015	BY10	56 38.00 N	019 35.00 E	Aranda / SYKE	143	x	x		x	x	x	x	x						x				x																				
5.8.2015	BY20	58 00.00 N	019 53.81 E	Aranda / SYKE	195	x	x		x	x	x	x	x						x								x						x				x						
5.8.2015	BY15	57 19.20 N	020 03.00 E	Aranda / SYKE	238	x			x	x	x	x	x	x		x	x	x	x	x	x						x						x						x	x			x
6.8.2015	BY10	56 38.00 N	019 35.00 E	Aranda / SYKE	142	x	x		x	x	x	x	x						x				x																				
6.8.2015	BY38	57 07.00 N	017 40.00 E	Aranda / SYKE	109	x	x	x	x	x	x	x	x		x																												
7.8.2015	BY32	57 59.99 N	017 59.81 E	Aranda / SYKE	170	x	x	x	x	x	x	x	x						x								x					x											
24.10.2015	BY15	57 19.22 N	020 03.12 E	Salme / TTU	231	x			x	x	x	x	x			x		x	x	x	x						x						x						x	x			
25.10.2015	BY20	57 59.99 N	019 57.12 E	Salme / TTU	169				x	x	x	x	x						x								x				x												
8.12.2015	BY20	57 59.89 N	019 52.73 E	Aranda / SMHI	196	x	x		x	x	x	x	x						x								x						x			x							
8.12.2015	BY15	57 18.73 N	020 04.57 E	Aranda / SMHI	239	x	x	x	x	x	x	x	x						x								x	x	x	x		x	x						x	x	x		
9.12.2015	BY10	56 38.02 N	019 35.09 E	Aranda / SMHI	145	x	x		x	x	x	x	x						x						x																		
13.12.2015	BY38	57 07.03 N	017 40.12 E	Aranda / SMHI	111	x	x	x	x	x	x	x	x			x																											
13.12.2015	BY32	58 01.01 N	017 59.07 E	Aranda / SMHI	202	x	x	x	x	x	x	x	x						x								x						x						x				

† gas samples lost

II

Paper II

Jukka-Pekka Myllykangas, Susanna Hietanen, and Tom Jilbert

Legacy effects of eutrophication on mondern methane dynamics in a boreal estuary

In *Estuaries and Coasts*,
Volume 43, issue 2, 2020, pages 189–206.

Estuaries and Coasts
https://doi.org/10.1007/s12237-019-00677-0

Legacy Effects of Eutrophication on Modern Methane Dynamics in a Boreal Estuary

Jukka-Pekka Myllykangas [1,2] · Susanna Hietanen [1,2] · Tom Jilbert [1,2]

Received: 15 May 2019 / Revised: 2 December 2019 / Accepted: 10 December 2019

Abstract

Estuaries are important conduits between terrestrial and marine aquatic systems and function as hot spots in the aquatic methane cycle. Eutrophication and climate change may accelerate methane emissions from estuaries, causing positive feedbacks with global warming. Boreal regions will warm rapidly in the coming decades, increasing the need to understand methane cycling in these systems. In this 3-year study, we investigated seasonal and spatial variability of methane dynamics in a eutrophied boreal estuary, both in the water column and underlying sediments. The estuary and the connected archipelago were consistently a source of methane to the atmosphere, although the origin of emitted methane varied with distance offshore. In the estuary, the river was the primary source of atmospheric methane. In contrast, in the adjacent archipelago, sedimentary methanogenesis fueled by eutrophication over previous decades was the main source. Methane emissions to the atmosphere from the study area were highly variable and dependent on local hydrodynamics and environmental conditions. Despite evidence of highly active methanogenesis in the studied sediments, the vast majority of the upwards diffusive flux of methane was removed before it could escape to the atmosphere, indicating that oxidative filters are presently still functioning regardless of previous eutrophication and ongoing climate change.

Keywords Aquatic biogeochemistry · Organic matter cycling · Greenhouse gases · Baltic Sea · Anaerobic oxidation of methane · Communicated by Margaret R. Mulholland

Introduction

Methane (CH_4) is an important greenhouse gas that contributes significantly to global warming (IPCC 2014) and influences atmospheric chemistry through a complex chain of oxidation reactions (Cicerone and Oremland 1988). The majority of CH_4 on Earth is produced by microbial methanogenesis, which is the ultimate pathway of anaerobic fermentation of organic matter occurring in a multitude of environments (Knittel and Boetius 2009). Of the natural sources of atmospheric CH_4, wetlands and freshwater systems are among the most significant, while agriculture, fossil fuels, waste treatment, and other anthropogenic sources make up between 46 and 67% of global emissions (Kirschke et al. 2013). As a consequence of human activities, the concentration of CH_4 in the atmosphere has more than doubled since pre-industrial times (Blasing 2016).

Coastal regions globally are experiencing intensified anthropogenic influence. In 2010, 1.9 billion people lived within a 100 km of a coastline; this figure is expected to rise to 2.4 billion by 2050 (Kummu et al. 2016). Agriculture, wastewater, industrial activities, and transport all contribute to nutrient and organic carbon loading to coastal aquatic systems (Syvitski et al. 2005; Lotze 2006; Paerl et al. 2006). Due to their role as conduits of land-to-sea transfer, estuaries are hot spots for biogeochemical cycling and are among the most productive aquatic systems in the world (Bianchi 2007). Eutrophication has increased the organic matter loading to estuarine

Communicated by Margaret R. Mulholland

Electronic supplementary material The online version of this article (https://doi.org/10.1007/s12237-019-00677-0) contains supplementary material, which is available to authorized users.

✉ Jukka-Pekka Myllykangas
jukka-pekka.myllykangas@helsinki.fi

✉ Tom Jilbert
tom.jilbert@helsinki.fi

[1] Ecosystems and Environment Research Program, Faculty of Biological and Environmental Sciences, University of Helsinki, P.O. Box 65, FI-00014 Helsinki, Finland

[2] Tvärminne Zoological Station, University of Helsinki, J.A. Palménintie 260, 10900 Hanko, Finland

Published online: 23 December 2019

sediments, leading to expanded areas of oxygen stress (Diaz and Rosenberg 2008; Middelburg and Levin 2009).

An important consequence of the eutrophication-driven expansion of low-oxygen conditions in estuaries is the increased production of CH_4 in the underlying sediments, as remineralization of organic matter increasing proceeds by anaerobic pathways (Naqvi et al. 2010; Gelesh et al. 2016). Estuaries have long been considered a potential source of atmospheric CH_4 emissions (Reeburgh 1969), due to outgassing of allochthonous inflowing CH_4 from the terrestrial environment, as well as autochthonous production within the estuary itself (Upstill-Goddard et al. 2000). However, the relative importance of these two main sources is not always easy to quantify (Reeburgh 2007). Large spatial and temporal variability in CH_4 concentrations is observed within and between estuaries, hampering efforts to construct methane mass balances for estuarine systems or to quantify the extent of human impact. Yet, typical estuarine surface water CH_4 concentrations are well above atmospheric equilibrium (de Angelis and Scranton 1993; Abril and Borges 2004), implying that estuarine systems are indeed a source for atmospheric CH_4.

The anthropogenic impact on methane cycling in estuaries is potentially exacerbated by climate change. The combined effects of eutrophication and warmer temperatures have been shown to increase atmospheric fluxes of CH_4 from lakes (Davidson et al. 2018). Boreal regions are excepted to be especially vulnerable to the warming climate and the changes introduced might not be linear in nature (Soja et al. 2007). Furthermore, other effects of climate change such as increased or more variable runoff, decreased solubility of oxygen, and increased water mass stratification (Gelesh et al. 2016) can all potentially contribute to the methanogenic potential of estuaries.

Despite their productivity and potential for greenhouse gas emissions, the exact contribution of estuaries to the global CH_4 budget is still relatively poorly constrained and they have often been excluded from global carbon budgets (Kirschke et al. 2013). In estuaries, as in other methanogenic environments, the emissions reaching the atmosphere are dependent on the balance of methanogenic and methanotrophic processes. The microbial processes and communities involved in the production and consumption of CH_4 are both directly and indirectly affected by environmental conditions. Hence, it is important to understand how different environmental conditions may lead to cascading effects in the microbial communities mediating CH_4 processes, and impact directly on process rates, for example through influencing metabolic activity or substrate availability (Dean et al. 2018).

Of the biogeochemical processes occurring in estuarine sediments, anaerobic oxidation of methane (AOM) is the most important limiting the escape of CH_4 to the water column and eventually to the atmosphere. AOM is capable of removing up to 90% of all CH_4 produced by methanogenesis (Knittel and Boetius 2009). It is typically most active in sediments (Iversen and Blackburn 1981), though it has been also shown to be active in the water column in strongly stratified systems (Jakobs et al. 2014). In the water column, aerobic oxidation of methane (MOX) is also a major process removing significant amounts of methane (Fenchel et al. 1995). Although these processes are very effective at preventing methane from escaping to the atmosphere, the combined effects of climate change and eutrophication have the potential to drastically increase CH_4 emissions from estuaries (Davidson et al. 2018), and it remains unknown whether it is possible for these filters to be overcome, whether through large increases in methanogenesis, increased storm activity, or solubility effects of increased temperatures.

Here we report the results of a 3-year study investigating seasonal and spatial variability of methane dynamics in a eutrophied boreal estuary with a legacy of eutrophication. The legacy effect is the result of decades of heightened autochthonous and allochthonous carbon loading in response to eutrophication in the catchment of the estuary, as well as the Baltic Sea in general. This has decreased the depth of the sulfate-methane transition zone (SMTZ), leading to increased CH_4 fluxes from the sediment. Data presented here contain both water column and sediment porewater concentrations and calculated flux estimates from sediments to water column and from there to the atmosphere.

Materials and Methods

Study Area

This study was conducted in an estuary and adjacent archipelago area located in Southern Finland, east of the Hanko Peninsula (Fig. 1.). The estuary goes by several names in the literature (Jilbert et al. 2018) but will be referred to as Pojo Bay here. It has been a location for numerous scientific studies for more than a century (Stipa 1999). It is a microtidal, fjord-like estuary that receives fresh water primarily from the river Mustionjoki (also known as Karjaanjoki) and opens in to the Gulf of Finland. The catchment area of Mustionjoki is 2046 km^2, consisting of 46% forest, 19% agriculture, 11% lakes, and 10% urban area (Asmala et al. 2012). There is a shallow sill (< 5 m water depth) near the city of Ekenäs separating the inner estuary from the outer archipelago and restricts currents, which creates a strong salinity gradient in the basin (< 1 in the inner bay to 7–8 in the outer archipelago). The inner bay is typically strongly stratified and the stagnant deep water is renewed only during late autumn or winter, when wind-driven inflows push more saline water over the sill into the inner bay (Stipa 1999). The estuary freezes intermittently

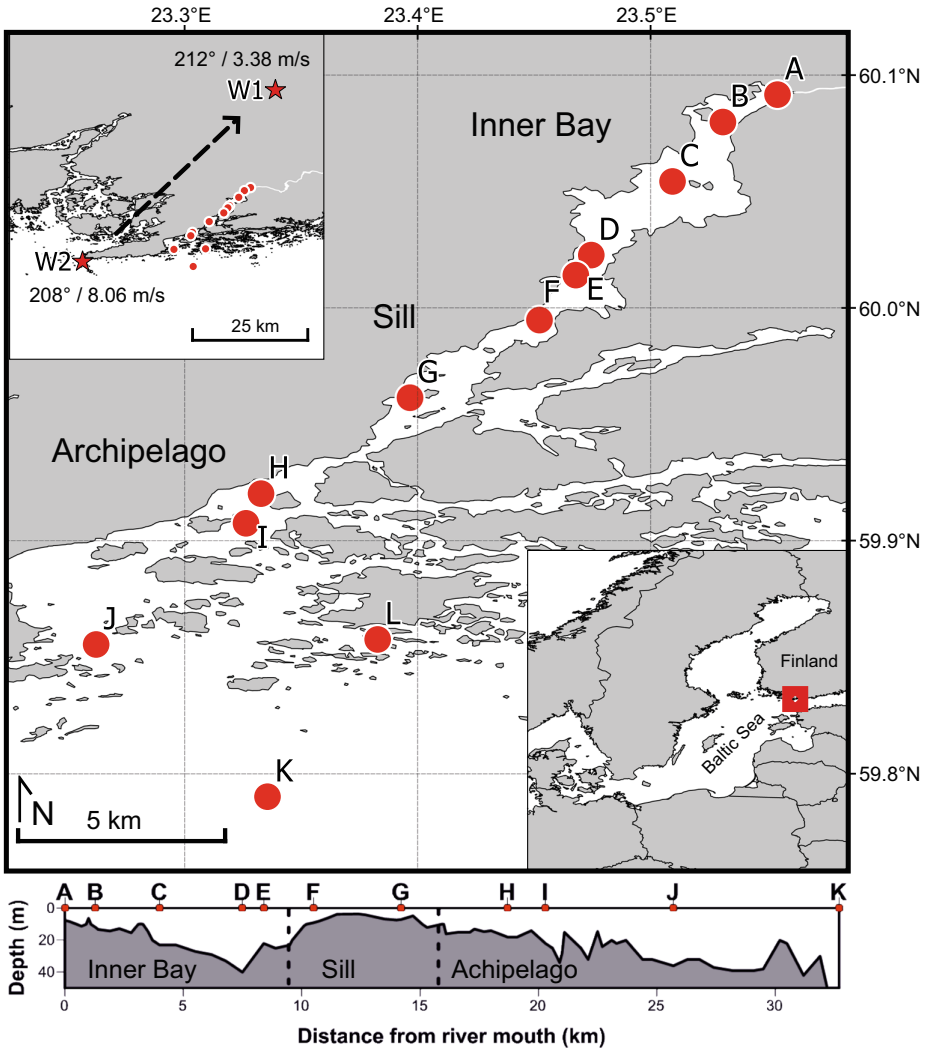

Fig. 1 Map of the study area and the stations along the transect. Stations J and L were used in the seasonal study. The inset in the top left corner shows the location of the weather stations used for wind data, and the dashed arrow the predominant wind direction between the stations. Average wind direction and speed in June 2015 is shown next to the station symbols. The inset in the lower right corner shows the position of the estuary in the Baltic Sea. The estuarine depth contour is shown in the bottom of the figure

during winter, with the inner bay typically freezing over completely and featuring several decimeters of ice. The inner bay has long suffered from periods of anoxia and sediment cores from the estuary feature distinct accumulation of solid-phase sulfur since the early 1970s, indicative of increased input of organic matter in response to eutrophication in the area (Jilbert et al. 2018). However, with improvements in communal wastewater treatment, limitations imposed on agricultural fertilizer usage and decreases in upstream industrial activity, modern nutrient and organic matter loading via the river is limited compared to similar estuaries along the Finnish coast (Meeuwig et al. 2000; Asmala et al. 2013). Annual mean loadings of carbon and nutrients determined during 2010–2011 are as follows: TOC = 4037 t year^{-1}, TN = 378 t year^{-1}, and TP = 12 t year^{-1} (Asmala et al., 2013). Two large lakes in the catchment also retain nutrients effectively (Koskiaho et al. 2015).

Sampling Strategy

Spatial methane dynamics in the estuary were studied along a 33-km transect consisting of 11 sites, which span from the river mouth of Mustionjoki in the inner estuary, out to open sea. The sites were selected for being representative of the various biogeochemical conditions along the estuary, both in the water column and in the sediments. The transect sites are labeled from A to K alphabetically and ordered by their distance offshore. The transect can be broadly split into three distinct parts: inner bay (A–E), sill (F–G), and archipelago (H–K) (Fig. 1). Sites D and J are both long-time monitoring stations also known in the literature as Sällvik deep and Storfjärden, respectively.

Seasonality of methane dynamics was studied at two sites: J and L, of which J is situated within the main channel and is deeper, relatively open and more dynamic, whereas L is a

more sheltered site surrounded by islands and features stronger seasonal stratification and is periodically hypoxic or anoxic below the pycnocline.

Sites along the transect were sampled three times for water column parameters (years 2015, 2016, and 2017) and twice for sediments (2014 and 2016). Three upstream sites in the Mustionjoki River (max 2 km from river mouth) were also sampled once in September 2015. The seasonal sites (J and L) were sampled four times during 2016 and once during 2017 (April, June, August, October, and March).

Water Sampling and CH_4 Analysis

Water samples were collected using a 5-L LIMNOS™ water sampler. Each site along the transect was sampled at 5-m depth intervals, with the first sample immediately below the surface (covering approximately 0–50 cm depth due to the length of the sampler). The two seasonal sites J and L were sampled at 2-m intervals. Complimentary temperature and salinity profiles were measured with a handheld CTD device at every station (Fig. S2). Samples were collected from small boats in the summer and from a hovercraft during winter sampling (March 2017).

Dissolved CH_4 samples were collected and prepared for analysis using a headspace equilibration method. Briefly, 30 mL of water was retrieved directly from the water sampler through a rubber tube, into a 60-mL plastic syringe and stored in a cooler. Within 6 h, a headspace of 30 mL of 5.0 purity N_2 was added and the samples were left to warm up for 30 min at room temperature. The samples were shaken vigorously for 3 min prior to transferring the headspace/gas in to a dry syringe through a three-way stopcock. From the dry syringe, the samples were injected into 12 mL glass tubes with butyl rubber septa (pre-evacuated LabCo Exetainer™ model 839W). The concentration of methane in the headspace was measured with a gas chromatograph equipped with a FID sensor (Agilent Technologies 7890B) against a three-point calibration of known gas concentrations (0.46, 5, and 47 ppm). Standards were measured before and after each sample series, and a 5-ppm standard was measured after every 10th sample, to account for between- and within-series drift, respectively. The original dissolved gas concentration of methane was then calculated using Henry's law and Bunsen solubility (Wiesenburg and Guinasso 1979). Samples were always analyzed within 2 weeks of sampling. For a more detailed description of the method, we refer the reader to Myllykangas et al. (2017). The method has limited sensitivity at CH_4 concentrations close to atmospheric equilibrium (1–3 nM). However, the lowest concentrations measured in this study were an order of magnitude higher than these values; hence, we consider the method reliable in this setting.

Sediment Sampling and Porewater Geochemical Analysis

Sediment cores were retrieved with a GEMAX™ twin gravity corer with 3 cm diameter holes pre-drilled at 1.5 cm intervals on the side of the core tube. The holes were closed with wide water-resistant electrical tape prior to sampling. After recovery, the holes were cut open and a cutoff syringe was quickly inserted into the core and filled with 10 cm^3 of sediment. The sediment in the syringe was then transferred to a 65-mL glass bottle containing supersaturated NaCl solution (Egger et al. 2015). The bottles were instantly capped with a butyl rubber septum and a screw cap and stored upside down while awaiting analysis. The transfers were always performed immediately after the core was brought on deck and as rapidly as possible to minimize degassing. Within 24 h, a headspace of 10 mL of 5.0 purity N_2 was introduced into the samples (with an equivalent amount of NaCl-slurry flowing out) and the samples were shaken to ensure all methane had evolved from the dissolved phase to the headspace.

Two 1-mL subsamples were taken from the headspace of each sample with a gas-tight 1-mL glass syringe and transferred to an evacuated 12-mL glass tube with a butyl rubber septum (LabCo Exetainer™ model 839W) and pressurized with 20 mL of 5.0 N_2, creating a dilution of 1:21. The mole fraction of methane in headspace of the samples was analyzed with a FID-equipped gas chromatograph (Agilent Technologies 7890B) against a standard series of known gas concentrations (5, 1000, and 10,000 ppm). As with water column samples, standard series were analyzed before and after each sample series and a 5-ppm standard was inserted after every 10 samples. The original porewater methane concentration was calculated assuming quantitative evolution of methane into the headspace. The volume of porewater in the 10-mL wet sediment sample was calculated directly from porosity values measured in parallel cores or estimated using assumed porosity profiles based on data from neighboring sites.

Vertical sulfate (SO_4^{2-}) and hydrogen sulfide (H_2S) profiles were generated from a parallel GEMAX™ core after Rhizon™ sampling. Two vertical series of holes at 2 cm intervals were drilled into the core tube, one for each sulfur species. The holes were taped prior to sampling, and after recovery, Rhizons™ were inserted into the holes and porewater was collected into 10 mL polyethylene syringes. The syringes for the H_2S series were pre-loaded with 1 mL 10% zinc acetate prior to sampling in order to trap sulfide in the form of zinc sulfide. The samples in the SO_4^{2-} series were acidified post-sampling with 1 M HNO_3.

The acidified SO_4^{2-} samples were analyzed using inductively coupled plasma-optical emission spectrometry (ICP-OES). The post-sampling acidification removes H_2S from the samples (Jilbert and Slomp 2013); hence, the measured S pool was considered to represent only SO_4^{2-}. The H_2S series

was analyzed spectrophotometrically at 670 nm wavelength according to a modified version of the methods of Cline (1969) and Reese et al. (2011). For a more detailed description of the method, see Jilbert et al. (2018).

Sediment Flux

Flux of methane from the sediment to water column was calculated using Fick's first law:

$$J = -\phi D_s \frac{\partial C}{\partial x} \quad (1)$$

Where J is the calculated flux of methane (mol m^{-2} s^{-1}), ϕ is the porosity of the surface sediment (determined from water content assuming sediment density of 2.65 g cm^{-3}), ∂C is the concentration difference between the surface sample from sediment (mol m^{-3}) and the deepest water sample (concentration assumed uniform between deepest sample and sediment surface), ∂x is the distance between the two different measurements (m), and D_s is the bulk sediment diffusion coefficient for methane, which was estimated according to (Berner 1980):

$$D_s = \frac{D_0}{\theta^2} \quad (2)$$

where D_0 is the molecular diffusion coefficient for methane in seawater at 4 °C ($0.87 \times 10^{-10} m^2 s^{-1}$) (Iversen and Jørgensen 1993) and θ is tortuosity, estimated as per (Boudreau 1997) as:

$$\theta^2 = 1 - \ln(\phi^2) \quad (3)$$

In addition to surface flux calculations described above, methane dynamics were studied also deeper in the sediment at seasonally studied sites J and L. A simple 1-D diagenetic model of CH_4 production and consumption was generated by using the software PROFILE (Berg et al. 1998). The software utilizes a simplified version of mass conservation equation of Boudreau (1997):

$$\frac{\partial}{\partial x}\left(\phi D_s \frac{\partial C}{\partial x}\right) + R = 0 \quad (4)$$

where R is the net production rate of CH_4. The software uses F tests and least squares fitting routines to determine optimum numbers of zones of production and consumption based on the concentration gradients of the porewater profiles. The model domain is defined by the whole interval sampled for porewater methane concentrations. In situ porosity values were used at each depth interval.

Atmospheric Flux

Flux of methane to the atmosphere was calculated with a two-layer model (Liss and Slater 1974):

$$F = k(C_{aq} - C_{eq}) \quad (5)$$

where F is the diffusive flux (mol m^{-2} s^{-1}), C_{aq} (mol m^{-3}) is the surface water concentration of CH_4 and C_{eq} the atmospheric equilibrium concentration calculated based on Henry's law, and k is the gas transfer velocity (m s^{-1}). C_{eq} was calculated using the atmospheric CH_4 concentrations of 1.91, 1.92, and 1.96 ppm for the years 2015, 2016, and 2017, respectively (data from the Utö monitoring station of the Finnish Meteorological Institute, approximately 100 km west of the estuary). The gas transfer velocity can be quantified in a number of ways, but it is commonly parameterized as a function of wind speed (e.g., Cole and Caraco 1998; Liss and Merlivat 1986; Wanninkhof 1992). Here we opted to use the exponential wind relationship formulated especially for estuaries by Raymond and Cole (2001), $1.91e^{0.35u}$, where u is the mean wind speed at 10 m height above sea level. Schmidt number is the ratio between the kinematic viscosity of water and the molecular diffusion coefficient (Jähne et al. 1987) and k values are commonly normalized to 600, which is the Schmidt number of CO_2 in freshwater at 20 °C.

Hence, the final atmospheric flux was calculated as:

$$F = 1.91e^{0.35u}\left(\frac{Sc_{CH4}}{600}\right)^{-0.5}(C_{aq} - C_{eq}) \quad (6)$$

where Sc_{CH4} is the Schmidt number for methane, calculated individually for all samples using in situ salinity and temperature values according to Wanninkhof (2014). Wind speed for each site was estimated by interpolating monthly wind speed averages between two weather stations of the Finnish Meteorological Institute situated roughly SW–NW along the transect (W1: Kiikala, Salo; W2: Tulliniemi, Hanko; Fig. 1). SW (the main fetch axis of the estuary) was the predominant wind direction and wind speeds were consistently higher at station W2 (Fig. S1, Online Resource). Due to wind speed having a strong effect on atmospheric exchange, atmospheric flux estimates in this study are presented as ranges of ± 1 standard deviation from the value estimated using the monthly mean wind speed.

Results

Transect

Water Column

Salinity in the inner bay was < 5 on all sampling occasions, with salinities offshore ranging between 6 and 8. Both summer transects displayed clear thermal stratification, although the thermocline was markedly deeper in the inner bay than in

the outer archipelago. At the two most offshore sites, the depth of the thermocline increased again (Fig. S2, Online Resource).

The highest dissolved CH_4 concentrations in the water column were consistently found near the river mouth at the surface of station A, with the highest value of 665 nM found in June of 2016 (Fig. 2). These values were similar to those measured in the inflowing river water in September 2015 (450 ± 7 nM, not shown), indicating a clear signal of river-derived CH_4 in the surface waters of the inner estuary. Surface concentrations decreased offshore consistently throughout all the sampling years, with a midwater minimum at 15 m depth in the estuary. CH_4 concentrations were elevated in the near-bottom samples at most sites on most sampling occasions, suggesting efflux from the sediments. However, these values were consistently lower than those close to the river mouth. For example, in June 2015, the deepest estuary site D had a near-bottom value of 156 nM, while in June 2016, the deepest open sea site K had a near-bottom value of 153 nM. In the archipelago areas, CH_4 concentrations were comparatively high throughout the water column, while concentrations at the offshore site K were consistently among the lowest measured. During winter, ice cover had a strong influence on the CH_4 distribution in the estuary; concentrations at the river mouth were lower than during summer, the CH_4-rich surface plume expanded further into the inner estuary with concentrations of 130–245 nM in the surface, and also the midwater minimum was expanded vertically from summer. Overall, the surface water concentrations were the highest in winter throughout the whole estuary.

During both summers, the highest atmospheric CH_4 fluxes were found at site A near the river mouth, from which the fluxes steadily decreased offshore (Fig. 3). The highest mean flux was calculated in June of 2016 (− 1.56 mmol m^{-2} day^{-1}, min − 0.7, max − 3.46), while the lowest fluxes were consistently found from the furthest offshore site K during all years. During winter, sites under ice were considered to have an atmospheric flux of 0, but potential fluxes are still shown in Fig. 3 because they are indicative of fluxes at the ice margins or gaps in the ice. At completely ice-free sites in March 2017 (H, J, and K), the mean atmospheric fluxes were higher than at the same sites during summer, and due to stronger winds, the maximum flux at site J (−1.12 mmol m^{-2} day^{-1}) was among the highest in the whole study.

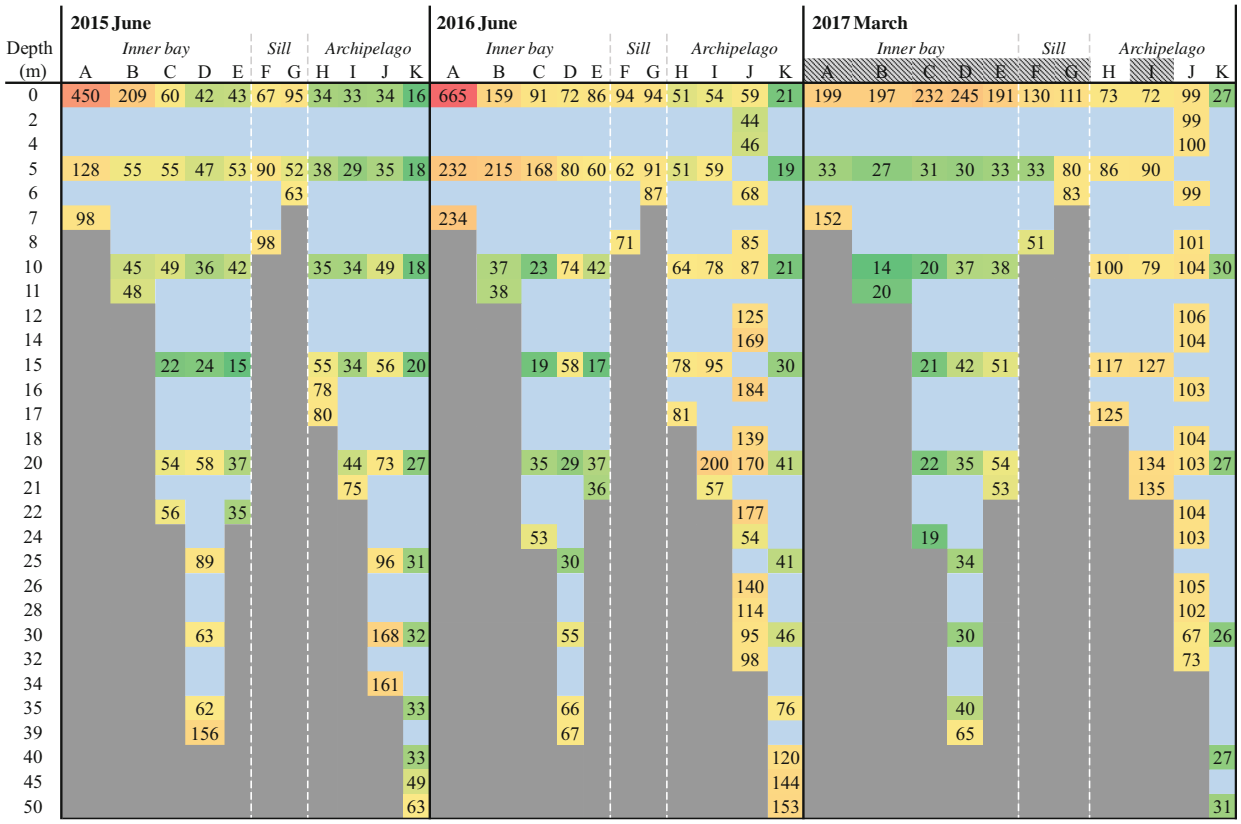

Fig. 2 Transect water column dissolved CH_4 concentrations (nmol L^{-1}) along the transect sites during three sampling campaigns. Note the irregular depths and that station distances are not to scale. The colors represent the relative change in the concentration throughout the whole data set, with the highest concentration presented in bright red and the lowest concentration in deep green. The shaded sites in March represent ice cover. For references to color, we refer the reader to the online version of the paper

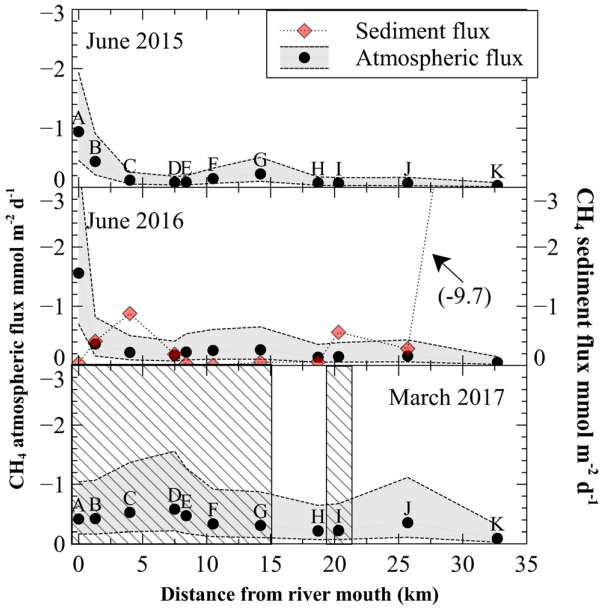

Fig. 3 Calculated atmospheric flux of methane along the transect during June 2015, June 2016, and March 2017. Dots indicate values estimated from monthly mean wind speed using Eq. 6. Gray-shaded areas indicate range of fluxes estimated from ± 1 standard deviation from monthly mean wind speed. Due to the nonlinearity of Eq. 6, the range is asymmetric about the mean. Also presented in the middle panel is the calculated sediment flux along the transect during June 2016. The hatched area in March 2017 represents ice cover, where true flux is assumed to be 0. Hence, the values presented are potential ice-free fluxes only

Sediment

Sediment porewater CH_4 concentrations measured in June 2016 are typically in the millimolar range, indicating significant methanogenesis in shallow sediments throughout the transect (Fig. 4). The highest CH_4 concentration, 6.19 mM, was found at site K from 12 cm depth, although the offshore trends in absolute CH_4 concentrations and the depth of the SMTZ are complex. Sediments near the sill (sites E–G) were typically devoid of methane, most likely due to the fact that these locations are characterized by transport rather than accumulation bottoms and, hence, lower concentrations of degrading organic matter. Sediments in bathymetric depressions (e.g., sites D and K), conversely, show elevated values. However, the shape of SO_4^{2-} profiles suggests that SO_4^{2-} reduction occurs at all sites.

The depth of the SMTZ (here defined as the depth of equivalent CH_4 and SO_4^{2-} concentration in the porewater profiles) is determined both by the upwards flux of methane and the bottom water SO_4^{2-} concentration. The latter show a clear increasing trend with distance offshore (Fig. 4). The depth of the SMTZ, in turn, is the primary control on the flux of methane across the sediment–water interface. Fluxes are typically highest in the bathymetric depressions (Fig. 3), consistent with high methane concentrations in the sediments at these locations. However, despite higher absolute porewater CH_4 concentrations at site D, site C shows a higher flux across the sediment–water interface, due to its lower bottom water SO_4^{2-} concentration and hence shallower SMTZ.

The highest fluxes anywhere on the transect were calculated at the offshore site K (− 9.66 mmol m^{-2} day^{-1}), a bathymetric depression where porewater CH_4 concentrations in the upper centimeter of the sediments are > 1 mM (Figs. 3 and 4). The sediment and atmospheric fluxes showed no correlation along the transect sites (Pearson's product-moment correlation $p > 0.5$).

Seasonal

Water Column

Water column CH_4 concentration patterns, as well as atmospheric and sediment fluxes, varied significantly during the seasonal cycle at both study sites J and L. Bottom water CH_4 concentrations at site L were generally higher than at site J. The highest bottom water value of 611 nM was found in June from the deepest sampling point at site L (Fig. 5), consistent with the stronger stratification at this site and

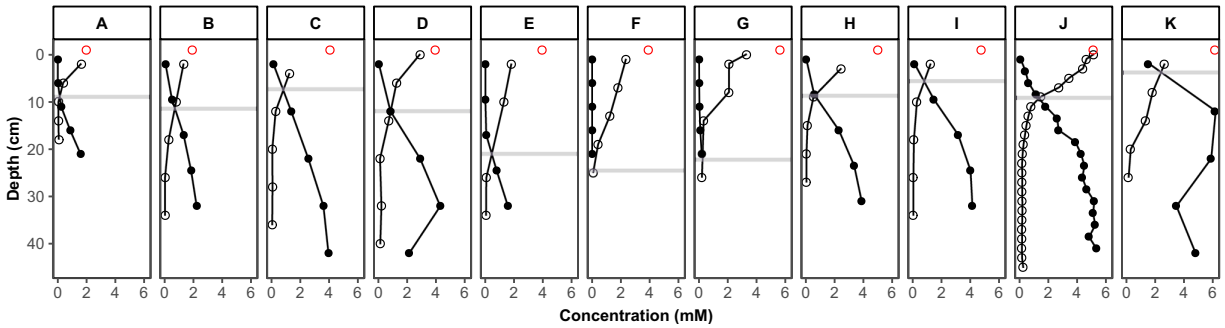

Fig. 4 Sediment porewater concentration profiles of methane from June 2016 (black circles) and sulfate from September 2014 (white circles) along the whole transect. The red circles represent bottom water sulfate concentration, and the horizontal gray line the depth of SMTZ at the sites (defines as equivalent concentrations of CH_4 and SO_4^{2-}

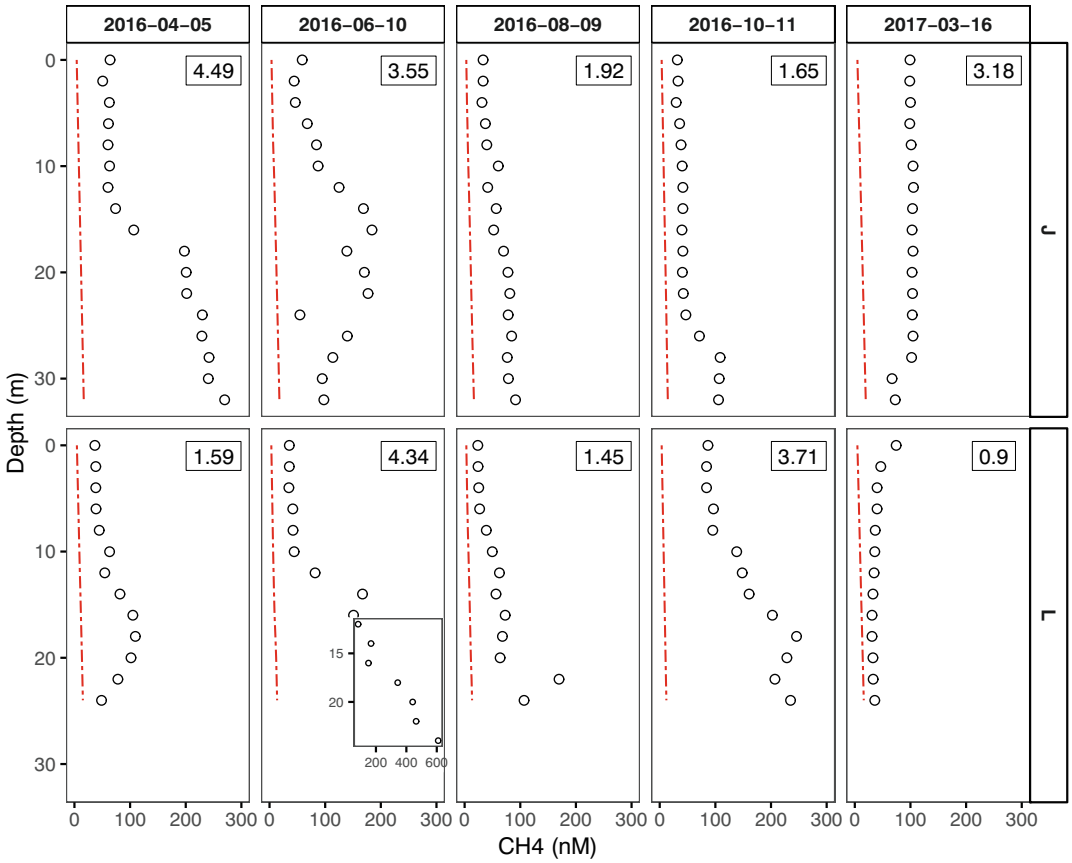

Fig. 5 Water column CH_4 concentrations at seasonally sampled sites J and L. The red dashed line represents in situ atmospheric equilibrium concentration. Note the different scale in the x axis of the inset. The number in the top right corner of each panel is the total CH_4 inventory in mmol L^{-1} m^{-2}

consequent accumulation of sediment-derived CH_4 in the bottom water. However, surface water concentrations at both sites were similar, and both sites showed their highest respective surface water concentrations in March. In terms of total CH_4 inventories per square meter, the seasonal evolution of the two sites varied. Site J featured the largest inventory in April with 4.49 mmol L^{-1} m^{-2} from where the inventory decreased throughout the year before increasing again in next March. At site L two maxima were observed, in June and October.

Atmospheric fluxes were generally higher at site J (Table 1), although the highest atmospheric flux in the dataset was calculated at L in October (− 0.39 mmol m^{-2} day^{-1}). No

Table 1 Sediment flux and atmospheric flux of CH_4 based on monthly mean wind values at sites J and L. Min and max represent monthly mean wind ± SD. SMTZ depth is defined as the depth where CH_4 and SO_4^{2-} concentrations are equal

Site	Date (year–month)	Atmospheric flux (mmol m^{-2} day^{-1})	Min	Max	Sediment flux (mmol m^{-2} day^{-1})	SMTZ depth (cm)
J	2016–04	− 0.14	− 0.05	− 0.39	− 0.61	11.6
	2016–06	− 0.18	− 0.07	− 0.49	− 0.25	9.3
	2016–08	− 0.12	− 0.05	− 0.3	− 0.25	7.9
	2016–10	− 0.13	− 0.04	− 0.42	− 0.66	9.5
	2017–03	− 0.34	− 0.11	− 1.09	N/A	N/A
L	2016–04	− 0.08	− 0.03	− 0.21	− 4.32	6.7
	2016–06	− 0.09	− 0.04	− 0.25	− 5.73	5.8
	2016–08	− 0.08	− 0.03	− 0.2	− 5.69	5.2
	2016–10	− 0.39	− 0.13	− 1.24	− 4.11	4.7
	2017–03	− 0.25*	− 0.08*	− 0.79*	N/A	N/A

*Potential value (under ice cover at the time of sampling)

flux is reported for site L in March because the site was under ice. Site J was ice-free and in March had the second highest seasonal flux value in the study of − 0.34 mmol m^{-2} day^{-1}.

Sediments

Surface sediment porewater CH_4 concentrations were generally higher at site L, with the highest concentration of 0.96 mM found in June. Accordingly, the SMTZ at this site was consistently shallower in the sediment column at site L (Fig. 6). The SMTZ, as defined by the depth of equivalent concentrations of CH_4 and SO_4^{2-}, is also indicated by the maximum in porewater H_2S, which was also generally observed close to this depth. The accumulation of CH_4 above this suggests intensive methanogenesis despite active sulfate-mediated AOM, evidenced by the presence of H_2S.

The overall shape of the CH_4 profiles at the two sites also differs considerably. Site J shows a concave profile in the uppermost 15 cm, while site L shows a convex profile in this interval. Also, concentrations at site L begin decreasing after 20 cm, whereas they generally keep increasing with depth at site J, with the highest concentration 5.33 mM found from 40 cm depth in June. The profiles

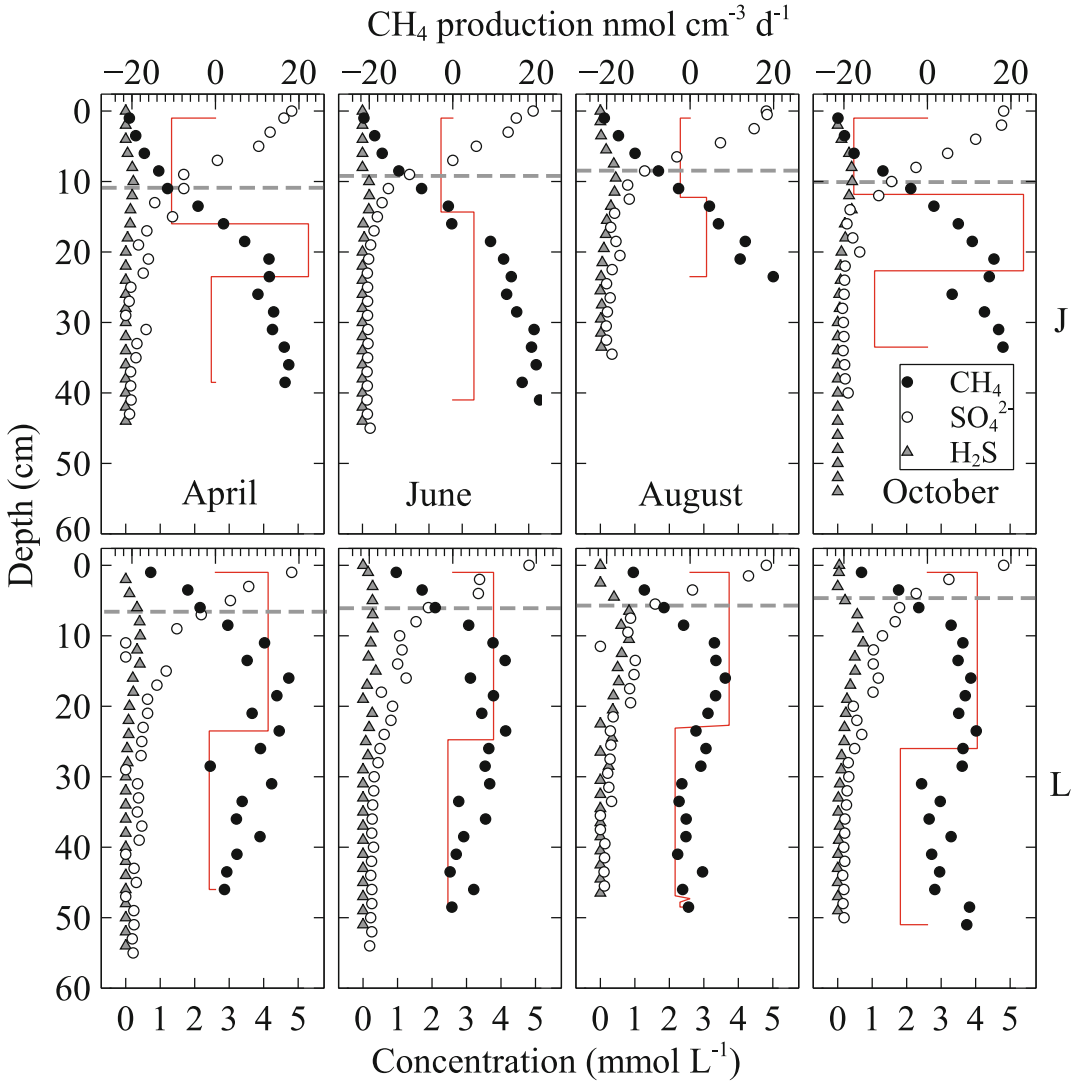

Fig. 6 Porewater concentrations of methane (black circles), sulfate (white circles), and hydrogen sulfide (triangles) at the seasonally sampled sites J and L. The concentrations of methane are from 2016, while concentrations of SO_4^{2-} and H_2S are from 2015. The red line represents modeled production and consumption of methane (secondary x axis) and the dashed gray line represents approximate depth of the SMTZ, as given by the equivalent concentration of CH_4 and SO_4^{2-}

from site J in April and October show some evidence for decreasing concentrations in the deepest samples.

The PROFILE outputs, too, show a clear zone of net methane consumption in the surface sediments at site J, while the corresponding interval at site L shows net production. Conversely, site L shows net production below ~ 15 cm, with evidence for net consumption in the deepest interval during April and October, while site L always shows a clear zone of net consumption below ~ 25 cm.

The sediment CH_4 flux was considerably higher at site L throughout all sampling months (Table 1). At site J, the highest sediment fluxes (− 0.61 to − 0.66 mmol m^{-2} day^{-1}) are found in April and October with lower fluxes (− 0.25 mmol m^{-2} day^{-1}) during the summer, while site L displays an opposite trend, with the highest sediment fluxes (− 5.69 to − 5.73 mmol m^{-2} day^{-1}) found during summer and lower in spring and autumn (− 4.11 to − 4.32 mmol m^{-2} day^{-1}).

Discussion

Pojo Bay and Its Archipelago as Net Sources of Methane to the Atmosphere

The Pojo Bay estuary surface waters were consistently supersaturated with CH_4 throughout the whole study across all sampling years and sites, making it a net source of CH_4. In terms of site-specific values on our study transect, highest fluxes were measured in the estuary. However, due to the spatial extent of the archipelago regions along the coast of the Gulf of Finland, the contribution of these areas is expected to dominate the net methane flux to the atmosphere in this coastal setting.

Many of the patterns in CH_4 fluxes to the atmosphere seen along the transect are well established in previous literature. The seaward decrease of surface water CH_4 concentrations is a commonly observed phenomenon in estuaries (Bartlett et al. 1987; de Angelis and Scranton 1993; Middelburg et al. 1996; Upstill-Goddard et al. 2000), and overall CH_4 concentrations in estuaries are lower than in fresh waters (Wik et al. 2016b), which was also true at Pojo Bay. The average surface water saturation in the whole Pojo Bay estuary was 4148% (range 561–21,234%), which is broadly comparable to other European estuaries (Bange 2006; Upstill-Goddard and Barnes 2016). Surface waters of the open Baltic are typically only slightly supersaturated and rarely exceed 500% (Bange et al. 1994; Gülzow et al. 2013). This shows that while coastal areas and estuaries are smaller in area, they are still likely an important part in total CH_4 emissions from the Baltic Sea.

Major Sources of Methane to the Water Column in Pojo Bay and Its Archipelago

Mustionjoki River

Rivers effectively accumulate methane from their drainage and are very active in methanogenesis (Stanley et al. 2016) and are therefore strong sources of atmospheric methane themselves (Upstill-Goddard et al. 2000). In this study, the inflowing river was a perpetual source of CH_4 in to the inner bay of the estuary. Although the input of CH_4 from the river to the estuary during the sampling period in June 2016 was limited due to low discharge at this time (~ 7 m^3 s^{-1}), the average input is likely to be higher. Concentrations up to 2.5 times higher in the river mouth have been measured at this location (e.g., 1660 nM, unpublished data). Also, based on long-term monitoring data from The Finnish Environment Institute, periods of discharge up to six times higher (~ 50 m^3 s^{-1}) were observed in 2016 alone.

Methanogenesis in the Sediment Column

The strong gradients in CH_4 concentrations in the sediment porewaters indicate a diffusive flux of CH_4 from sediments to the water column throughout the transect (Fig. 4). Only in the area of organic-poor sediments close to the sill (sites F, G) are low porewater CH_4 concentrations observed at all depths in the sediments. Coastal sediments in this region are characterized by high concentrations of organic carbon (3–6%) and sedimentation rates of 0.5–0.9 cm/year (Jilbert et al. 2018), leading to short oxygen exposure times for sedimenting organic matter and high rates of anaerobic remineralization processes, including methanogenesis (Middelburg and Levin 2009; Sobek et al. 2009). The flux of CH_4 from sediments to the water column leads to elevated bottom water CH_4 concentrations, especially in deeper, more stratified locations (e.g., sites C, D, L, Figs. 2 and 5).

Potential Role of Ebullition

The flux from sediments to water column may be enhanced by ebullition. If porewater CH_4 concentrations exceed local hydrostatic pressure, the formation of gas bubbles may occur (Wever et al. 1998). Although we did not observe supersaturation of CH_4 in the porewaters within the sampled depth interval in our sediment cores, bubble formation may initiate well below saturation (Chanton et al. 1989), implying that ebullition is possible in this setting. While we did not measure ebullition directly, we made several visual observations of bubbles in the water column during sampling at various sites along the transect. Also, at site L, water column gas replicates occasionally had extremely high CH_4 content (> 20 μM),

suggestive of gas bubbles becoming trapped within the sampling syringe.

The simultaneous presence of CH_4 and H_2S and SO_4^{2-} in the shallow sediments at site L (Fig. 6) indicates a strong overlap of the diagenetic zones in the sediments, as observed previously in the northern Baltic Sea (Sawicka and Brüchert 2017; Jilbert et al. 2018). This shows that methanogenesis is occurring in the upper sediments simultaneously with sulfate reduction, potentially due to the use of noncompetitive substrates by the microbial communities (Maltby et al. 2018). These high CH_4 concentrations close to the sediment–water interface increase the possibility that ebullition could occur, due to subannual temperature changes or sediment destabilization. Furthermore, ebullition could also partially explain the stochastic nature of the water column CH_4 concentrations observed in the archipelago in this study. Not only does ebullition commonly display high spatiotemporal variability (e.g., Scandella et al. 2016), it also has been shown to enhance diffusive sedimentary fluxes by making the sediment more porous (Flury et al. 2015).

Regulation of Sediment Flux by Oxidation Processes

AOM in the SMTZ

The accumulation of H_2S in conjunction with a downward decline of SO_4^{2-} and upward decline of CH_4 at around 10 cm depth at sites J and L is suggestive of SO_4^{2-}-AOM. The depth of the SMTZ was considerably deeper at site J compared to site L and varied in depth between sites along the transect (Fig. 4, Table 1).

At all sites, the SMTZ is expected to act as a strong filter to CH_4 fluxes from sediments to the water column (Knittel and Boetius 2009). However, the significant differences in the depth of the SMTZ between sites indicate that the efficiency of this filter function is variable with space in the coastal environment. Sites such as D, K, and L are characterized by high sedimentations rates and organic matter contents, leading to relatively compressed redox zonation and a shallow SMTZ (Figs. 4 and 6). We did not observe a consistent effect of bottom water sulfate concentration on the depth of the SMTZ as given by the depth of equivalent concentrations of CH_4 and SO_4^{2-} (Fig. 4), implying that the flux of organic matter to the sediments is the main factor controlling the SMTZ depth. Our detailed comparison of sites J and L confirms that locations with a shallower SMTZ (site L) also show higher fluxes of CH_4 to the water column (Table 1), implying a less efficient filter function of SO_4^{2-}-AOM.

MOX at the Sediment Surface

The uppermost 10–15 cm of the sediments at site J showed consistent net consumption of porewater CH_4 (Fig. 6.). We interpret this as evidence of enhanced MOX in the zone above the SMTZ due to the presence of benthic fauna. Benthic animals have an important role in many sedimentary solute fluxes (Middelburg and Levin 2009). Our results show strong evidence of bioirrigation, i.e., the introduction of oxic bottom water via animal burrows down to 10 cm or more in the sediment, which greatly reduces sediment flux of methane. Indeed, site J was recently shown to have an active community of benthic fauna that affects solute fluxes seasonally (Kauppi et al. 2018), whereas in comparison at site L, there is no benthic fauna, likely due to recurrent seasonal hypoxia or anoxia (e.g., Gammal et al. 2017 report 0.0 mg/L O_2 at this site for August 2010). We suggest that this is reflected in the porewater profiles, with CH_4 found much closer to the sediment surface at the hypoxic site L due to the absence of bioirrigation. Similarly, Abril and Iversen (2002) observed that sediment cores that contained large amounts of burrowing animals exhibited porewater CH_4 minima close to the sediment surface, not observed in parallel cores without animals.

While we do not have detailed CH_4 porewater profiles from all transect stations, we expect non-hypoxic bottom areas in both the estuary and archipelago to exhibit some degree of bioirrigation; hence, this may be an important process regulating the sediment CH_4 flux in this system.

In contrast to our findings, Bonaglia et al. (2017) observed that macrofauna enhanced CH_4 fluxes from the sediment by a factor of 8 compared to fauna-free sediment. However, they based their flux estimates on changes in concentration over time in an oxic incubation chamber, which makes direct comparison with our results difficult. For example, it is possible that the addition of benthic organisms to previously uncolonized sediments stimulated transient release of CH_4, including through ebullition, whereas in our study locations, the porewater signals of bioirrigation-induced MOX appear to be largely stable over time (Fig. 6).

Quantitative Budget of Methane Fluxes in Pojo Bay and Its Archipelago

A highly simplified budget of CH_4 flows in the estuary and archipelago areas was estimated assuming a set of constraints as outlined in Table S1 (Online Resource). The goal of this exercise is to establish the relative orders of magnitude and ranges of CH_4 flows in different parts of the system. Due to the required extrapolation, it is not possible to refine these estimates further with the available data. Nevertheless, the exercise yields some key findings. For example, the results suggest that the surface waters of the estuary at the time of sampling contained a reservoir of 12,853 mol CH_4 (Fig. 7). The estimated efflux to the atmosphere from the estuary was 5589 mol/day, indicating a turnover time of the surface-water inventory on a timescale of days, which is considerably less than the residence time of the bay (1.5 years, Meeuwig et al.

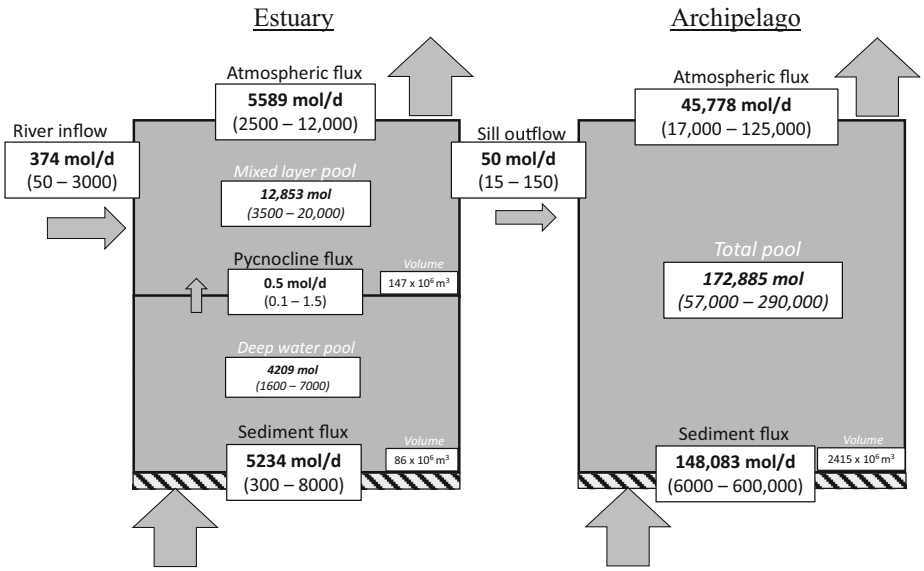

Fig. 7 Quantitative budget of the main sinks and sources of CH_4 in the estuary and archipelago compartments of the study system. The arrows in the figure indicate the direction of fluxes. Derivation of all values is presented in Table S1 (Online Resource) and the areal definition of the archipelago is presented in Fig. S3 (Online Resource). The gray-shaded area behind the sediment flux value conceptually represents the oxidative filter, i.e., real sediment flux is likely much less than presented here as most of the upwards-diffusing CH_4 will be oxidized before it enters the water column

2000). The estimated input of CH_4 from the river at the time of sampling was 374 mol/day, while the calculated diffusive flux from the isolated deep-water layer was only 0.5 mol/day. This indicates that the combined inputs to the surface waters at the time of sampling were significantly less than the amount required to balance the efflux to the atmosphere (Fig. 7). Hence, we conclude that the estuarine system was far from steady state with respect to CH_4 at the time of sampling. Furthermore, the system likely displays continuous high-amplitude variation in reservoir size, as well as riverine input and atmospheric fluxes, on very short timescales as a consequence of variable weather conditions.

The estimated range for atmospheric fluxes shown in Fig. 7 is based on the measured surface water CH_4 concentrations and the climatological range of wind stress in the month of June. Hence, the values are strongly dependent on the conditions during our sampling campaigns. The true range of values is also expected to be influenced by variability in the size of the surface water CH_4 reservoir over time. This in turn is likely to be controlled by variable inputs from the river. The budget shows that the river is the principal source of CH_4 to surface waters in the estuary, being orders of magnitude higher than the diffusive flux from the isolated deep-water layer. Theoretically, periods of high river discharge may lead to accumulation of the surface-water inventory, followed by rapid pulse-like expulsion to the atmosphere during high-wind stress storm events (Gelesh et al. 2016).

The flux of CH_4 from the sediments to the deep waters is estimated to be 5676 mol/day, a value that appears high compared to the deep-water reservoir of 4209 mol. However, the coarse resolution of our sediment sampling method is insufficient to resolve the fine-scale details of the porewater CH_4 gradient close to the sediment–water interface. It is likely that the vast majority of the upwards-diffusing CH_4 is oxidized by AOM and MOX in the uppermost sediment layers and, hence, that the true flux to the bottom waters is considerably lower than calculated here.

Despite extensive oxidation at the sediment–water interface, a fraction of sediment-derived CH_4 is clearly observed as elevated values in the deep waters of the estuary (Fig. 2). This drives an upwards diffusive flux toward the pycnocline and, hence, an additional, if small, contribution to surface water CH_4 concentrations in the estuary (Fig. 7). Processes in the water column, including dilution and oxidation, appear to attenuate the sediment-derived CH_4 signal in the intermediate-depth layers of the estuarine water column, leading to the development of a midwater minimum ($CH_4 <$ 30 nmol L^{-1}). This is likely maintained by the strong stratification, which also prevents downward advection of CH_4 introduced by the river water.

The budget shows that only a small fraction of the CH_4 introduced to surface waters of the estuary is transported across the sill to the archipelago area (Fig. 7). This indicates that the estuary behaves as a largely self-contained system with respect to CH_4 cycling. Conversely, the archipelago area displays its own internal CH_4 cycle, in which inputs are dominated by diffusion from sediments. Although the same oxidation filters are active in the archipelago as in the estuary, the flux from sediments is sufficient to raise deep-water CH_4 concentrations in some areas up to 600 nmol L^{-1} (Fig. 5). The heterogeneous nature of the archipelago environment makes spatial extrapolation of fluxes even more difficult than in the estuary. However, even if a small fraction of the archipelago area (as defined in Fig. S3, Online Resource) behaves similarly to our study locations, the estimated atmospheric fluxes are orders of magnitude higher than the flux of CH_4 introduced to

the archipelago via the sill (Fig. 7), indicating the importance of the sediment CH_4 source in this environment.

Overall, we can conclude from the budget that sedimentary methanogenesis obviously contributes to the total inventory of CH_4 in the estuary, especially during times of low discharge. However, in terms of atmospheric methane emissions originating from the estuary, current allochthonous CH_4 loading (i.e., input from the river) is likely far more important than the autochthonous loading caused by the legacy of eutrophication and sediment methanogenesis. This finding is similar to Abril and Iversen (2002) who calculated that annual CH_4 input by the river in Randers Fjord was equivalent to two thirds of total atmospheric emissions in that system, implying a lesser role for autochthonous estuarine CH_4 production. In the archipelago, the situation is reversed and methanogenesis fueled by the legacy of eutrophication is the main source of atmospheric methane.

Controls on Intra-annual Variability in Water Column Methane Concentrations

Seasonal Solubility and Oxidation Effects

Apart from the river-influenced surface layer, CH_4 concentrations in the estuary were overall lower in winter than in summer (Fig. 2). This runs contrary to the expectation of higher solubility of CH_4 at lower temperature, indicating that some additional processes control CH_4 saturation in the estuary in winter. Rates of water column MOX are sensitive to both temperature and salinity. MOX has an inverse relationship with salinity and is more efficient at low-salinity environments (de Angelis and Scranton 1993; Abril and Iversen 2002). The low salinity in the estuary could therefore favor MOX and cancel out the MOX inhibition caused by the cold temperatures (Steinle et al. 2017). Water column AOM, which may be active in low-oxygen regions of the study transect, has also been shown to have relatively high temperature optimum of 25–37 °C (Zehnder and Brock 1980). Furthermore, both AOM and MOX are most effective at the interfaces of strong gradients such as the pycnocline (Borges and Abril 2011), which are not present in a mixed water column. Therefore, the cold, more saline, and well-mixed conditions in the archipelago might be inhibiting both MOX and AOM, thus explaining the elevated concentrations of CH_4 in the archipelago during winter (Fig. 2).

Seasonal Changes in Stratification and Mixing

In the archipelago areas, CH_4 accumulated in the deeper waters is transported to the surface through physical mixing processes during winter, leading to a more uniform profile of CH_4 concentrations with higher surface concentrations (Figs. 2 and 5). Breakdown of stratification in late autumn could potentially lead to intermittent, "pulse-like," atmospheric emissions with large amounts of CH_4 escaping into the atmosphere over a relatively short period of time (Gelesh et al. 2016). Our results from site L suggest that stronger stratification coupled with low-oxygen bottom water in summer leads to decreased atmospheric flux of methane, whereas a large flux is detected during autumn, when mixing events are more likely (Fig. 5, Table 1). Silvennoinen et al. (2008) also observed the highest supersaturations of CH_4 during winter in Liminganlahti Bay in Northern Finland and also measured the highest atmospheric fluxes during winter in the unfrozen parts of the estuary.

In the Pojo Bay estuary, winter is characterized by extensive ice cover (Fig. 2). The inflowing river remained a strong source of methane during our winter sampling campaign, though the spatial signal of river-derived CH_4 differed from summer. The signal extended further offshore but was more diffuse in terms of the absolute concentrations. This was likely due to the river water creating a more compressed, laterally expanded freshwater lens under the ice. In previous studies, the influence of the river and especially spring melt water has been found to extend all the way to site J (Niemi 1975; Heiskanen and Tallberg 1999).

Subseasonal Exchange of Water Masses in the Archipelago

There was a remarkable drop in the water column CH_4 inventory from June to August at site L (Fig. 5), which can be explained by a large intrusion of saline water into the relatively secluded basin where this site is located, which displaced the CH_4-rich deep-water layer (Fig. S2, Online Resource). The same phenomenon can be seen at site J also, but to a lesser extent, and there it seems that only the surface water becomes more saline. A combination of both oxidation and displacement is likely behind the large decrease in CH_4 inventory (Schmale et al. 2016; Myllykangas et al. 2017).

Seasonal Migration of SMTZ

There were slight seasonal changes in the SMTZ depth and rates of methane production and consumption at the studied locations (Fig. 6). At site J, the SMTZ (defined as the depth of equivalent CH_4 and SO_4^{2-} concentration) was slightly deeper in spring and autumn and slightly shallower during summer (Fig. 6). Contrary to expectations, the calculated CH_4 fluxes were slightly suppressed during summer months (Table 1). At site L, the SMTZ was deepest in spring and became shallower with the passage of the year. Yet, there was no coincident trend in methane flux (Table 1). We note that the seasonal pattern differs slightly if the SMTZ is defined by the maximum concentration of H_2S (e.g., SMTZ at site L is deeper in October than August, Fig. 6). However, the small changes in methane-related processes in the sediments appear to be insufficient to

drive major seasonal changes in the flux of CH_4 to the water column in these locations. In the study of Schmaljohann (1996) from the Kiel harbor, clear seasonality was observed in the depth of the SMTZ over a range of 10–20 cm depth in sediment, potentially related to organic matter loading to the sediments. However, this author also observed a complex seasonal pattern of deep-water CH_4 concentrations, which could not be readily attributed to the mobility of the SMTZ and sediment fluxes. In other studies by Dale et al. (2008) and Mogollón et al. (2011), significant seasonal changes in AOM rates in sediments occurred due to temperature variations. Still, in these study locations, the SMTZ was located at > 2 m sediment depth, making a comparison with our setting difficult. In conclusion, the relationship between seasonal changes in temperature and organic matter loading, and sediment methane fluxes, are difficult to constrain in our study.

Long-Term Evolution of Methane Emissions in Eutrophied Estuaries

Pojo Bay Estuary and Archipelago

Like many other coastal regions of the Baltic Sea, the Pojo Bay estuary and the adjacent archipelago suffered from anthropogenic eutrophication during the twentieth century, leading to the expansion of seasonally hypoxic bottom waters in stratified areas (Conley et al. 2011; Jokinen et al. 2018). In the Pojo Bay estuary itself, there was a brief recovery period in the early 1980s, but oxygen conditions soon deteriorated again and the estuary suffered from extensive hypoxia in the 1990s (Malve et al. 2000). During that time, enhanced primary production in the estuary and archipelago led to high rates of carbon accumulation in the sediments (Heiskanen and Tallberg 1999). In a recent study, Raateoja and Kauppila (2019) studied eutrophication development of three estuaries in Northern Baltic, including Pojo Bay, from the 1970s onwards. In accordance with other studies of SW Finland archipelago areas (Conley et al. 2011; Jokinen et al. 2018), they did not find any evidence of oligotrophication in the recent past, but note that the two large lakes in the catchment of Mustionjoki may buffer changes in coastal nutrient levels, by delaying land-to-sea nutrient transfer. Bryhn et al. (2017) also argue that direct nutrient loading reduction to coastal catchments rarely controls the recovery of these systems from eutrophication, due to import of nutrients from the open Baltic Sea. This phenomenon is expected to be particularly important in open archipelago areas such as the outer stations of our study transect. They found that in 95% of their 656 coastal study sites along the Swedish coast, the influence of offshore nutrient contributions had a much greater impact on local nutrient concentrations than either catchment loading or atmospheric deposition. Therefore, the future recovery from eutrophication in our study region is likely closely coupled to that of the Baltic Sea as a whole.

Eutrophication and increased oxygen demand in the northern Baltic Sea have been shown to strongly influence diagenetic zonation in sediments, favoring a shallow SMTZ and enhanced rates of methanogenesis (Egger et al. 2015; Rooze et al. 2016). This situation is favored by the low salinity and, hence, low bottom water sulfate concentrations in this system (Capone and Kiene 1988). The high porewater CH_4 concentrations and shallow SMTZ depths observed in the sediments along the entire transect (Figs. 2 and 6) are therefore likely a modern phenomenon that is observed in response to nutrient loading in this region. This configuration of the diagenetic zones in the sediments contributes to high diffusive efflux of CH_4. In the archipelago areas, where sediments contribute the majority of the CH_4 fluxes to the atmosphere (Fig. 7), the legacy of eutrophication is therefore a potential key driver of methane emissions today. The theory of a recent acceleration of sedimentary methanogenesis is supported by the observation that CH_4 concentrations at some locations decline in the deeper sediments (e.g., below 20 cm at station L, Fig. 6). This implies lower rates of methanogenesis in layers deposited before peak eutrophication and carbon loading. However, we acknowledge that Fe-mediated AOM in the sub-SMTZ sediments (Egger et al. 2015) may also impact on these profiles.

Outlook and Implications

In a recent study, Borges et al. (2018) suggested a close coupling between eutrophication of the Belgian coastal zone and methane emissions from sediments. These authors compared methane concentrations 26 years apart and found a significant decrease in water column CH_4 concentrations, which they attribute to oligotrophication of the coastal zone during that time period. Our results confirm this close coupling, by showing that the shift toward eutrophication in the northern Baltic Sea has likely enhanced methanogenesis rates in the coastal sediments of this system.

Most findings of this study reinforce the patterns found in previous studies (e.g. Silvennoinen et al. 2008). The future evolution of methane emissions from our study area will likely depend on a combination of factors: first, the trajectory of nutrient loading from the catchment and import from the open Baltic Sea, which is expected to dictate rates of primary production and carbon loading to sediments. Secondly, climate change effects may play a strong role. For example, Wik et al. (2016b) found that the increased duration of the ice-free period caused by the warming climate was the main factor contributing to increased CH_4 emissions from Northern lakes. Many areas of the northern Baltic Sea currently experience significant ice cover during winter months. According to our results, the distribution of sea ice strongly influences the distribution of methane in the water column in

winter and the location of its eventual emission to the atmosphere (Figs. 2 and 3). In particular, the offshore propagation of terrestrial methane away from riverine sources may change if the extent and duration of ice cover is reduced in the future (Schneider et al. 2014). Climate change is also expected to increase precipitation especially in the Northern Hemisphere (Putnam and Broecker 2017). This would likely affect the freshwater balance in Pojo Bay in other similar estuaries and cause changes in stratification, solubility of CH_4 and, combined with increased discharge and ground runoff, increase land-to-sea CH_4 transport via increased methanogenesis in adjacent wetland areas (Corbett et al. 2015).

The role of ebullition in methane transfer from coastal sediments to the atmosphere requires further investigation. This process may be important both in our study system and in other coastal regions and may be sensitive to future changes in carbon loading, as well as bottom water temperatures and sediment resuspension importance of ebullition in controlling fluxes of methane directly from the sediment column. Bubbles rapidly rising through the water column to the surface may bypass the oxidative filter functions of AOM and MOX entirely (Knittel and Boetius 2009). The importance of ebullition as a source of atmospheric emissions of CH_4 has become more evident in recent studies. Schilder et al. (2016) found that in many lakes ebullitive fluxes to the atmosphere were almost 10 times higher than the diffusive flux, and it has been suggested that ebullition is behind up to 90% of all CH_4 emissions from aquatic systems (Wik et al. 2016a). It was also recently shown by Davidson et al. (2018) that while increased temperature and nutrient availability had little direct effect on diffusive fluxes of CH_4, their effects combined caused a considerable increase in ebullition.

Summary

- The whole estuary and its connecting archipelago were consistently a source of CH_4 to the atmosphere.
- According to our results, the allochthonous river input was consistently the main factor behind CH_4 supersaturation in the estuary, while sedimentary methanogenesis fueled by past eutrophication was the main source of CH_4 in the archipelago. The strong flux of CH_4 from the sediments was primarily caused by a shallow SMTZ and, where present, the action of benthic biota.
- Seasonal variability had a strong influence on atmospheric fluxes of methane and their spatial distribution. In the estuary, the CH_4-rich river plume reached much farther offshore, and in the archipelago areas, physical mixing brought methane from the deeper water layers to the surface. Patterns of atmospheric and sedimentary fluxes of methane in the archipelago appeared more complex and less directly affected by seasonality.
- The estuary displayed large variability in the sinks and sources of CH_4 implying that CH_4 fluxes to the atmosphere are equally variable and dependent on both local hydrodynamics as well as the larger climate system.
- The strong CH_4 fluxes from the sediments are likely a recent (decadal timescale) phenomenon. Our porewater CH_4 profiles show declining concentrations at greater depth in the sediment column, implying that the main zone of methanogenesis in this system is the shallow sediments.
- Despite the clear evidence of strong methanogenic activity throughout the sediments both in the estuary and the adjacent archipelago, atmospheric fluxes were generally at least an order of magnitude lower than respective sedimentary fluxes. This indicates that the oxidative filters are still functioning efficiently, although phenomena such as ebullition bypass these filters and future changes in temperature and eutrophication development might further modify the balance of these processes.

Acknowledgments We thank the personnel and trainees of Tvärminne Zoological Station for providing invaluable support to the field campaigns of this study, as well as the staff of the Department of Food and Environmental Sciences at University of Helsinki for assistance with ICP-OES analyses. The comments of two anonymous reviewers greatly improved the manuscript.

Funding Information Open access funding provided by University of Helsinki including Helsinki University Central Hospital. This research was funded by the Academy of Finland projects 139267, 272964, and 267112; Walter and Andrée de Nottbeck Foundation project COOLGAS; and Onni Talas Foundation (personal grant to JPM).

References

Abril, G., and N. Iversen. 2002. Methane dynamics in a shallow non-tidal estuary (Randers Fjord, Denmark). *Marine Ecology Progress Series* 230: 171–181. https://doi.org/10.3354/meps230171.

Abril, G., and A.V. Borges. 2004. *Carbon dioxide and methane emissions from estuaries. In Greenhouse gas emissions—fluxes and processes*, 187–207. Berlin/Heidelberg: Springer. https://doi.org/10.1007/3-540-26643-7_7 .

de Angelis, M.A., and M.I. Scranton. 1993. Fate of methane in the Hudson River and Estuary. *Global Biogeochemical Cycles* 7: 509–523. https://doi.org/10.1029/93GB01636.

Asmala, E., R. Autio, H. Kaartokallio, L. Pitkänen, C.A. Stedmon, and D.N. Thomas. 2013. Bioavailability of riverine dissolved organic matter in three Baltic Sea estuaries and the effect of catchment land use. *Biogeosciences* 10: 6969–6986. https://doi.org/10.5194/bg-10-6969-2013.

Asmala, E., C.A. Stedmon, and D.N. Thomas. 2012. Linking CDOM spectral absorption to dissolved organic carbon concentrations and loadings in boreal estuaries. *Estuarine, Coastal and Shelf Science* 111: 107–117. https://doi.org/10.1016/j.ecss.2012.06.015 .

Bange, H.W. 2006. Nitrous oxide and methane in European coastal waters. *Estuarine, Coastal and Shelf Science* 70: 361–374. https://doi.org/10.1016/j.ecss.2006.05.042.

Bange, H.W., U.H. Bartell, S. Rapsomanikis, and M.O. Andreae. 1994. Methane in the Baltic and North Seas and a reassessment of the marine emissions of methane. *Global Biogeochemical Cycles* 8: 465–480.

Bartlett, K.B., D.S. Bartlett, R.C. Harriss, and D.I. Sebacher. 1987. Methane emissions along a salt marsh salinity gradient. *Biogeochemistry* 4: 183–202. https://doi.org/10.1007/BF02187365.

Berg, P., N. Risgaard-Petersen, and S. Rysgaard. 1998. Interpretation of measured concentration profiles in sediment pore water. *Limnology and Oceanography* 43: 1500–1510. https://doi.org/10.4319/lo.1998.43.7.1500.

Berner, R.A. 1980. Early diagenesis: A theoretical approach. Princeton University Press, 1980.

Bianchi, T.S. 2007. *Biogeochemistry of estuaries*. New York: Oxford University Press, Inc..

Blasing, T.J. 2016. *Recent greenhouse gas concentrations*. https://doi.org/10.3334/CDIAC/atg.032.

Bonaglia, S., V. Brüchert, N. Callac, A. Vicenzi, E. Chi Fru, and F.J.A. Nascimento. 2017. Methane fluxes from coastal sediments are enhanced by macrofauna. *Scientific Reports* 7 (1): 1–10. https://doi.org/10.1038/s41598-017-13263-w.

Borges, A.V., and G. Abril. 2011. Carbon dioxide and methane dynamics in estuaries. *Treatise on Estuarine and Coastal Science* 5: 119–161. https://doi.org/10.1016/B978-0-12-374711-2.00504-0.

Borges, A.V., G. Speeckaert, W. Champenois, M.I. Scranton, and N. Gypens. 2018. Productivity and temperature as drivers of seasonal and spatial variations of dissolved methane in the Southern Bight of the North Sea. *Ecosystems* 21 (4): 583–599. https://doi.org/10.1007/s10021-017-0171-7.

Boudreau, B.P. 1997. *Diagenetic models and their implementation*. New York: Springer. https://doi.org/10.1007/978-3-642-60421-8.

Bryhn, A.C., P.H. Dimberg, L. Bergström, R.E. Fredriksson, J. Mattila, and U. Bergström. 2017. External nutrient loading from land, sea and atmosphere to all 656 Swedish coastal water bodies. *Marine Pollution Bulletin* 114: 664–670. https://doi.org/10.1016/j.marpolbul.2016.10.054.

Capone, D.G., and R.P. Kiene. 1988. Comparison of microbial dynamics in marine and freshwater sediments: Contrasts in anaerobic carbon catabolism. *Limnology and Oceanography* 33: 725–749. https://doi.org/10.4319/lo.1988.33.4part2.0725.

Chanton, J.P., C.S. Martens, and C.A. Kelley. 1989. Gas transport from methane-saturated, tidal freshwater and wetland sediments. *Limnology and Oceanography* 34: 807–819. https://doi.org/10.4319/lo.1989.34.5.0807.

Cicerone, R.J., and R.S. Oremland. 1988. Biogeochemical aspects of atmospheric methane. *Global Biogeochemical Cycles* 2: 299–327. https://doi.org/10.1029/GB002i004p00299.

Cline, J.D. 1969. Spectrophotometric determination of hydrogen sulfide in natural waters. *Limnology and Oceanography* 14: 454–458. https://doi.org/10.4319/lo.1969.14.3.0454.

Cole, J.J., and N.F. Caraco. 1998. Atmospheric exchange of carbon dioxide in a low-wind oligotrophic lake measured by the addition of SF 6. *Limnology and Oceanography* 43: 647–656. https://doi.org/10.4319/lo.1998.43.4.0647.

Conley, D.J., J. Carstensen, J. Aigars, P. Axe, E. Bonsdorff, T. Eremina, B.-M. Haahti, C. Humborg, P. Jonsson, J. Kotta, C. Lännegren, U. Larsson, A. Maximov, M.R. Medina, E. Lysiak-Pastuszak, N. Remeikaité-Nikiené, J. Walve, S. Wilhelms, and L. Zillén. 2011. Hypoxia is increasing in the coastal zone of the Baltic Sea. *Environmental Science & Technology* 45 (16): 6777–6783. https://doi.org/10.1021/es201212r.

Corbett, J.E., M.M. Tfaily, D.J. Burdige, P.H. Glaser, and J.P. Chanton. 2015. The relative importance of methanogenesis in the decomposition of organic matter in northern peatlands. *Journal of Geophysical Research – Biogeosciences* 120: 280–293. https://doi.org/10.1002/2014JG002797.

Dale, A.W., D.R. Aguilera, P. Regnier, H. Fossing, N.J. Knab, and B.B. Jørgensen. 2008. Seasonal dynamics of the depth and rate of anaerobic oxidation of methane in Aarhus Bay (Denmark) sediments. *Journal of Marine Research* 66: 127–155. https://doi.org/10.1357/002224008784815775.

Davidson, T.A., J. Audet, E. Jeppesen, F. Landkildehus, T.L. Lauridsen, M. Søndergaard, and J. Syväranta. 2018. Synergy between nutrients and warming enhances methane ebullition from experimental lakes. *Nature Climate Change* 8 (2): 156–160. https://doi.org/10.1038/s41558-017-0063-z.

Dean, J.F., J.J. Middelburg, T. Röckmann, R. Aerts, L.G. Blauw, M. Egger, M.S.M.M. Jetten, et al. 2018. Methane feedbacks to the global climate system in a warmer world. *Reviews of Geophysics* 56: 207–250. https://doi.org/10.1002/2017RG000559.

Diaz, R.J., and R. Rosenberg. 2008. Spreading dead zones and consequences for marine ecosystems. *Science* 321: 926–929. https://doi.org/10.1126/science.1156401.

Egger, M., O. Rasigraf, C.J. Sapart, T. Jilbert, M.S.M. Jetten, T. Röckmann, C. van der Veen, et al. 2015. Iron-mediated anaerobic oxidation of methane in brackish coastal sediments. *Environmental Science & Technology* 49 (1): 277–283. https://doi.org/10.1021/es503663z.

Fenchel, T., C. Bernard, G. Esteban, B.J. Finlay, P.J. Hansen, and N. Iversen. 1995. Microbial diversity and activity in a Danish Fjord with anoxic deep water. *Ophelia* 43: 45–100. https://doi.org/10.1080/00785326.1995.10430576.

Flury, S., R.N. Glud, K. Premke, and D.F. McGinnis. 2015. Effect of sediment gas voids and ebullition on benthic solute exchange. *Environmental Science and Technology* 49: 10413–10420. https://doi.org/10.1021/acs.est.5b01967.

Gammal, J., J. Norkko, C.A. Pilditch, and A. Norkko. 2017. Coastal hypoxia and the importance of benthic macrofauna communities for ecosystem functioning. *Estuaries and Coasts* 40 (2): 457–468. https://doi.org/10.1007/s12237-016-0152-7.

Gelesh, L., K. Marshall, W. Boicourt, and L. Lapham. 2016. Methane concentrations increase in bottom waters during summertime anoxia in the highly eutrophic estuary, Chesapeake Bay, U.S.A. *Limnology and Oceanography* 61: S253–S266. https://doi.org/10.1002/lno.10272.

Gülzow, W., G. Rehder, J.S.V. Deimling, T. Seifert, Z. Tóth, and J. Schneider Von Deimling. 2013. One year of continuous measurements constraining methane emissions from the Baltic Sea to the atmosphere using a ship of opportunity. *Biogeosciences* 10: 81–99. https://doi.org/10.5194/bg-10-81-2013.

Heiskanen, A., and P. Tallberg. 1999. Sedimentation and particulate nutrient dynamics along a coastal gradient from a fjord-like bay to the open sea. *Hydrobiologia* 393: 127–140. https://doi.org/10.1023/A:1003539230715.

IPCC. 2014. *Climate change 2013—The physical science basis. Edited by Intergovernmental Panel on Climate Change*. Cambridge: Cambridge University Press. https://doi.org/10.1017/CBO9781107415324.

Iversen, N., and T.H. Blackburn. 1981. Seasonal rates of methane oxidation in anoxic marine sediments. *Deep Sea Research Part B.*

Oceanographic Literature Review 28: 888. https://doi.org/10.1016/0198-0254(81)91600-9.

Iversen, Niels, and B. Jørgensen. 1993. Diffusion coefficients of sulfate and methane in marine sediments: Influence of porosity. *Geochimica et Cosmochimica Acta* 57: 571–578. https://doi.org/10.1016/0016-7037(93)90368-7.

Jähne, B., K.O. Münnich, R. Bösinger, A. Dutzi, W. Huber, and P. Libner. 1987. On the parameters influencing air-water gas exchange. *Journal of Geophysical Research* 92: 1937. https://doi.org/10.1029/JC092iC02p01937.

Jakobs, G., P. Holtermann, C. Berndmeyer, G. Rehder, M. Blumenberg, G. Jost, G. Nausch, and O. Schmale. 2014. Seasonal and spatial methane dynamics in the water column of the central Baltic Sea (Gotland Sea). *Continental Shelf Research* 91: 12–25. https://doi.org/10.1016/j.csr.2014.07.005.

Jilbert, T., E. Asmala, C. Schröder, R. Tiihonen, J.-P. Myllykangas, J.J. Virtasalo, A. Kotilainen, P. Peltola, P. Ekholm, and S. Hietanen. 2018. Impacts of flocculation on the distribution and diagenesis of iron in boreal estuarine sediments. *Biogeosciences* 15: 1243–1271. https://doi.org/10.5194/bg-15-1243-2018.

Jilbert, T., and C.P. Slomp. 2013. Iron and manganese shuttles control the formation of authigenic phosphorus minerals in the euxinic basins of the Baltic Sea. *Geochimica et Cosmochimica Acta* 107: 155–169. https://doi.org/10.1016/j.gca.2013.01.005.

Jokinen, S.A., J.J. Virtasalo, T. Jilbert, J. Kaiser, O. Dellwig, H.W. Arz, J. Hänninen, L. Arppe, M. Collander, and T. Saarinen. 2018. A 1500-year multiproxy record of coastal hypoxia from the northern Baltic Sea indicates unprecedented deoxygenation over the 20th century. *Biogeosciences* 15: 3975–4001. https://doi.org/10.5194/bg-15-3975-2018.

Kauppi, L., G. Bernard, R. Bastrop, A. Norkko, and J. Norkko. 2018. Increasing densities of an invasive polychaete enhance bioturbation with variable effects on solute fluxes. *Scientific Reports* 8: 1–12. https://doi.org/10.1038/s41598-018-25989-2.

Kirschke, S., P. Bousquet, P. Ciais, M. Saunois, J.G. Canadell, E.J. Dlugokencky, P. Bergamaschi, et al. 2013. Three decades of global methane sources and sinks. *Nature Geoscience* 6: 813–823. https://doi.org/10.1038/ngeo1955.

Knittel, K., and A. Boetius. 2009. Anaerobic oxidation of methane: Progress with an unknown process. *Annual Review of Microbiology* 63: 311–334. https://doi.org/10.1146/annurev.micro.61.080706.093130.

Koskiaho, J., S. Tattari, and E. Röman. 2015. Suspended solids and total phosphorus loads and their spatial differences in a lake-rich river basin as determined by automatic monitoring network. *Environmental Monitoring and Assessment* 187 (4): 187. https://doi.org/10.1007/s10661-015-4397-6.

Kummu, M., H. de Moel, G. Salvucci, D. Viviroli, P.J. Ward, and O. Varis. 2016. Over the hills and further away from coast: Global geospatial patterns of human and environment over the 20th–21st centuries. *Environmental Research Letters* 11: 034010. https://doi.org/10.1088/1748-9326/11/3/034010.

Liss, P.S., and L. Merlivat. 1986. Air-sea gas exchange rates: Introduction and synthesis. In *The role of air-sea exchange in geochemical cycling*, 113–127. Dordrecht: Springer. https://doi.org/10.1007/978-94-009-4738-2_5.

Liss, P.S., and P.G. Slater. 1974. Flux of gases across the air-sea interface. *Nature* 247: 181–184. https://doi.org/10.1038/247181a0.

Lotze, H.K. 2006. Depletion, degradation, and recovery potential of estuaries and coastal seas. *Science* 312: 1806–1809. https://doi.org/10.1126/science.1128035.

Maltby, J., L. Steinle, C.R. Löscher, H.W. Bange, M.A. Fischer, M. Schmidt, and T. Treude. 2018. Microbial methanogenesis in the sulfate-reducing zone of sediments in the Eckernförde Bay, SW Baltic Sea. *Biogeosciences* 15: 137–157. https://doi.org/10.5194/bg-15-137-2018.

Malve, O., M. Virtanen, L. Villa, M. Karonen, H. Aakerla, A.S. Heiskanen, K.M. Lappalainen, and R. Holmberg. 2000. Artificial oxygenation experiment in hypolimnion of Pojo Bay estuary in 1995 and 1996: Factors regulating estuary circulation and oxygen and salt balances. Helsinki .

Meeuwig, J.J., P. Kauppila, and H. Pitkänen. 2000. Predicting coastal eutrophication in the Baltic: A limnological approach. *Canadian Journal of Fisheries and Aquatic Sciences* 57: 844–855. https://doi.org/10.1139/f00-013.

Middelburg, J.J., G. Klaver, J. Nieuwenhuize, A. Wielemaker, W. De Haas, T. Vlug, and J.F.W.A. Van Der Nat. 1996. Organic matter mineralization in intertidal sediments along an estuarine gradient. *Marine Ecology Progress Series* 132: 157–168. https://doi.org/10.3354/meps132157.

Middelburg, J.J., and L.A. Levin. 2009. Coastal hypoxia and sediment biogeochemistry. *Biogeosciences* 6: 1273–1293. https://doi.org/10.5194/bg-6-1273-2009.

Mogollón, J.M., A.W. Dale, I. L'Heureux, and P. Regnier. 2011. Impact of seasonal temperature and pressure changes on methane gas production, dissolution, and transport in unfractured sediments. *Journal of Geophysical Research* 116: G03031. https://doi.org/10.1029/2010JG001592.

Myllykangas, J.-P., T. Jilbert, G. Jakobs, G. Rehder, J. Werner, and S. Hietanen. 2017. Effects of the 2014 major Baltic inflow on methane and nitrous oxide dynamics in the water column of the central Baltic Sea. *Earth System Dynamics* 8: 817–826. https://doi.org/10.5194/esd-8-817-2017.

Naqvi, S.W.A., H.W. Bange, L. Farías, P.M.S. Monteiro, M.I. Scranton, and J. Zhang. 2010. Marine hypoxia/anoxia as a source of CH_4 and N_2O. *Biogeosciences* 7: 2159–2190. https://doi.org/10.5194/bg-7-2159-2010.

Niemi, Å. 1975. Ecology of phytoplankton in the Tvärminne area, SW coast of Finland II. Primary production and environmental conditions in the archipelago and the sea zone. Annales Botanici Fennici 105. Finnish Zoological and Botanical Publishing Board

Paerl, H.W., L.M. Valdes, B.L. Peierls, J.E. Adolf, and L.J.W. Harding. 2006. Anthropogenic and climatic influences on the eutrophication of large estuarine ecosystems. *Limnology and Oceanography* 51: 448–462. https://doi.org/10.4319/lo.2006.51.1_part_2.0448.

Putnam, A.E., and W.S. Broecker. 2017. Human-induced changes in the distribution of rainfall. *Science Advances* 3: 1–15. https://doi.org/10.1126/sciadv.1600871.

Raateoja, M., and P. Kauppila. 2019. Interaction between the land and the sea: Sources and patterns of nutrients in the scattered coastal zone of a eutrophied sea. *Environmental Monitoring and Assessment* 191: 24. https://doi.org/10.1007/s10661-018-7143-z.

Raymond, P.A., and J.J. Cole. 2001. Gas exchange in rivers and estuaries: Choosing a gas transfer velocity. *Estuaries* 24: 312–317.

Reeburgh, W.S. 1969. Observations of gases in Chesapeake Bay sediments. *Limnology and Oceanography* 14: 368–375. https://doi.org/10.4319/lo.1969.14.3.0368.

Reeburgh, W.S. 2007. Oceanic methane biogeochemistry. *Chemical Reviews* 107: 486–513. https://doi.org/10.1021/cr050362v.

Reese, B.K., D.W. Finneran, H.J. Mills, M.-X. Zhu, and J.W. Morse. 2011. Examination and refinement of the determination of aqueous hydrogen sulfide by the methylene blue method. *Aquatic Geochemistry* 17 (4-5): 567–582. https://doi.org/10.1007/s10498-011-9128-1.

Rooze, J., M. Egger, I. Tsandev, and C.P. Slomp. 2016. Iron-dependent anaerobic oxidation of methane in coastal surface sediments: Potential controls and impact. *Limnology and Oceanography* 61: S267–S282. https://doi.org/10.1002/lno.10275.

Sawicka, J.E., and V. Brüchert. 2017. Annual variability and regulation of methane and sulfate fluxes in Baltic Sea estuarine sediments. *Biogeosciences* 14: 325–339. https://doi.org/10.5194/bg-14-325-2017.

Scandella, B.P., L. Pillsbury, T. Weber, C.D. Ruppel, H.F. Hemond, and R. Juanes. 2016. Ephemerality of discrete methane vents in lake sediments. *Geophysical Research Letters* 43: 4374–4381. https://doi.org/10.1002/2016GL068668.

Schilder, J., D. Bastviken, M. van Hardenbroek, and O. Heiri. 2016. Spatiotemporal patterns in methane flux and gas transfer velocity at low wind speeds: Implications for upscaling studies on small lakes. *Journal of Geophysical Research – Biogeosciences* 121: 1456–1467. https://doi.org/10.1002/2016JG003346.

Schmale, O., S. Krause, P. Holtermann, N.C. Power Guerra, and L. Umlauf. 2016. Dense bottom gravity currents and their impact on pelagic methanotrophy at oxic/anoxic transition zones. *Geophysical Research Letters* 43: 5225–5232. https://doi.org/10.1002/2016GL069032.

Schmaljohann, R. 1996. Methane dynamics in the sediment and water column of Kiel Harbour (Baltic Sea). *Marine Ecology Progress Series* 131: 263–273. https://doi.org/10.3354/meps131263.

Schneider, B., W. Gülzow, B. Sadkowiak, and G. Rehder. 2014. Detecting sinks and sources of CO2 and CH4 by ferrybox-based measurements in the Baltic Sea: Three case studies. *Journal of Marine Systems* 140: 13–25. https://doi.org/10.1016/j.jmarsys.2014.03.014.

Silvennoinen, H., A. Liikanen, J. Rintala, and P.J. Martikainen. 2008. Greenhouse gas fluxes from the eutrophic Temmesjoki River and its estuary in the Liminganlahti Bay (the Baltic Sea). *Biogeochemistry* 90 (2): 193–208. https://doi.org/10.1007/s10533-008-9244-1.

Sobek, S., E. Durisch-Kaiser, R. Zurbrügg, N. Wongfun, M. Wessels, N. Pasche, and B. Wehrli. 2009. Organic carbon burial efficiency in lake sediments controlled by oxygen exposure time and sediment source. *Limnology and Oceanography* 54: 2243–2254. https://doi.org/10.4319/lo.2009.54.6.2243.

Soja, A.J., N.M. Tchebakova, N.H.F. French, M.D. Flannigan, H.H. Shugart, B.J. Stocks, A.I. Sukhinin, E.I. Parfenova, F.S. Chapin, and P.W. Stackhouse. 2007. Climate-induced boreal forest change: Predictions versus current observations. *Global and Planetary Change* 56: 274–296. https://doi.org/10.1016/j.gloplacha.2006.07.028.

Stanley, E.H., N.J. Casson, S.T. Christel, J.T. Crawford, L.C. Loken, and S.K. Oliver. 2016. The ecology of methane in streams and rivers: Patterns, controls, and global significance. *Ecological Monographs* 86: 146–171. https://doi.org/10.1890/15-1027.

Steinle, L., J. Maltby, T. Treude, A. Kock, H.W. Bange, N. Engbersen, J. Zopfi, M.F. Lehmann, and H. Niemann. 2017. Effects of low oxygen concentrations on aerobic methane oxidation in seasonally hypoxic coastal waters. *Biogeosciences* 14: 1631–1645. https://doi.org/10.5194/bg-14-1631-2017.

Stipa, T. 1999. Water exchange and mixing in a semi-enclosed coastal basin (Pohja Bay). *Boreal Environment Research* 4: 307–317.

Syvitski, J.P.M., C.J. Vörösmarty, A.J. Kettner, and P. Green. 2005. Impact of humans on the flux of terrestrial sediment to the global coastal ocean. *Science* 308 (5720): 376–380. https://doi.org/10.1126/science.1109454.

Upstill-Goddard, R.C., and J. Barnes. 2016. Methane emissions from UK estuaries: re-evaluating the estuarine source of tropospheric methane from Europe. *Marine Chemistry* 180: 14–23. https://doi.org/10.1016/j.marchem.2016.01.010.

Upstill-Goddard, R.C., J. Barnes, T. Frost, S. Punshon, and N.J.P. Owens. 2000. Methane in the southern North Sea: Low-salinity inputs, estuarine removal, and atmospheric flux. *Global Biogeochemical Cycles* 14: 1205–1217. https://doi.org/10.1029/1999GB001236.

Wanninkhof, R.H. 1992. Relationship between wind speed and gas exchange. *Journal of Geophysical Research* 97: 7373–7382. https://doi.org/10.1029/92JC00188.

Wanninkhof, R.H. 2014. Relationship between wind speed and gas exchange over the ocean revisited. *Limnology and Oceanography: Methods* 12: 351–362. https://doi.org/10.4319/lom.2014.12.351.

Wever, T.F., F. Abegg, H.M. Fiedler, G. Fechner, and I.H. Stender. 1998. Shallow gas in the muddy sediments of Eckernforde Bay, Germany. *Continental Shelf Research* 18: 1715–1739. https://doi.org/10.1016/S0278-4343(98)00055-7.

Wiesenburg, D.A., and N.L. Guinasso. 1979. Equilibrium solubilities of methane, carbon monoxide, and hydrogen in water and sea water. *Journal of Chemical & Engineering Data* 24: 356–360. https://doi.org/10.1021/je60083a006.

Wik, M., B.F. Thornton, D. Bastviken, J. Uhlbäck, and P.M. Crill. 2016a. Biased sampling of methane release from northern lakes: A problem for extrapolation. *Geophysical Research Letters* 43: 1256–1262. https://doi.org/10.1002/2015GL066501.

Wik, M., R.K. Varner, K.W. Anthony, S. MacIntyre, and D. Bastviken. 2016b. Climate-sensitive northern lakes and ponds are critical components of methane release. *Nature Geoscience* 9: 99–105. https://doi.org/10.1038/ngeo2578.

Zehnder, A.J., and T.D. Brock. 1980. Anaerobic methane oxidation: Occurrence and ecology. *Applied and Environmental Microbiology* 39 (1): 194–204.

LEGACY EFFECTS OF EUTROPHICATION ON MODERN METHANE DYNAMICS IN A BOREAL ESTUARY

Online Resource

Estuaries and Coasts

Jukka-Pekka Myllykangas[1,2], Tom Jilbert[1,2], and Susanna Hietanen[1,2]

[1] Ecosystems and Environment Research Programme, Faculty of Biological and Environmental Sciences, University of Helsinki, P.O. Box 65, FIN-00014 University of Helsinki, Finland
[2] Tvärminne Zoological Station, University of Helsinki, J.A. Palménintie 260, 10900 Hanko, Finland

Corresponding author: JP Myllykangas (jukka-pekka.myllykangas@helsinki.fi

Contents

Fig. S1

Fig. S2

Fig. S3

Table S1

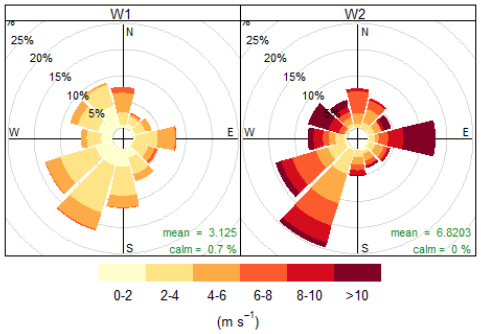

Fig. S1 Frequency of counts by wind direction (%) in June 2016 and distribution of average windspeeds in m s^{-1}

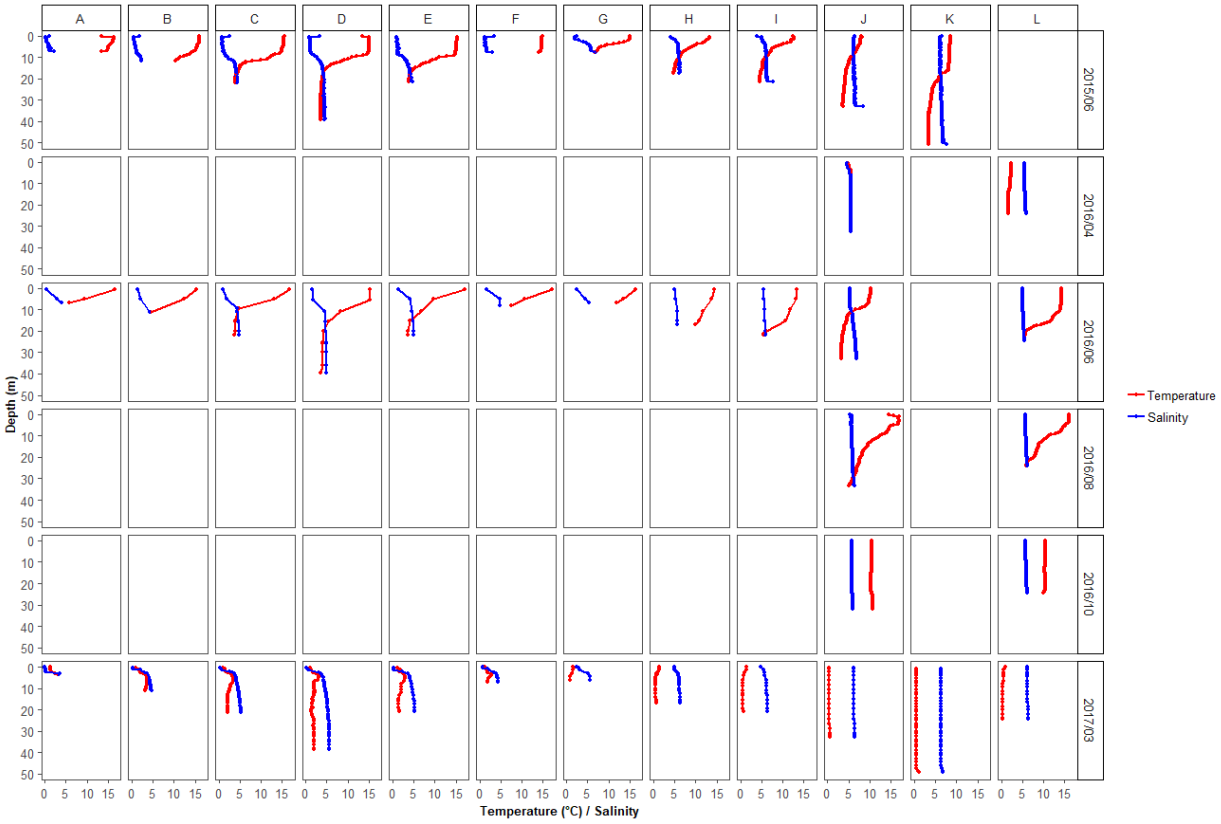

Fig. S2 Salinity and temperature profiles of all sites measured with hand-held CTD devices

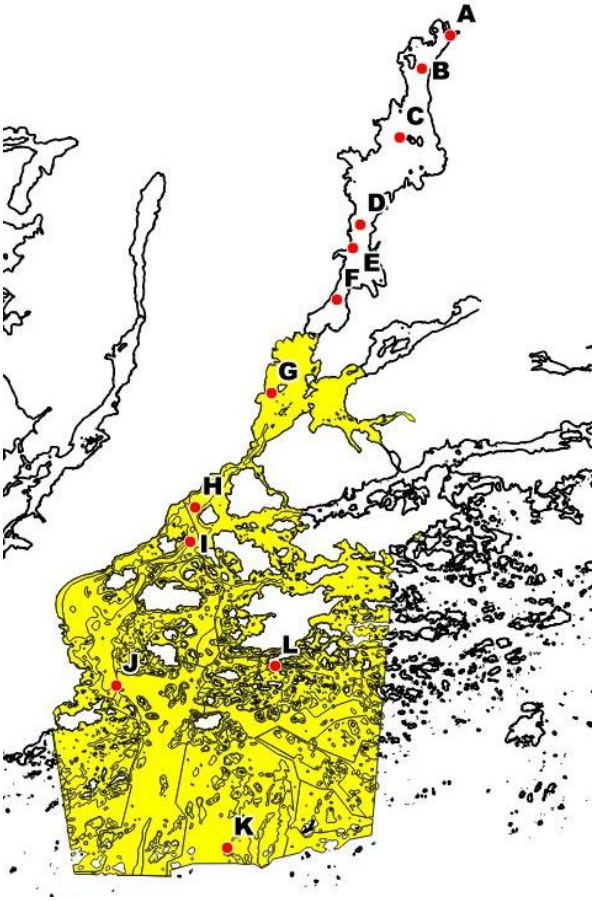

Fig. S3 Map of the area used for calculating the budget for the archipelago in Fig 7

Table S1 The parameters, their values and derivations used in calculation of the budget in Fig 7

Parameter	Value	Unit	Variable	Source / Derivation
Estuary surface volume	147.0	10^{-6} m^3	*V(surf)*	Virta 1977[1]
Estuary bottom water volume	86.2	10^{-6} m^3	*V(bot)*	Virta 1977[1]
Estuary area	21.8	10^{-6} m^2	*A(est)*	Virta 1977[1]
Estuary pycnocline area (~10 m depth)	9.2	10^{-6} m^2	*A(pyc)*	Virta 1977[1]
Estuary methanogenic bottom area (>10 m depth)	9.2	10^{-6} m^2	*A(bot_est)*	Virta 1977[1]
River mean June discharge 2015-2016	7.06	m^3 s^{-1}	*Q*	Finnish Environment Institute
Lowest monthly discharge 2015-2016	2.43	m^3 s^{-1}	*Q(min)*	Finnish Environment Institute
Highest monthly discharge 2015-2016	17.21	m^3 s^{-1}	*Q(max)*	Finnish Environment Institute
Diffuse flow multiplier	1.11		*d*	Stipa 1999[2]
River mouth mean CH_4 concentration	557	nmol L^{-1}	*c(riv)*	Measured June 2015 & 2016
Lowest CH_4 concentration measured at river mouth	199	nmol L^{-1}	*c(riv_min)*	Measured 2015-2017
Highest CH_4 concentration measured at river mouth	1666.1	nmol L^{-1}	*c(riv_max)*	Measured 2015-2017
Total river input	373.7	mol d^{-1}	*J(riv)*	*J(riv) = Q x d x c(riv)*
Minimum total river input	46.0	mol d^{-1}	*J(riv_min)*	*J(riv_min) = Q(min) x d x c(riv_min)*
Maximum total river input	2725.1	mol d^{-1}	*J(riv_max)*	*J(riv_max) = Q(max) x d x c(riv_max)*
Mean atmospheric flux of CH_4 in the estuary	-0.3	mmol m^2 d^{-1}	*F(atm_est)*	Calculated*
Low atmospheric flux	-0.1	mmol m^2 d^{-1}	*F(atm_est_min)*	Calculated†
High atmospheric flux	-0.6	mmol m^2 d^{-1}	*F(atm_est_max)*	Calculated†
Total estuary atmospheric CH_4 flux	-5589.3	mol d^{-1}	*J(atm_est)*	*J(atm_est) = A(est) x F(atm_est)*
Minimum total atmospheric flux	-2548.0	mol d^{-1}	*J(atm_est_min)*	*J(atm_est_min) = A(est) x F(atm_est_min)*
Maximum total atmospheric flux	-12285.9	mol d^{-1}	*J(atm_est_max)*	*J(atm_est_max) = A(est) x F(atm_est_max)*
Mean pycnocline diffusive CH_4 flux 2015–2016	0.00005	mmol m^2 d^{-1}	*F(pyc)*	Calculated*
Lowest calculated pycnocline flux 2015–2016	0.00001	mmol m^2 d^{-1}	*F(pyc_min)*	Calculated†
Highest calculated pycnocline flux 2015–2016	0.00014	mmol m^2 d^{-1}	*F(pyc_max)*	Calculated†
Total pycnocline CH_4 flux	0.5	mol d^{-1}	*J(pyc)*	*J(pyc) = A(pyc) x F(pyc)*
Minimum total pycnocline flux	0.1	mol d^{-1}	*J(pyc_min)*	*J(pyc_min) = A(pyc) x F(pyc_min)*
Maximum total pycnocline flux	1.4	mol d^{-1}	*J(pyc_max)*	*J(pyc_max) = A(pyc) x F(pyc_max)*

Mean sediment to water CH_4 flux 2016	-0.6	mmol m^2 d^{-1}	*F(sed_est)*	Calculated*
Lowest calculated sediment flux 2016	0.0	mmol m^2 d^{-1}	*F(sed_est_min)*	Calculated†
Highest calculated sediment flux 2016	-0.9	mmol m^2 d^{-1}	*F(sed_est_max)*	Calculated†
Total sediment CH_4 flux	-5233.9	mol d^{-1}	*J(sed_est)*	*J(sed_est) = A(bot_est) x F(sed_est)*
Minimum total sediment flux	-284.6	mol d^{-1}	*J(sed_est_min)*	*J(sed_est_min) = A(bot_est) x F(sed_est_min)*
Maximum total sediment flux	-8092.9	mol d^{-1}	*J(sed_est_max)*	*J(sed_est_max) = A(bot_est) x F(sed_est_max)*
Mean water CH_4 concentration at sill	80.0	mol d^{-1}	*c(sill)*	Measured June 2015 & 2016
Mean - 1SD concentration at sill 2015–2016	64.4	nmol L^{-1}	*c(sill_min)*	Measured June 2015 & 2016
Mean + 1SD concentration at sill 2015–2016	96.5	nmol L^{-1}	*c(sill_max)*	Measured June 2015 & 2016
Total CH_4 outflow removal	-48.8	mol d^{-1}	*J(out)*	*J(out) = Q x d x c(sill)*
Minimum total outflow removal	-13.5	mol d^{-1}	*J(out_min)*	*J(out_min) = Q(min) x d x c(sill_min)*
Maximum total outflow removal	-143.5	mol d^{-1}	*J(out_max)*	*J(out_max) = Q(max) x d x c(sill_max)*
Mean estuary surface water CH_4 concentration	87.4	nmol L^{-1}	*c(surf)*	Measured June 2015 & 2016
Mean - 1SD estuary surface water CH_4	23.5	nmol L^{-1}	*c(surf_min)*	Measured June 2015 & 2016
Mean + 1SD estuary surface water CH_4	151.3	nmol L^{-1}	*c(surf_max)*	Measured June 2015 & 2016
Mean estuary bottom water CH_4 concentration	48.8	nmol L^{-1}	*c(bot)*	Measured June 2015 & 2016
Mean - 1SD estuary bottom water CH_4	19.2	nmol L^{-1}	*c(bot_min)*	Measured June 2015 & 2016
Mean + 1SD estuary bottom water CH_4	78.5	nmol L^{-1}	*c(bot_max)*	Measured June 2015 & 2016
Estuary surface water CH_4 pool	12852.7	mol	*C(surf)*	*C(surf) = V(surf) x c(surf)*
Estuary surface water CH_4 minimum pool	3461.2	mol	*C(surf_min)*	*C(surf_min) = V(surf) x c(surf_min)*
Estuary surface water CH_4 maximum pool	22244.3	mol	*C(surf_max)*	*C(surf_max) = V(surf) x c(surf_max)*
Estuary bottom water CH_4 pool	4209.5	mol	*C(bot)*	*C(bot) = V(surf) x c(bot)*
Estuary bottom water CH_4 minimum pool	1654.4	mol	*C(bot_min)*	*C(bot_min) = V(surf) x c(bot_min)*
Estuary bottom water CH_4 maximum pool	6764.6	mol	*C(bot_max)*	*C(bot_max) = V(surf) x c(bot_max)*
Archipelago volume	2414.6	10^{-6} m^3	*V(arc)*	GIS (Fig. S3)
Archipelago area	165.5	10^{-6} m^2	*A(arc)*	GIS (Fig. S3)
Archipelago methanogenic bottom area	100.1	10^{-6} m^2	*A(bot_arc)*	GIS (Fig. S3)
Mean atmospheric flux of CH_4 in the archipelago	0.3	mmol m^2 d^{-1}	*F(atm_arc)*	Calculated*
Lowest atmospheric flux of CH_4 in the archipelago	0.1	mmol m^2 d^{-1}	*F(atm_arc_min)*	Calculated†

Highest atmospheric flux of CH_4 in the archipelago	0.8	mmol m^2 d^{-1}	*F(atm_arc_min)*	Calculated†
Total archipelago atmospheric CH_4 flux	45778.2	mol d^{-1}	*J(atm_arc)*	*J(atm_arc) = A(arc) x F(atm_arc)*
Minimum total archipelago atmospheric flux	17162.6	mol d^{-1}	*J(atm_arc_min)*	*J(atm_arc_min) = A(arc) x F(atm_arc)*
Maximum total archipelago atmospheric flux	124326.2	mol d^{-1}	*J(atm_arc_max)*	*J(atm_arc_min) = A(arc) x F(atm_arc)*
Mean archipelago sediment CH_4 flux	-1.5	mmol m^2 d^{-1}	*F(sed_arc)*	Calculated*
Lowest calculated archipelago sediment flux	-0.1	mmol m^2 d^{-1}	*F(sed_arc_min)*	Calculated†
Highest calculated archipelago sediment flux	-6.2	mmol m^2 d^{-1}	*F(sed_arc_min)*	Calculated†
Total archipelago sediment CH_4 flux	-148082	mol d^{-1}	*J(sed_arc)*	*J(sed_arc) = A(arc) x F(sed_arc)*
Minimum total archipelago sediment flux	-6033.6	mol d^{-1}	*J(sed_arc_min)*	*J(sed_arc_min) = A(arc) x F(sed_arc)*
Maximum total archipelago sediment flux	-623111	mol d^{-1}	*J(sed_arc_max)*	*J(sed_arc_min) = A(arc) x F(sed_arc)*
Archipelago mean water CH_4 concentration	71.6	nmol L^{-1}	*c(arc)*	Measured June 2015 & 2016
Mean - 1SD archipelago water CH_4	23.7	nmol L^{-1}	*c(arc_min)*	Measured June 2015 & 2016
Mean + 1SD archipelago water CH_4	119.5	nmol L^{-1}	*c(arc_max)*	Measured June 2015 & 2016
Total archipelago CH_4 pool	172885.2	mol	*C(arc)*	*C(arc) = V(arc) x C(arc)*
Minimum total archipelago CH_4 pool	57261.5	mol	*C(arc_min)*	*C(arc_min) = V(arc) x C(arc_min)*
Maximum total archipelago CH_4 pool	288508.9	mol	*C(arc_max)*	*C(arc_max) = V(arc) x C(arc_max)*

[1] Niemi, Å. 1977. Hydrography and oxygen fluctuations in Pojoviken, southern Coast of Finland, 1972-1975. *Meri* 4: 23–35.

[2] Stipa, Tapani. 1999. Water exchange and mixing in a semi-enclosed coastal basin (Pohja Bay). *Boreal Environment Research* 4: 307–317.

Note on the calculations:

* Atmospheric fluxes were calculated using Eq. 6 in the main text. The estuary and archipelago areas were subdivided latitudinally between the sampling stations in GIS software and the areas were used as weights in calculating a single weighted average flux from the point values shown in Fig. 4 of the main text. Sedimentary fluxes were calculated with Eq. 1 using the similar area weights as the atmospheric fluxes, except applied only to water areas deeper than 10 m. Hence, sediment flux calculations do not account for shallower than 10 m depth methanogenesis, riparian inputs or diffuse flow in the archipelago. Mean pycnocline diffusive flux was calculated using eq. 1 without porosity, i.e. $J = -D_s \frac{\partial C}{\partial x}$, where ∂C is the average concentration difference between concentrations

immediately above and below the steepest temperature gradient at sites C, D and E (i.e. the only sites with a properly defined thermocline in June 2016, Fig. S2).

† The minimum and maximum values for atmospheric fluxes were calculated as described above, with the exception that the flux point values used were the +/-1 SD monthly wind speed fluxes presented in Fig. 4 (i.e. the upper and lower limits of the grey bands). For sediment and pycnocline fluxes, minimum and maximum absolute values across all sites during the period reported in Table S1 were used.

Paper III

III

Jukka-Pekka Myllykangas, Antti J. Rissanen, Susanna Hietanen, and Tom Jilbert

Influence of electron acceptor availability and microbial community structure on sedimentary methane in oxidation in a boreal estuary

In *Biogeochemistry*,
Volume 148, issue 3, 2020, pages 291–309.

Biogeochemistry (2020) 148:291–309
https://doi.org/10.1007/s10533-020-00660-z

Influence of electron acceptor availability and microbial community structure on sedimentary methane oxidation in a boreal estuary

Jukka-Pekka Myllykangas · Antti J. Rissanen · Susanna Hietanen · Tom Jilbert

Received: 1 October 2019 / Accepted: 27 March 2020 / Published online: 6 April 2020

Abstract Methane is produced microbially in vast quantities in sediments throughout the world's oceans. However, anaerobic oxidation of methane (AOM) provides a near-quantitative sink for the produced methane and is primarily responsible for preventing methane emissions from the oceans to the atmosphere. AOM is a complex microbial process that involves several different microbial groups and metabolic pathways. The role of different electron acceptors in AOM has been studied for decades, yet large uncertainties remain, especially in terms of understanding the processes in natural settings. This study reports whole-core incubation methane oxidation rates along an estuarine gradient ranging from near fresh water to brackish conditions, and investigates the potential role of different electron acceptors in AOM. Microbial community structure involved in different methane processes is also studied in the same estuarine system using high throughput sequencing tools. Methane oxidation in the sediments was active in three distinct depth layers throughout the studied transect, with total oxidation rates increasing seawards. We find extensive evidence of non-sulphate AOM throughout the transect. The highest absolute AOM rates were observed below the sulphate-methane transition zone (SMTZ), strongly implicating the role of alternative electron acceptors (most likely iron and manganese oxides). However, oxidation rates were ultimately limited by methane availability. ANME-2a/b were the most abundant microbial phyla associated with AOM throughout the study sites, followed by ANME-2d in much lower abundances. Similarly to oxidation rates, highest abundances of microbial groups commonly associated with AOM were found well below the SMTZ, further reinforcing the importance of non-sulphate AOM in this system.

Keywords Baltic sea · Methanotrophy · Radiotracer incubation · High throughput sequencing · 16S rRNA gene

Responsible Editor: R. Kelman Wieder

Electronic supplementary material The online version of this article (https://doi.org/10.1007/s10533-020-00660-z) contains supplementary material, which is available to authorized users.

J.-P. Myllykangas (✉) · S. Hietanen · T. Jilbert
Ecosystems and Environment Research Program, Faculty of Biological and Environmental Sciences, University of Helsinki, P.O. Box 65, 00014 Helsinki, Finland
e-mail: jukka-pekka.myllykangas@helsinki.fi

J.-P. Myllykangas · S. Hietanen · T. Jilbert
Tvärminne Zoological Station, University of Helsinki, J.A. Palménintie 260, 10900 Hanko, Finland

A. J. Rissanen
Bio and Circular Economy Research Group, Faculty of Engineering and Natural Sciences, Tampere University, Korkeakoulunkatu 10, 33720 Tampere, Finland

Introduction

Methane (CH_4) is a powerful greenhouse gas affecting the global climate. Its atmospheric concentrations have more than doubled since the industrial revolution, due to anthropogenic activities (IPCC 2014). In aquatic systems, production of CH_4 primarily takes place in sediments through methanogenesis, which is the final step in anaerobic breakdown of organic matter that occurs when other electron acceptors (EA) have been depleted and carbon dioxide (CO_2) is the only viable electron acceptor remaining (Thauer 1998). The exact sediment depth of the primary methanogenic zone depends on the organic matter loading of the system, spanning from a few centimeters in productive coastal systems to several meters in the oligotrophic open ocean seabed (Jørgensen et al. 2001). Methanogenesis is also typically more active in freshwater sediments than in marine sediments, due to the presence of sulphate (SO_4^{2-}) in seawater (Capone and Kiene 1988), which provides a more energetically favorable pathway for anaerobic remineralization. Eutrophication is expected to increase methanogenesis globally due to enhanced carbon loading (Beaulieu et al. 2019).

Although CH_4 is produced in sediments in large quantities, as a highly reduced compound it is susceptible to microbial oxidation. These oxidative processes create a "filter" which prevent CH_4 from escaping to the atmosphere (Knittel and Boetius 2009). In aquatic systems, CH_4 is oxidized through both oxic and anoxic processes. Of these, aerobic oxidation of methane (MOX) is typically more prevalent in fresh waters (de Angelis and Scranton 1993). It is typically most prominent at steep oxyclines, such as the pycnocline of a stratified water column (Schmale et al. 2010; Jakobs et al. 2013) or the sediment–water interface (Fenchel et al. 1995).

Unlike MOX, anaerobic oxidation of methane (AOM) tends to be more efficient at higher salinities, due to increased availability of SO_4^{2-} in seawater (Knittel and Boetius 2009). Of these two processes, AOM is thus the major sink of CH_4 in marine systems, though extreme variability in process rates exists. Globally, AOM has been shown to be a near-quantitative sink for CH_4 produced by sedimentary methanogenesis (Egger et al. 2018). It was originally thought that due to its SO_4^{2-}-dependence, AOM is an exclusively marine process, but it has since been shown to be active also in lakes (Eller et al. 2005; Sivan et al. 2011; Martinez-Cruz et al. 2018).

SO_4^{2-} mediated AOM (S-AOM) is mainly performed by anaerobic methanotrophic (ANME) archaea with sulfate reducing bacteria (SRB) via direct interspecies electron transfer (McGlynn et al. 2015). It is the most important AOM reaction in marine systems (Knittel and Boetius 2009) and the stoichiometry has been formulated as follows (Hoehler et al. 1994):

$$CH_4 + SO_4^{2-} \rightarrow HS^- + HCO_3^- + H_2O$$

It has later been established that at least nitrite/nitrate (Ettwig et al. 2010; Timmers et al. 2017), as well as oxides of iron (Fe, Egger et al. 2015; Ettwig et al. 2016) and manganese (Mn, Beal et al. 2009) can also be used as alternatives to SO_4^{2-} as terminal electron acceptors by the different ANME clades.

Iron mediated AOM (Fe-AOM):

$$CH_4 + 8\,Fe(OH)_3 + 15\,H^+ \rightarrow HCO_3^- + 8\,Fe^{2+} + 21\,H_2O$$

Manganese mediated AOM (Mn-AOM):

$$CH_4 + 4\,MnO_2 + 7\,H^+ \rightarrow HCO_3^- + 4\,Mn^{2+} + 5\,H_2O$$

Fe-AOM requires the concurrent presence of CH_4 and reducible iron (i.e. $Fe(OH)_3$) below the sulphate-methane transition zone (SMTZ). This is possible either under sedimentation regimes with high $Fe(OH)_3$ deposition or recent shoaling of the SMTZ due to carbon loading, both of which are typical in eutrophied coastal systems (Rooze et al. 2016; Jilbert et al. 2018). Most microbes capable of Fe reduction can also reduce Mn and may do so preferentially due to the higher energy yield of the process (Lovley and Phillips 1988). Beal et al. (2009) showed that though Mn-AOM exhibits slower process rates compared to SO_4^{2-}-AOM, energetically Mn-AOM can be up to 10 times more favorable. Mn-AOM and Fe-AOM will be collectively referred to as Me-AOM henceforth in this paper.

Many methanotrophic archaea are capable of AOM. These have been divided into three main groups and a number of subclusters: ANME-1 (subgroups a and b), ANME-2 (subgroups a, b, c and d, of which the two latter are distinct from the two former, and also from each other) and ANME-3 (Haroon et al. 2013; Ettwig et al. 2016; Timmers et al. 2017). Outside the ANME, a group of bacteria called *Candidatus* Methylomirablis

(in phylum NC10) are capable of AOM (Ettwig et al. 2010). It has been suggested that the main biochemical pathway of CH_4 oxidation in ANME is the enzymatic reversal of methanogenesis (McGlynn 2017). However, complexity arises from the fact that several of the ANME clades have been shown to have the capacity also for methanogenesis (Ding et al. 2016).

Understanding AOM, and the role of different compounds as electron acceptors is important, not only because of the global warming potential of CH_4, but also because of the influence of AOM on other biogeochemical cycles, such as those of phosphorus (P), sulphur (S), Fe and Mn. As an example, Fe-AOM and Mn-AOM could potentially lead to increases in sediment release and subsequent lateral transfer ("shuttling") of Fe, Mn and P from the coastal zone to offshore regions in systems such as the Baltic Sea (Jilbert and Slomp 2013; Reed et al. 2016; Rooze et al. 2016). In this study our aim was to investigate the factors controlling sedimentary AOM rates along an estuarine gradient in the northern Baltic Sea. To do this, we conducted full-core incubations on sediments from three sites in the estuary, spanning large vertical and lateral gradients in potential electron acceptor availability, thus allowing us to investigate the influence of electron acceptors on methane oxidation rates. In addition to the oxidation rate measurements, we make use of sediment microbial community compositional data from a parallel study in the same estuarine system, in order to investigate the key microbial groups involved in CH_4 cycling. We hypothesize that the estuarine gradient is characterized by increasing availability of sulfate offshore, and that this in turn determines the depth of the SMTZ and vertical distribution of methane oxidation zones and related microbial communities in the sediments.

Materials and methods

Study area

Samples were collected along a transect in the Pojo Bay estuary, located in Southwestern Finland, from four sites: A, C, D and J (Fig. 1). The non-sequential lettering for the sites is used to maintain compatibility with a companion paper detailing the wider CH_4 dynamics in the same system (Myllykangas et al. 2020). The sites span a water column salinity gradient of 0–7.

Site A is located in the river mouth of River Karjaa, which is the primary freshwater source of the estuary. Site A is permanently oxic, with bottom water salinity 0–2, and receives organic carbon of primarily terrestrial origin (Jilbert et al. 2018). Due to its proximity to rivermouth flocculation of Fe, from both natural and anthropogenic sources, site A also has strongly elevated concentrations of Fe in the sediments (up to 10–20% by weight). Approximately half of the sedimentary Fe is expected to be in reducible oxide forms as determined by sequential extraction (Jilbert et al. 2018).

Sites C and D are in the main depression of the inner bay (bottom water salinity 3–5), which is separated from the connecting archipelago by a narrow sill close to the city of Ekenäs. These sites experience seasonal hypoxia and sediment focusing, and are subject to relatively intense carbon accumulation from both terrestrial and phytoplankton sources (Jilbert et al. 2018). These sites have intermediate sedimentary Fe concentrations, but are strongly enriched in Mn due to redox shuttling of Mn-oxides during seasonal hypoxia in the inner bay (Tiihonen 2016).

Site J is seawards in the archipelago (bottom water salinity 6–7) along the main channel of the estuary. It is typically fully oxic and receives primarily phytoplankton-derived organic carbon (Jilbert et al. 2018). The sediments contain lower concentrations of Fe and Mn than those at sites A, C and D, but concentrations are nevertheless significantly elevated (e.g. Fe = 6–7%) with respect to sites offshore in the Baltic Sea (Jilbert et al. 2018).

In coastal sediments of the Gulf of Finland generally, bioturbation is known to be important at oxic sites but restricted at sites showing seasonal hypoxia (Gammal et al. 2017; Kauppi et al. 2018). Hence, of our sites, A and J are expected to show intense bioturbation, while sites C and D are expected to be relatively undisturbed by benthic fauna.

Sediment sampling for incubation experiments and pore water profiling

Sediment was retrieved using a GEMAX^{TM}—twin corer in August 2017 from sites A, C, and J on board R/V *Saduria*. Four acrylic minicores (26 ID × 400 mm) were taken from each site for incubation (three replicates and one control). During transport, minicores were capped from both ends and stored upright submersed in site bottom water at in situ temperature.

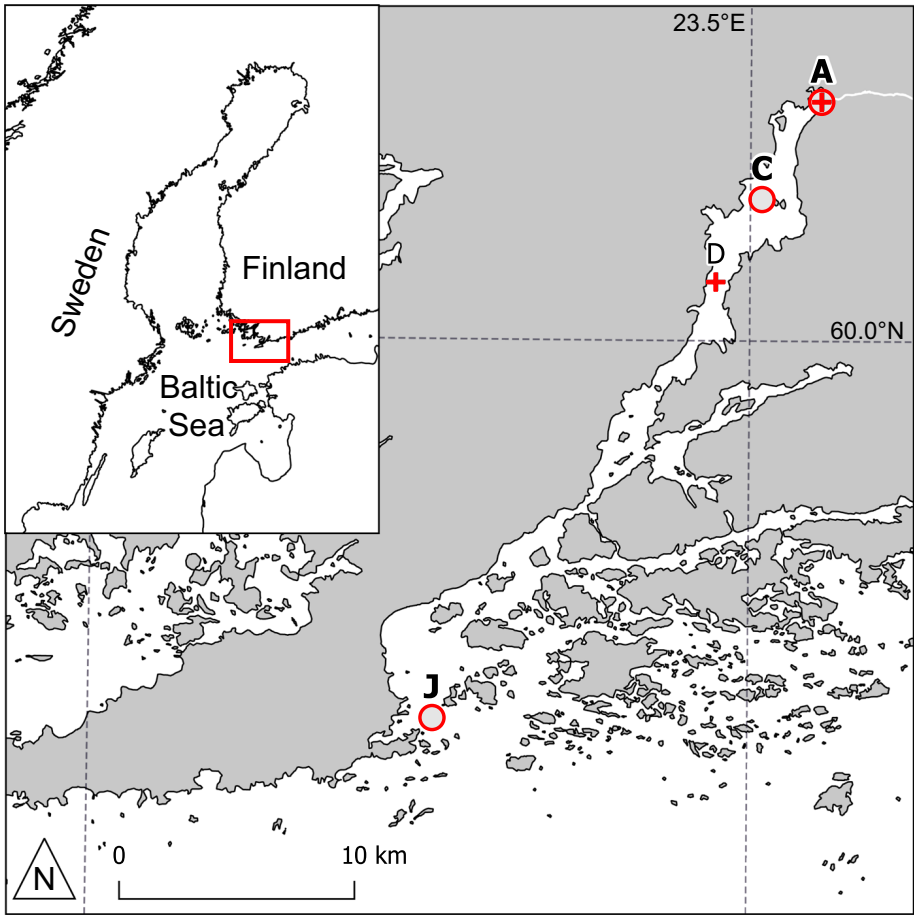

Fig. 1 Map of the Pojo Bay estuary and the connected archipelago. Sites A and D (cross) were sampled for microbial data, sites A, C and J (circle) for oxidation rate

Samples for vertical porewater CH_4 profiles were measured from a parallel core directly following retrieval. 10 ml of wet sediment was extracted at 2.5 cm intervals using cutoff plastic syringes. Sediment was immediately transferred into 65 mL glass bottles pre-loaded with supersaturated NaCl solution, which were immediately capped with butyl rubber septa and screw caps and stored upside down. Within 24 h, 10 mL of N_2 headspace was injected by needle through the stopper, and an equivalent volume of sediment slurry removed through a second needle. After equilibration, two 1 mL subsamples of the headspace were analyzed with a gas chromatograph equipped with a flame ionization detector (Agilent Technologies 7890B). Sediment volume in the original sample was calculated from complementary porosity profiles.

One additional GEMAX-core was retrieved per site and sampled at 1 cm intervals with Rhizons™ for porewater extraction and later analyzed for Fe, Mn, S and Ca with inductively coupled plasma—optical emission spectrometry (ICP-OES). The samples were acidified with 10 µL of 65% HNO_3 per mL of porewater in order to keep metals in solution. ICP-OES-derived S is interpreted to represent SO_4^{2-}, since H_2S is lost upon the addition of HNO_3. The analyzed metals are interpreted to be present as divalent ions. For full details see Jilbert et al. (2018).

Determination of methane oxidation rates

Incubation

Each of the minicores was pre-drilled with holes at 1 cm intervals on the side. The holes were plugged with silicone and taped from both sides with water resistant tape. In the lab, a 25 µL of 0.25 KBq activity $^{14}CH_4$ (Biotrend Chemikalien) label (2.26 nmol)

dissolved in oxygen-free artificial seawater was injected into the cores through the side ports with a gastight glass syringe (Hamilton). The needle was first pushed through the core horizontally and then simultaneously withdrawn during the injection, in order to ensure even distribution of the tracer. The cores were incubated without top caps in a temperature-controlled water bath at in situ temperature for 24 h.

The incubation was stopped and microbial activity was halted by sectioning the cores at 2 cm intervals (total volume per slice approximately 11 cm^3) and funneling the slices into pre-weighed 100 mL glass bottles containing 40 mL of 2.5% NaOH. Following the NaOH addition, pH in the slurry was consistently > 12, ensuring that all DIC in the slurry was present as carbonate (CO_3^{2-}). The bottles were immediately closed with a septum cap (PFTA, 5 mm) and stored upside down.

Analysis

The total amount of CH_4 in the samples after incubation and storage was calculated from a 1 mL subsample taken from the headspace through the septum cap, which was subsequently analyzed with a gas chromatograph equipped with a flame ionization detector (Agilent Technologies 7890B). To capture residual $^{14}CH_4$ tracer not converted to $^{14}CO_2$ during incubation, the headspace of samples was purged with synthetic air through a glass tube containing copper oxide and combusted in a tube oven at 850 °C. The combusted $^{14}CO_2$ was trapped in a 20 mL scintillation vial containing 10 mL of CO_2-absorbant (2-phenylethylamine and 2-methoxyethanol, 1:7 v/v). After 15 min of purging, 10 mL of Ultima Gold™ scintillation cocktail (Perkin Elmer) was added and samples were subsequently analyzed using a liquid scintillation counter (Wallac® 1415). The bottles were weighed again to assess total sediment volume of each sample.

Following combustion, the slurry jars were left uncapped for 10 min to allow all residual CH_4 to escape. Subsequently, a 20 mL glass scintillation vial containing CO_2-absorbant (6 mL of 0.5 M NaOH and 2-phynyethylamine solution, 1:1 v/v) was gently inserted into the sediment slurry bottle. The slurry was then acidified with 12 mL of 6 M HCl injected to the bottom of the slurry and capped rapidly. The acidification procedure lowered the pH of the slurry to < 1, which caused the release of all DIC in the slurry as CO_2, which was subsequently trapped in the amine solution in the headspace. After 12 h under gentle magnetic stirring, the scintillation vials were removed and wiped thoroughly with ethanol, after which 10 mL of scintillation liquid was added, and the samples were analyzed for $^{14}CO_2$ with a liquid scintillation counter.

Controls

One full minicore from each site was dedicated as a control and treated the same way as the replicates, except that the tracer was added only after the core had been sliced and fixed in NaOH. Controls were analyzed from five different depths from each site. The volume of injected tracer was identical to that during the sample incubations.

Rate calculations

In situ rates of AOM were calculated from the fraction of produced $^{14}CO_2$ in the total ^{14}C pool using Eq. 1 (modified from Treude et al. 2005):

$$AOM = \frac{^{14}CO_2 \times CH_4}{(^{14}CH_4 + ^{14}CO_2) \times t \times v} \quad (1)$$

where $^{14}CO_2$ and $^{14}CH_4$ are the activities (disintegrations per minute, DPM) of microbially produced CO_2 during incubation and the activity of the injected CH_4 not incorporated into CO_2, respectively, CH_4 is the total amount of CH_4 in the sample in nmol at time zero, t is the incubation time in days and v volume of slices in cm^3. Average of DPM values from the blanks were subtracted from the $^{14}CO_2$ values, and only samples with activity more than 3 × SD of the blanks were considered active. The DPM values of $^{14}CH_4$were corrected with the ratio between T_0 and post-incubation CH_4 concentrations to account for losses of CH_4 during storage, which are assumed to occur at the same rate for both $^{14}CH_4$ and $^{12}CH_4$ (Treude et al. 2005). Total ^{14}C label recovered in both combustion and acidification steps was 85–95%.

Depth-integrated oxidation rates were calculated from the mean oxidation rates between 0 and 31 cm depths utilizing the trapezoid rule:

$$\int_{31\text{cm}}^{0\text{cm}} f(x)dx \approx \frac{1}{2}\sum_{k=1}^{N}(x_{k+1}-x_k)(f(x_{k+1})+f(x_k)) \quad (2)$$

where $f(x)$ is oxidation rate in mmol m^{-3} day^{-1}, x is the sediment depth zone in cm.

Microbial communities

Analysis of bacterial and archaeal community composition

Samples for community composition analysis were collected in June 2015 from sites A and D with a GEMAX^{TM} corer. This work was carried out as part of a parallel project, and data was made available to the current study. The presence of a well-defined shallow (5–15 cm) SMTZ at all muddy sites in the Pojo Bay system (Myllykangas et al. 2020) facilitates qualitative comparison of the vertical structure of the microbial communities and CH_4 oxidation rates, regardless of spatial offset in sampling locations.

Sediment was sliced at 2.5 cm intervals and stored in 2 mL sterilized plastic vials at − 80 °C. DNA was extracted from frozen sediment samples (200–400 mg) using a previously published protocol based on bead-beating and phenol–chloroform extraction (Griffiths et al. 2000). DNA yields of extractions were determined with Qubit 3.0 Fluorometer and Qubit^{TM} dsDNA HS Assay Kit for DNA (Thermo Fisher Scientific). DNA extractions were stored at −20 °C before sequencing analyses.

PCR of 16S rRNA genes and amplicon sequencing took place commercially at FISABIO (Valencia, Spain; https://fisabio.san.gva.es/en/inicio). For each sample, V3-V4 region of the bacterial and archaeal 16S rRNA genes were simultaneously targeted using primer pair Pro341F (5′-CCTACGGGNBGCASCAG-3′)/Pro805R (5′-GACTACNVGGGTATCTAATCC-3′) (Takahashi et al. 2014). Archaea were also specifically studied from each sample by targeting the V3-V4 region of the archaeal 16S rRNA genes using primer pair 340F (5′-CCCTAYGGGGYGCASCAG-3′)/806R (5′-GGACTACVSGGGTATCTAAT-3′) (Takai and Horikoshi 2000; Gantner et al. 2011). PCR mixtures (total volume of 25 µL) included approximately 25 ng of template DNA, 12 µL of 2 × KAPA HiFi HotStart ReadyMix (KK2602, Roche) and 5 µL of each primer (1 µmol L^{-1}). DNA amplicon libraries were generated using a limited cycle PCR: initial denaturation at 95 °C for 3 min, followed by 25 cycles of annealing (95 °C for 30 s, 55 °C for 30 s, 72 °C for 30 s) extension at 72 °C for 5 min. Thereafter, Illumina sequencing adaptors and dual-index barcodes (Nextera XT index kit v2, FC-131-2001) were added to the amplicons. Libraries were purified with AMPure XP after each amplification. Their DNA content was measured using a Qubit 2.0 Fluorometer and a dsDNA HS Assay Kit (Thermo Fisher). Libraries were normalized and pooled in equal amounts prior to sequencing. The pool containing the indexed amplicons was then loaded onto the MiSeq reagent cartridge v3 (MS-102–3003) and 4 pM of this pool was spiked with 25% PhiX control to improve base calling during sequencing, as recommended by Illumina for amplicon sequencing. Sequencing was conducted using a paired-end 2 × 300 bp cycle run on an Illumina MiSeq sequencing system.

Bioinformatic analyses

Trimming of the raw data (parameters, min_length: 50; trim_qual_right: 30; trim_qual_type: mean; trim_qual_window: 20) was done using prinseq-lite (Schmieder and Edwards 2011). The paired end reads, R1 and R2, from Illumina sequencing were joined using FLASH program applying default parameters (Magoč and Salzberg 2011).

Mothur (Schloss et al. 2009) was used in subsequent sequence analyses. The sequences were aligned using Silva reference alignment (Release 123). Chimeric sequences, identified using UCHIME (Edgar et al. 2011), were removed from each library and a preclustering algorithm (Huse et al. 2010) was used to reduce the effect of sequencing errors. Sequences were assigned taxonomies with a naïve Bayesian classifier (bootstrap cut-off value 75%) (Wang et al. 2007), using the Silva database (Release 128). Thereafter, sequences classified as chloroplast, mitochondria and eukaryota were removed from each library, while in addition, bacterial sequences were removed from the archaeal V3-V4 library (340F/806R).

Sequences were divided into operational taxonomic units (OTUs) at a 97% similarity level. Singleton OTUs (OTUs with only one sequence) were removed, and the data were then normalized by subsampling to the same size, which was 20,755 for prokaryotic (i.e.

bacterial and archaeal) and 63,673 for archaeal libraries. Good´s coverage was over 0.88 and 0.99 in each prokaryotic and archaeal library, respectively, confirming that sequence variation was well covered (data not shown). This study focused specifically on OTUs assigned to known aerobic and anaerobic methanotrophic taxa and on known methanogenic taxa (Nazaries et al. 2013). In addition, as sulfate reducing bacteria are involved in S-AOM and as we also generally wanted to reveal genetic potential for anaerobic sulfate and Fe^{3+} respiration, we also focused on known sulfate and Fe^{3+} reducing taxa (Kuever et al. 2005; Youssef et al. 2009; Kuever 2013; Lovley 2013; Rabus et al. 2013).

Sequence accession numbers

Raw sequencing data has been submitted to National Center for Biotechnology Information's (NCBI) Short Read Archive (SRA) under accession number PRJNA574569.

Results

Porewater biogeochemistry

Profiles of SO_4^{2-} were broadly similar between the three sites (Figs. 2 and 3), though there was a seawards increase in maximum SO_4^{2-} values in the top sediment from 2.9 to 5.0 mmol L^{-1}, from site A to J. Similar to SO_4^{2-}, CH_4 profiles displayed similarity between sites, with key differences (Fig. 3). Lowest concentrations of 0.01 mmol L^{-1} were found at site A surface sediments and highest of 5 mmol L^{-1} at site J below 30 cm depth. At site A, CH_4 was largely absent in the upper sediments, whereas in contrast C was the only site studied with clearly discernible amounts of CH_4 near the sediment–water interface. Overall, CH_4 concentrations displayed a seaward increase, with both absolute concentrations and inventories increasing markedly from site A to J. Site A was the only station that showed a steep decrease in CH_4 concentration below 33 cm depth. All sites display a clear SMTZ, defined as the depth of equal porewater CH_4 and SO_4^{2-} concentrations. The depth of the SMTZ varied between the sites, being located at 13.0, 7.6 and 10.5 cm depth at sites A, C and J, respectively (Fig. 2).

Other biogeochemical parameters were similarly variable between the sites. Porewater Fe concentrations exhibited large variation between the study sites (Fig. 2). Highest concentrations were found at site A, nearest to the river mouth. Surface sediments at site A contained 898 µmol L^{-1} of Fe in porewaters. Concentrations declined rapidly towards the SMTZ, down to 253 µmol L^{-1}, after which they increased again reaching 655 µmol L^{-1} at 24 cm depth. Site C showed a slight elevation of Fe in the surface sediment (169 µmol L^{-1}), but there, too, concentrations decreased rapidly towards the SMTZ and were largely below the detection limit below it. Below 20 cm depth, the iron concentrations started increasing again. Site J Fe concentrations were low throughout, with only a small elevation of 22 and 23 µmol L^{-1} found at 2 cm depth and below 26 cm depth, respectively.

Porewater profiles of Mn were similarly highly variable between sites (Fig. 2). Site A displayed a mostly flat profile, with slightly lower concentrations near the sediment surface, but ca. 50 µmol L^{-1} concentrations throughout the rest of the sediment column. Site C contained a small peak near the sediment surface, followed by a rapid decrease towards the SMTZ, below which Mn increased again, reaching 196 µmol L^{-1} at 30 cm depth. Site J displayed a similar pattern, except that overall the concentrations were lower, reaching only 69 µmol L^{-1} at 30 cm depth, and the increase did not begin until clearly below the SMTZ.

Calcium profiles were included as a proxy for porewater salinity. Accordingly, the average porewater calcium concentrations increased with distance offshore (Fig. 2). At site A, porewater calcium concentration increased slightly with sediment depth from 1593 to 1715 µmol L^{-1}. At site D concentrations varied between 1775 and 2011 µmol L^{-1}, decreasing slightly with depth. At site J, concentrations increased slightly with depth and varied between 2392 to 2656 µmol L^{-1}.

Methane oxidation rates

CH_4 oxidation activity showed clear and distinct vertical zonation at all three sites (Fig. 3). The activity zones could be divided into three layers: 1. surface-sediment (above the SMTZ), 2. close to the SMTZ, and 3. below the SMTZ. CH_4 oxidation in the surface sediment layer was most evident at site C with a rate of

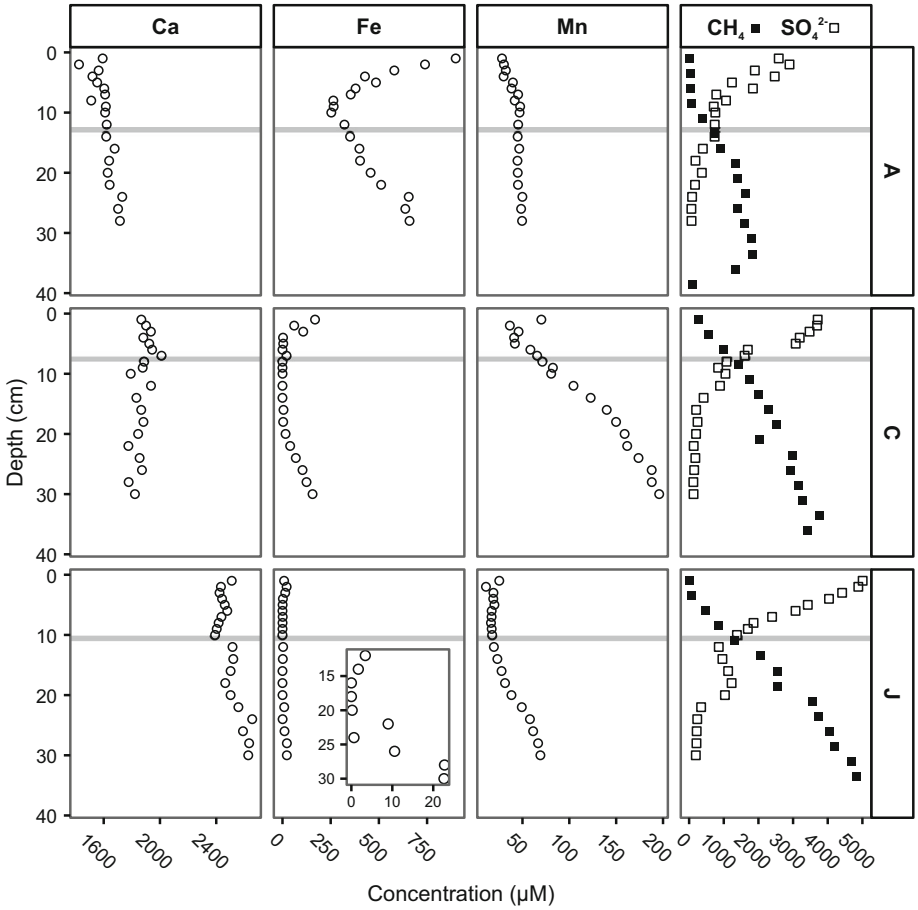

Fig. 2 Porewater chemistry at the different sampling sites. Note the different scales on the x-axes and the inset of the iron concentration at site J. The grey line represents the depth of the SMTZ at each site, defined as the depth of equal CH_4 and SO_4^{2-} concentrations

29.52 ± 7.21 nmol cm^{-3} day^{-1}. Site A featured a distinct peak in oxidation activity between the SMTZ and the sediment surface, while at site J oxidation above the SMTZ was low. Oxidation activity near and around the SMTZ was most evident at site J, with a peak of 32.09 ± 1.69 nmol cm^{-3} day^{-1} found at 11 cm depth, which was also the highest recorded rate throughout the study transect. Site C also featured a very apparent, albeit smaller, increase in oxidation activity near the SMTZ. Clearly elevated oxidation rates were found below the SMTZ at site J, with the highest rate of 13.89 ± 7.34 nmol cm^{-3} day^{-1} found from 31 cm depth. Site A also showed oxidation activity below the SMTZ, though in lesser degree, whereas at site C oxidation rates drop to near zero in the deepest parts of the core. Standard deviation between replicate oxidation rates was 4.1–93.9%, with an average of 33.97%.

To quantify the lateral (between stations) and vertical differences in CH_4 oxidation rates systematically, we divided each profile into three sections of equal thickness, and calculated depth-integrated rates for each. Full-core integrated rates displayed an overall seaward increase from 2.32 to 3.51 mmol m^{-2} day^{-1} from site A to J (Table 1). At site A, the highest integrated oxidation rate of 0.94 mmol m^{-2} day^{-1} was found at the 1–10 cm depth interval, with a decrease in the 11–20 cm depth interval and a slight increase in the deepest section. In contrast, site C displayed a downwards trend in the integrated rates, decreasing from 0.87 mmol m^{-2} day^{-1} in the topmost section, down to 0.46 mmol m^{-2} day^{-1} in the bottom section. While site J featured the lowest integrated rates of the whole study in the surface section (0.38 mmol m^{-2} day^{-1}), in contrast the highest (2.00 mmol m^{-2} day^{-1}) and second highest

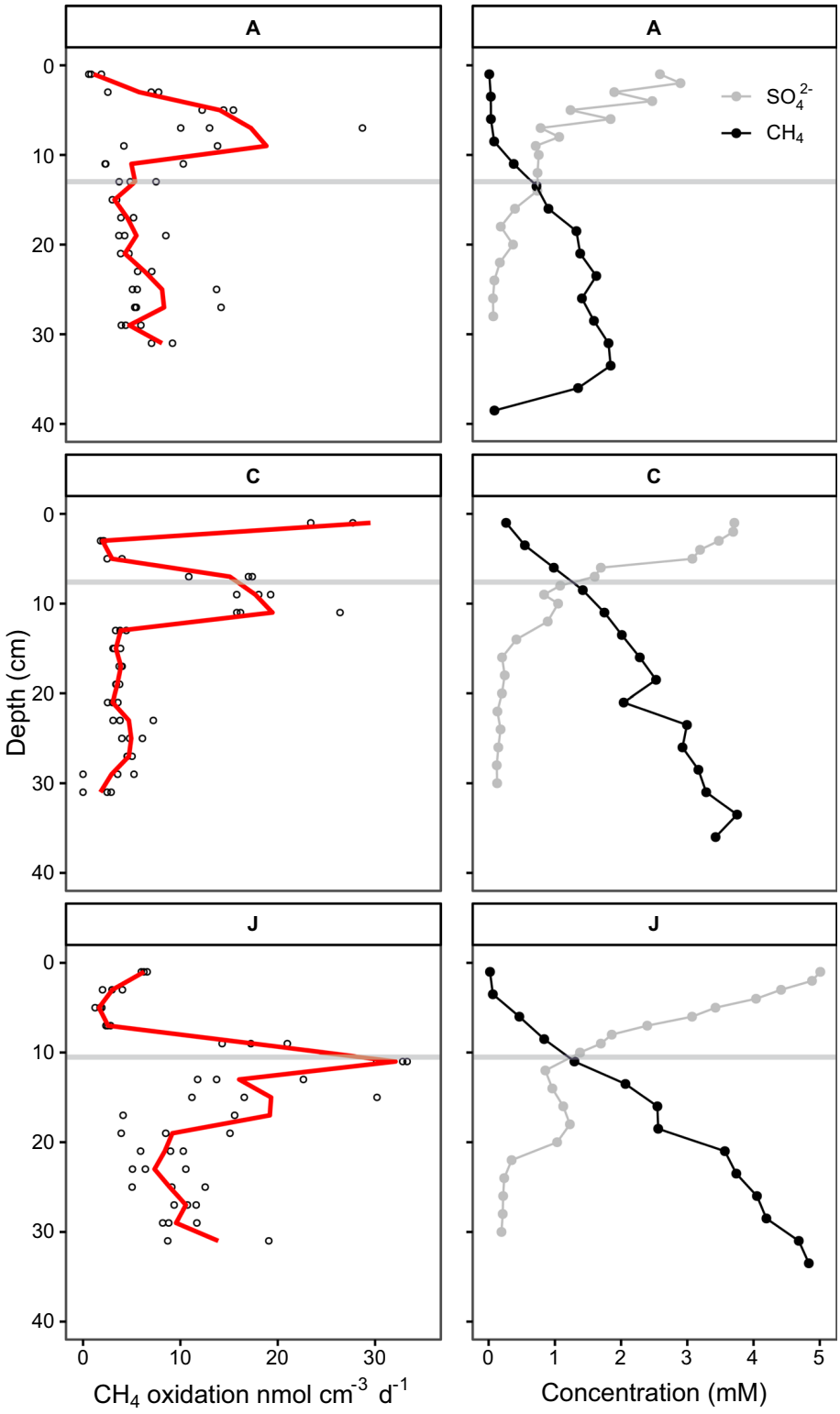

Fig. 3 Vertical sediment profiles of methane oxidation rates from all sites (three replicates per site shown with data points, mean rate at each depth interval shown with the red line), coupled with dissolved porewater CH_4 and SO_4^{2-} concentrations from the same sites. The grey line denotes the depth of the SMTZ, as defined by the depth of equivalent CH_4 and SO_4^{2-} concentration. Note the different x axes

Table 1 Depth integrated oxidation rates for all sites and depth zones in mmol m^{-2} day^{-1}

Depth	A	C	J
1–10 cm	**0.94**	0.87	0.38
11–20 cm	0.61	0.82	**2.00**
21–31 cm	0.77	0.46	**1.13**
Total	2.32	2.16	**3.51**

Highest values of each depth zone across all sites in bold typeface

(1.13 mmol m^{-2} day^{-1}) integrated rates of the whole study were found from the 11–20 cm and 21–31 cm depth zones respectively.

Microbial community structure

A clear vertical structure was observed in the microbial community composition at sites A and D as determined by relative abundances of 16S ribosomal RNA genes (Figs. 4 and 5, Supplementary Figs. 1 and 2). The dominant archaeal taxa in both sites were *Methanomicrobia* and *Thermoplasmata* (within *Euryarchaeota*) as well as *Bathyarcheota*, *Thaumarcheota* and *Woesearcheota* (Supplementary Fig. 1). The bacterial community was more diverse than the archaeal community. The most dominant bacterial taxa in both sites included e.g. *Deltaproteobacteria*, *Gammaproteobacteria* and *Betaproteobacteria* (within *Proteobacteria*) as well as *Bacteroidetes*, *Chloroflexi* and *Verrucomicrobia* (Supplementary Fig. 2). In the following, we report the relative abundance of microbial groups associated with specific CH_4-related processes and with sulfate and Fe^{3+} reduction within this vertical structure, as well as differences between sites A and D. Since the microbial data is derived from cores sampled in June 2015, we report the depth of the SMTZ as determined from these cores by Jilbert et al. (2018), rather than from the 2017 profiles shown in Figs. 2 and 3.

Vertical structure of methane-related as well as sulfate and Fe^{3+} reducing microbial communities

The relative abundances of taxa associated with AOM, MOX and MOG showed a clear vertical zonation at both sites (Fig. 4k–n). MOX-related taxa dominate in the surface sediments, while AOM and MOG taxa became more dominant with increasing depth in the sediment column. The contrasting depth of the SMTZ at these two sites is reflected in the depth of the switch from MOX-to AOM-dominance of the CH_4 oxidizer community, which occurs deeper at site D (Fig. 4m–n). Below the SMTZ, AOM-related groups show a similar abundance to methanogens at site D, while at site A, methanogens dominate over AOM-related groups throughout the deeper sediments (Fig. 4k–l). Putative sulfate and Fe^{3+} reducing bacteria were present all through the sediment columns at both sites (Fig. 5). The vertical variations in the total relative abundance of Fe^{3+} reducers were quite minor at both sites, yet at site A they were highest in the surface above SMTZ and in the bottom layers, while multiple minor peaks in their relative abundance were observed along the sediment column in site D (Fig. 5). In contrast, sulfate reducers had lower relative abundance at the surface layers and at SMTZ than deeper in the sediment column at site A, while at site D they had highest relative abundance at the surface layers above the SMTZ and decreased drastically in deeper layers especially from 30 to 40 cm depth (Fig. 5).

Groups associated with AOM

From the microbial groups commonly associated with AOM, ANME-2a/b was the most abundant at both sites. The relative abundance of ANME-2a/b generally increased with depth in the sediment column (Fig. 4a–d). When reported as a fraction of total prokaryotes, relative abundances of this group were thus highest below the SMTZ at both sites (Fig. 4c–d). This effect was most pronounced at site D, where ANME-2a/b also dominated AOM-related groups (Fig. 4d). At site A, high relative abundances of ANME-2a/b were also observed in the uppermost 10 cm, broadly within the SMTZ at this site (Fig. 4a). ANME-2d contributed an additional important group at site A, with a clear increase below the SMTZ (Fig. 4a, c). At site D, ANME-2d was present in small numbers (0.01–0.32%) in the archaeal community throughout the sediment column (Fig. 4b). ANME-1 was present in even smaller numbers at throughout the sediment column at site A (0.002–0.009% of archaeal 16S rRNA genes) but entirely absent at site D (Fig. 4a-b). *Ca*. Methylomirabilis (*NC10* phylum) was also present in very small numbers (0.002–0.005% of 16S

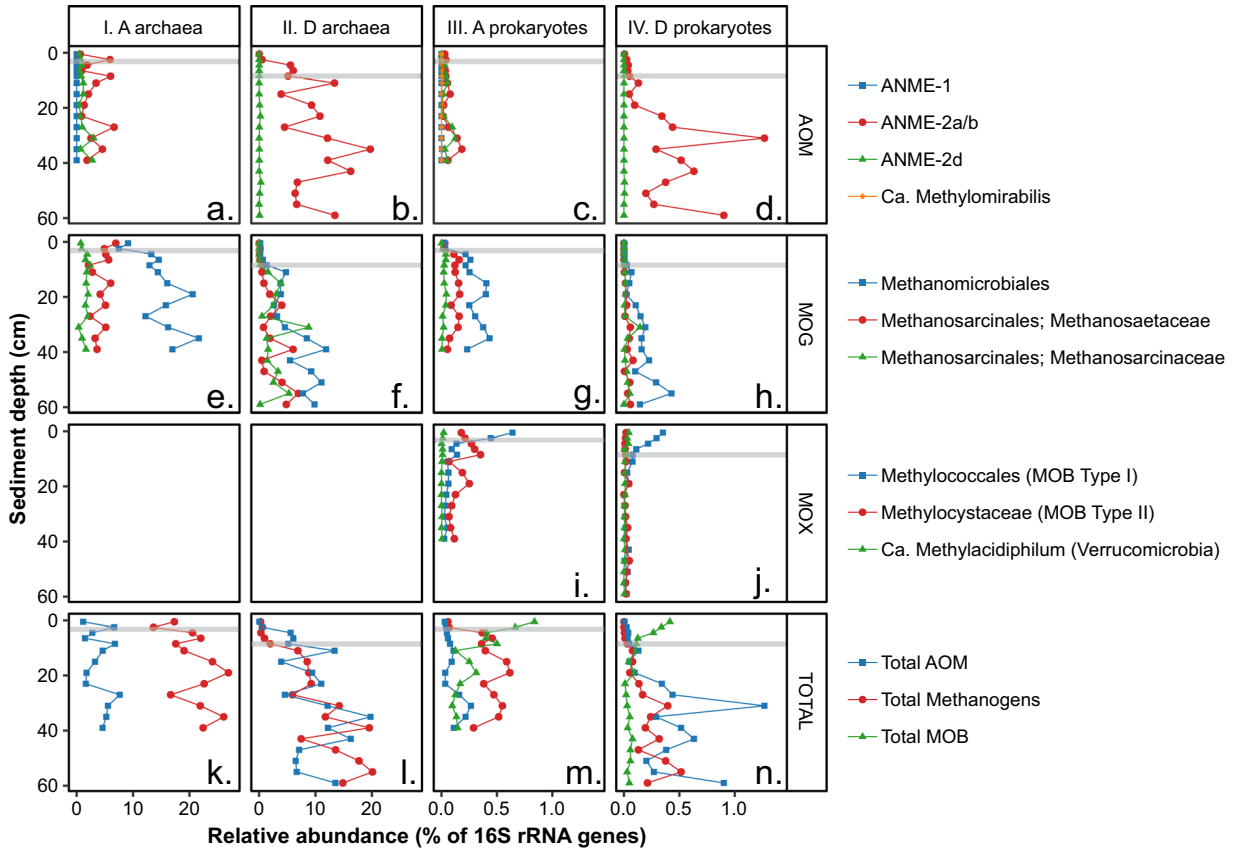

Fig. 4 Relative abundances of different microbial groups (AOM = clades associated with AOM, MOG = clades of methanogens, MOX = clades of bacteria capable of MOX, TOTAL = groups summed up) at sites A and D in June 2015. Note the different scales on the x-axes for archaea (columns I–II) and prokaryotes (III–IV). Abundances of archaea are reported as a fraction of total archaea and abundances of prokaryotes reported as a fraction of total prokaryotes (archaea + bacteria). The grey line represents the depth of the SMTZ in June 2015 (Jilbert et al. 2018)

prokaryotic rRNA genes at 4–12 cm depth) and only at site A, with the highest abundance of 0.010% found from 20 cm depth (Fig. 4c).

Groups associated with MOX

Methylococcales (Type I) were the most abundant group of MOB in surface sediment at both sites, remaining more abundant deeper in the sediment at site A (Fig. 4i). However, their abundance decreased rapidly below the SMTZ. *Methylocystaceae* (Type II) MOB showed two peaks in abundance below the SMTZ at site A, but were largely absent from site D (Fig. 4i-j). MOB belonging to the phylum *Verrucomicrobia*, i.e. *Ca*. Methylacidiphilum sp., were present in small numbers in the surface sediment of both sites.

Groups associated with methanogenesis (MOG)

Methanomicrobiales, *Methanosaetaceae* and *Methanosarcinaceae* were the most abundant methanogen taxa at both sites, while other methanogens, i.e. *Methermicoccaceae*, *Methanobacteria*, *Methanocellales* and *Methanomassiliicoccus* sp. were scarce (Fig. 4). *Methanomicrobiales*, which consisted dominantly of *Methanoregulaceae*, were the most abundant at site A and made up to 20% of all archaea at 35 cm depth (Fig. 4e), while the MOG community at site D was less abundant but more varied in distribution between *Methanomicrobiales*, *Methanosaetaceae* and *Methanosarcinaceae* (Fig. 4f). At both sites, the relative abundance of all the dominant taxa of methanogens generally increased below the SMTZ. However, at site D the largest increase was observed deeper in the sediment column (Fig. 4h).

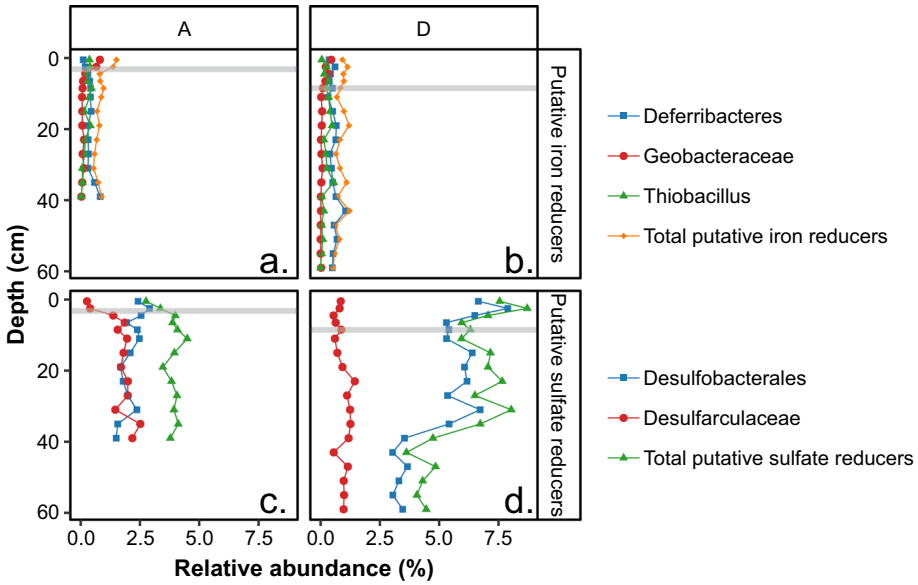

Fig. 5 Relative abundances of dominant microbial taxa and sum of relative abundances of all microbial taxa putatively involved in sulfate and Fe^{3+} reduction. Relative abundances are presented as a fraction of total prokaryotes (archaea + bacteria)

Groups associated with sulfate and Fe^{3+} reduction

The relative abundance of sulfate reducers was higher at site D than A. Sulfate reducers were also more abundant than Fe^{3+} reducers at both sites (Fig. 5). The putative sulfate reducing community in both sites consisted mostly of *Desulfobacterales* and *Desulfarculaceae* with minor contribution also from *Desulfobacca* sp., *Desulfomonile* sp, *Desulfosporosinus* sp. and *Desulfovibrionales* (Fig. 5). *Desulfobacterales* and *Desulfarculaceae* were generally of similar relative abundance at site A, except at surface layers and at SMTZ, where *Desulfobacterales* were at their highest and *Desulfarculaceae* at their lowest levels (Fig. 5). In contrast, in site D, *Desulfobacterales* significantly outnumbered *Desulfarculaceae* at all layers and generally followed the same depth pattern as total sulfate reducing community, while the relative abundance of *Desulfarculaceae* was quite stable through the sediment column (Fig. 5).

The putative Fe^{3+} reducing bacterial community in both sites consisted mostly of *Deferribacteres*, *Geobacteraceae* and *Thiobacillus* with minor contribution also from *Geothrix* sp., *Pseudomonas* sp., *Thermotogae*, *Bacillus* sp., *Desulfuromonas* sp., *Shewanella* sp., *Ferribacterium* sp. and *Aeromonas* sp. (Fig. 5). The dominant taxa differed in their vertical distribution patterns. *Geobacteraceae* generally had highest relative abundance at surface layers above SMTZ, whereas *Deferribacteres* were more abundant at deeper layers (Fig. 5).

Discussion

Vertical structure of methane oxidation rates in the context of porewater data

The oxidation rates measured in this study (Fig. 3) are broadly comparable to those of previous studies in the Baltic Sea, e.g. Thang et al. (2013) reported maximum rates of 16 nmol cm^{-3} day^{-1} from Sweden (Himmerfjärden bay) and Treude et al. (2005) reported rates of 1–14 nmol cm^{-3} day^{-1} in the upper 20 cm of the sediment in Germany (Eckernförde bay). However, while the rate profiles of Thang et al. and Treude et al. typically contained only a single clear peak of oxidation near the SMTZ, the oxidation rate profiles in this study can broadly be divided into three distinct layers: 1. surface-sediment (above the SMTZ), 2. close to the SMTZ, and 3. below the SMTZ. Oxidation in each layer was most likely mediated by different EAs. In layer 1, above the SMTZ, and especially close to the sediment surface, the observed oxidation was most likely related to MOX (Osudar et al. 2015; Steinle et al. 2017). In layer 2, the steep converging CH_4 and

SO_4^{2-} gradients, forming a well-defined SMTZ at all three sites, strongly suggest S-AOM at this depth (Iversen and Jørgensen 1985). Indeed, the most conspicuous peaks in oxidation at sites C and J are observed at the SMTZ (Fig. 3). However, we also measured oxidation activity in layer 3 at all sites, well below the SMTZ, at depths where porewater SO_4^{2-} was completely depleted. Therefore, we must attribute this activity to AOM mediated by other EAs than SO_4^{2-}, most likely by oxides of either Fe (Egger et al. 2015; Rooze et al. 2016) or Mn (Beal et al. 2009). The porewater profiles show evidence for reduction of Fe and Mn oxides below the SMTZ at all sites (Fig. 2). Accumulation of porewater Fe is most apparent at site A, while accumulation of Mn is most apparent at site C, likely reflecting the contrasting availability of Fe and Mn oxides at these two sites.

Lateral variability in methane oxidation along transect

One key finding of the study is that the maximum depth-integrated rates of CH_4 oxidation at any site were observed at site J. Moreover, this site also showed higher rates of oxidation in layer 3 (below the SMTZ), with respect to the other sites (Table 1). This observation suggests that non-SO_4^{2-} AOM may be an important biogeochemical process in the archipelago regions of the northern Baltic Sea, and apparently more prevalent in the archipelago sediments than in the low-salinity estuaries that drain into these areas. This conclusion appears surprising, since the availability of Fe and Mn oxides is greater in the inner estuarine areas (sites A and C in this study), and the porewater data from these sites suggest more active reduction of oxides. However, we note that there are several reasons why the accumulation of porewater Fe^{2+} and Mn^{2+} may not directly reflect rates of Fe- and Mn-AOM. Principally, dissimilatory reduction of oxides coupled to organic matter respiration may also generate these dissolved species (e.g. Egger et al. 2015). Also, the presence of excess porewater H_2S at the SMTZ will draw down their concentrations through precipitation of sulphide minerals (e.g. Reed et al. 2011). Jilbert et al. (2018) showed that site J is characterized by a strongly developed H_2S maximum at the SMTZ, which could explain the relatively low porewater Fe and Mn accumulation at this site despite high rates of AOM.

We therefore suggest that rates of non-SO_4^{2-} AOM are not controlled by EA availability in our study transect. Apparently, all the studied sites have sufficient Fe and/or Mn oxides in the sediments to facilitate AOM below the depth of SO_4^{2-} penetration. Rather, the availability of CH_4 (i.e. the rate of methanogenesis) controls the observed rate of non-SO_4^{2-} AOM at any given site. Depth-integrated oxidation rates below the SMTZ were highest at site J (Fig. 3), which is also characterized by the highest porewater CH_4 concentrations (Fig. 2). The reason for the high porewater CH_4 at site J is likely related to the high accumulation rate of degradable organic material at this location. Rates of CH_4 production in the 12–20 cm interval of the sediment column at site J have been estimated from porewater profiles as 8–10 nmol cm^{-3} day^{-1} (Jilbert et al. 2018). That study showed that the sediments of the archipelago are dominated by phytoplankton-derived organic carbon, while the inner estuarine sites have a mixed phytoplankton-terrestrial organic matter composition. Hence, for an equivalent total accumulation rate of carbon, archipelago areas are likely to have higher overall rates of remineralization reactions—including methanogenesis—due to the relative lability of the carbon source (Arndt et al. 2013).

Site-specific characteristics in the oxidation rate profiles

Due to the presence of oxygen in bottom waters, we expected to find evidence of MOX in the surface sediments at all sites (Fenchel et al. 1995). In addition, we expected to find the surface sediment at the nearly freshwater site A to contain the highest oxidation rates of the three sites. This is motivated by previous observations that MOX has a strong inverse relationship with salinity (de Angelis and Scranton 1993), likely caused by changes in the relative availability of oxygen, sulfate and methane along salinity gradients. However, while the integrated rates in the surface sediment layer were indeed highest at site A (Table 1), it lacked the distinct oxidation peak seen especially at site C and to a lesser degree at site J (Fig. 3).

We suggest that the differences in oxidation activity in the surface sediments can again be explained partly by CH_4 availability: site C was the only site to contain appreciable amounts of porewater CH_4 close to the sediment–water interface, and accordingly displayed

the shallowest SMTZ of the three sites (Fig. 2). Also, given that sites A and J are consistently oxic, strong bioturbation is expected (Vaquer-Sunyer and Duarte 2008). This may blur the diagenetic zones, allowing MOX to co-occur with S-AOM in the vicinity of burrows and hence to obscure the development of a distinct double-peak structure in the oxidation rate profile.

All three sites featured distinct oxidation maxima near the depth of SMTZ, interpreted as S-AOM, though the peak became more pronounced offshore (Fig. 2). Integrated oxidation rates in layer 2 (close to the SMTZ) increased considerably offshore and highest integrated rates of the whole study were found at site J in this layer (Table 1). The increased rates of S-AOM offshore are likely a reflection of dual substrate availability. S-AOM is dependent on both the availability of CH_4 and SO_4^{2-} (Valentine 2002). As outlined above, CH_4 concentrations are highest at site J due to organic matter degradability. Moreover, due to higher bottom water salinity, SO_4^{2-} availability is also greater at this site.

Microbial communities at the study sites

The sediment archaeal and bacterial communities at sites A and D generally consisted of the same taxa as in coastal and offshore sites of another northern Baltic Sea area, the Bothnian Sea (Rasigraf et al. 2019) (Supplementary Figs. 1 and 2). Furthermore, the same dominant methanogen taxa, *Methanomicrobiales* (*Methanoregulaceae*), *Methanosaetaceae* and *Methanosarcinaceae*, were present both at our study sites and in Bothnian Sea sediments (Rasigraf et al. 2019) (Fig. 4). Although Rasigraf et al. (2019) were able to construct a metagenome-assembled-genome of *Methanomassiliicoccaceae* thriving in Bothnian Sea sediments, this family, alongside other methanogenic taxa, were at very low levels both at ours and their study sites. *Methanomicrobiales* and *Methanosaetaceae* are considered to drive hydrogenotrophic and acetoclastic methanogenic pathways, respectively, while both acetoclastic and methylotrophic pathways have been suggested for *Methanosarcinaceae* (Nazaries et al. 2013). However, in environments with Fe^{3+} reducing bacteria and conductive minerals such as in iron-rich sediments of our study sites, *Methanosaetaceae* and *Methanosarcinaceae* could also drive CO_2 – reduction (to CH_4) coupled with either direct or indirect (via conductive materials) electron transfer from iron-reducing bacteria, such as *Geobacter* (Rotaru et al. 2014, 2018). Some metagenomic datasets also indicate *Bathyarchaeota*, which were dominant archaea both at our study sites and Bothnian Sea sediments (Rasigraf et al. 2019) (Supplementary Fig. 1), can be both methanogenic and methanotrophic (Evans et al. 2015). Shotgun metagenomic data would be needed to assess genetic potential of *Bathyarchaeota* at our study sites. However, the metagenomes of Rasigraf et al. (2019) suggest a non-methanogenic/non-methanotrophic fermentative lifestyle for *Bathyarchaeota* in Bothnian Sea sediments.

Genetic potential for sulfate and Fe^{3+} reduction was present throughout the sediment columns based on distribution of sulfate and Fe^{3+} reducing bacteria (Fig. 5). Because many of the Fe^{3+} reducing bacteria can also reduce Mn^{4+}, genetic potential for Mn^{4+} reduction was also present (Lovley 2013). The higher relative abundance of sulfate reducers at site D very likely represented higher marine influence, thus higher availability of sulfate (Fig. 5). Quite surprisingly, except for *Desulfobacterales* at site A, the relative abundance of sulfate reducers was not highest at the SMTZ. In addition, sulfate reducers were present in significant relative abundance also in deeper sulfate-depleted layers (Fig. 5). These deviations can be explained by sulfate reducing bacteria having also alternative metabolism strategies. For example, many sulfate reducers can switch to fermentation if sulfate is depleted (Rabus et al. 2013). We acknowledge that the deviations can also represent a bias in functional grouping, since this was based mostly on data from isolated bacteria. Modern metagenomic studies have shown that potential for both sulfate and Fe^{3+} reduction is spread also beyond the taxa from which isolates exist (Rasigraf et al. 2019; Garber et al. 2020).

Microbial community data in the context of oxidation rate data

Our theory that availability of CH_4 was the key factor controlling the observed oxidation rates is supported by the microbial data. At both stations sampled for microbial communities, MOG generally occur concurrently with ANME (Fig. 4k–n), implying that AOM co-occurs with methanogenesis regardless of depth in the sediment column. Importantly, both MOG

and ANME taxa increase in abundance below the SMTZ at both sites (Fig. 4m–n). There is also significant overlap in the presence of MOB and ANME, especially at site A, and MOB are found in much greater abundances deeper in the sediment than at site D (Fig. 4m–n). This also supports our previous conclusions regarding the potential effects of bioturbation and the blurring of diagenetic zones above the SMTZ.

Of the AOM related clades included in this study, ANME-1 is generally considered the least flexible in terms of EAs and is mainly associated with S-AOM (Timmers et al. 2017). By contrast, ANME-2a/b have been shown to be capable of both S-AOM and Me-AOM (Timmers et al. 2017), and ANME-2d is suggested to be capable of at least S-AOM, N-AOM, Fe-AOM and Mn-AOM (Haroon et al. 2013; Ettwig et al. 2016; Timmers et al. 2017). The presence of sulfate and Fe^{3+} reducing (and Mn^{4+} reducing) bacteria throughout the sediment columns further support the role of sulfate reducers as bacterial partners in S-AOM and also more generally the role of SO_4^{2-} and Fe^{3+} (and Mn^{4+}) as electron acceptors in anaerobic processes. The dominance of ANME 2a/b in our data likely reflects the mixed-EA environment of the estuarine system in general, with relatively low SO_4^{2-} and high oxide availability when compared to fully marine settings. Treude et al. (2005) and Rasigraf et al. (2019) also found that in Eckernförde bay (southern Baltic) and Bothnian Sea (northern Baltic), respectively, which also feature relatively shallow SMTZs, ANME-2 were the dominant clade. ANME-2 have also been shown to dominate other shallow SMTZ sediments in the ocean (Losekann et al. 2007).

ANME-2d has previously been found the most abundant AOM clade in some lakes (Weber et al. 2017; Rissanen et al. 2017). We also observed the highest abundances of ANME-2d at the river mouth-site, while at the slightly more saline site D, ANME-2d was still present, but in much lower abundances (Fig. 4a–d). Thus, despite multiple EAs that ANME-2d could potentially utilize (Timmers et al. 2017), it seems that salinity strongly inhibits the presence of ANME-2d, reinforcing previous interpretations of this as a primarily freshwater clade (Timmers et al. 2017).

The anaerobic taxa *Ca*. Methylomirablis (NC10 phyla), also capable of N-AOM (Welte et al. 2016), was also present in our study, but only at site A (Fig. 4c, d). These taxa has previously been found from both freshwater and marine environments (Welte et al. 2016). Its environmental significance remains unknown, as some studies have found no significant contributions from bacteria of the NC10 phyla to CH_4 oxidation (Beck et al. 2013; Martinez-Cruz et al. 2018), while others have shown the clade capable of very active nitrite N-AOM in lakes, though only in the first few millimeters of the sediment surface (Deutzmann et al. 2014). In our study it was most abundant relatively deep (20 cm) in the sediment, though we have no way of showing whether it was active at those depths. Nevertheless, it is possible that bioirrigation may introduce nitrite deeper in the sediment and enable N-AOM to occur there intermittently. This, too, could further contribute to the blurring of the diagenetic zones as discussed previously, as Deutzmann et al. (2014) also note that N-AOM by the NC10 bacteria could potentially be confused with MOX.

The MOB present in the surface sediment of site A were predominantly type I, which was to be expected as they are considered to be most common in estuaries (Dean et al. 2018). However, there was also a clear enrichment of type II MOB below the SMTZ (Fig. 4i). The co-occurrence of aerobic and anaerobic methanotrophs has previously been observed in lakes (Deutzmann et al. 2014; Martinez-Cruz et al. 2018). While it is possible that MOX occurs below the SMTZ at site A due to bioturbation, it is unlikely. More likely, the presence of type II MOB deeper in the sediments is the combined result of burial due to intensive sedimentation and selective survival (Rissanen et al. 2019). Indeed, Type II MOB have been shown to be able to survive for extended periods in a dormant state and recover CH_4 oxidation capability even after decades of anoxic conditions (Roslev and King 1994).

Alternative interpretations of oxidation pathways

Here we present a number of alternative potential biogeochemical pathways that could lead to the observed diagenetic zonation, and assess the likelihood that they may play a role in our study system.

All the sites studied here have been previously shown to accumulate porewater Fe^{2+} below the SMTZ, which we interpret to be linked to Fe-AOM and organoclastic Fe reduction (Jilbert et al. 2018). However, such accumulation has also been postulated to reflect the "cryptic sulphur cycle" (Holmkvist et al. 2011). While it is possible that this process is taking

place in this location, it is most likely confined to the vicinity of the SMTZ or immediately below. H2S is required to sustain the cryptic sulphur cycle, and this is rapidly depleted below the SMTZ at these sites (Jilbert et al. 2018).

AOM coupled to denitrification (N-AOM) has been shown to be potentially an even more energetically favorable pathway than Me-AOM (Raghoebarsing et al. 2006; Ettwig et al. 2010). This process is expected to be confined to the oxic/anoxic interface in the sediment, which in our study area is so close to the sediment surface that the sampling resolution used is insufficient to capture it. However, as indicated above, given the potential for bioturbation and the presence of *Ca*. Methylomirablis (NC10 phyla) and ANME-2d, it is possible that N-AOM is also taking place at least at site A.

Methanogens are capable of also oxidizing CH_4, while on the other hand methanotrophs are capable of reducing CO2 to CH_4 (Timmers et al. 2017). This potentially creates a "cryptic CH_4" cycle, in which CH_4 is being oxidized and produced concurrently. These processes may be mediated partly by the same microbes or via syntrophic couplings, both within the SMTZ (Beulig et al. 2019) and shallower in the sediment column (Maltby et al. 2016; Xiao et al. 2017). While we cannot rule out these processes being present from the SMTZ upwards, no evidence yet exists of such processes deeper in the sediments in conjunction with Me-AOM.

Implications and conclusions

Our estimates for CH_4 oxidation rates are broadly similar in magnitude to rates of CH_4 production in sediments from the Pojo Bay estuary (Jilbert et al. 2018; Myllykangas et al. 2020). Thus, our results suggest that sedimentary CH_4 oxidation filters in this estuary and its connected archipelago are functioning efficiently and removing the vast majority of the produced CH_4 in situ, preventing its escape to the water column. This is supported by similarities in the abundances of methanogenic and methanotrophic microbial taxa in sediment profiles, indicating strong co-occurrence of these processes.

We identify three distinct layers of oxidation activity each contributing to the function of the oxidative filter; MOX, S-AOM and Me-AOM. Me-AOM below the SMTZ is clearly very active throughout the transect, with maximum rates observed at site J. Similarly, S-AOM rates are highest in this site. Overall it is likely the increased availability of CH_4 caused the total integrated rates of both processes to increase offshore. Similarly to the oxidation rates, in the microbial community structure, ANME-2a/b were relatively most abundant below the SMTZ, especially in higher salinity conditions whereas MOB and methanogens were more abundant in the lower salinity.

In many coastal systems, rates of both methanogenesis and methanotrophy have increased as a consequence of anthropogenic eutrophication (Borges et al. 2018). As well as potential impacts on CH_4 fluxes to the atmosphere, the links between CH_4 processes and other elemental cycles may lead to broader impacts on coastal sediment biogeochemistry. Our study shows that non-SO_4^{2-} AOM is important in coastal sediments of the northern Baltic Sea, highlighting in particular the coupling between CH_4 and Fe cycling. The Fe-AOM model of Rooze et al. (2016) found that only 9% of all CH_4 oxidation was performed by Fe-AOM. However, according to their results Fe-AOM had a significant role in Fe cycling, accounting for 46% of all $Fe(OH)_3$ reduction. Our study suggests that in coastal areas, the role of Fe-AOM may be even greater, leading to even stronger impacts on Fe cycling. This could have further downstream effects on other biogeochemical cycles, such as phosphorus transport to deep basins of the Baltic (Jilbert and Slomp 2013).

Acknowledgements Open access funding provided by University of Helsinki including Helsinki University Central Hospital. This project was funded by the Academy of Finland project 267112 to SH and 286642 to AJR, and the foundation of Onni Talas (personal grant to JPM). We extend our gratitude to Tina Treude for her invaluable insights and comments on the design of the radiotracer experiments. We also wish to thank the staff and field crew at the Tvärminne Zoological station for providing field and laboratory work infrastructure. Finally, we wish to thank Kaj-Roger Hurme for his invaluable assistance in the radiotracer analysis. We thank two anonymous reviewers for their comments, which greatly improved the paper.

References

Arndt S, Jørgensen BB, LaRowe DE et al (2013) Quantifying the degradation of organic matter in marine sediments: a review and synthesis. Earth Sci Rev 123:53–86. https://doi.org/10.1016/j.earscirev.2013.02.008

Beal EJ, House CH, Orphan VJ (2009) Manganese- and iron-dependent marine methane oxidation. Science 325:184–187. https://doi.org/10.1126/science.1169984

Beaulieu JJ, DelSontro T, Downing JA (2019) Eutrophication will increase methane emissions from lakes and impoundments during the 21st century. Nat Commun 10:1375. https://doi.org/10.1038/s41467-019-09100-5

Beck DAC, Kalyuzhnaya MG, Malfatti S et al (2013) A metagenomic insight into freshwater methane-utilizing communities and evidence for cooperation between the Methylococcaceae and the Methylophilaceae. PeerJ 1:e23. https://doi.org/10.7717/peerj.23

Beulig F, Røy H, McGlynn SE, Jørgensen BB (4) Cryptic CH4 cycling in the sulfate–methane transition of marine sediments apparently mediated by ANME-1 archaea. ISME J 13:250–262. https://doi.org/10.1038/s41396-018-0273-z

Borges AV, Speeckaert G, Champenois W et al (2018) Productivity and temperature as drivers of seasonal and spatial variations of dissolved methane in the Southern Bight of the North Sea. Ecosystems 21:583–599. https://doi.org/10.1007/s10021-017-0171-7

Capone DG, Kiene RP (1988) Comparison of microbial dynamics in marine and freshwater sediments: contrasts in anaerobic carbon catabolism. Limnol Oceanogr 33:725–749. https://doi.org/10.4319/lo.1988.33.4part2.0725

de Angelis MA, Scranton MI (1993) Fate of methane in the Hudson River and Estuary. Glob Biogeochem Cycles 7:509–523. https://doi.org/10.1029/93GB01636

Dean JF, Middelburg JJ, Röckmann T et al (2018) Methane feedbacks to the global climate system in a warmer world. Rev Geophys 56:207–250. https://doi.org/10.1002/2017RG000559

Deutzmann JS, Stief P, Brandes J, Schink B (2014) Anaerobic methane oxidation coupled to denitrification is the dominant methane sink in a deep lake. Proc Natl Acad Sci 111:18273–18278. https://doi.org/10.1073/pnas.1411617111

Ding J, Fu L, Ding ZW et al (2016) Experimental evaluation of the metabolic reversibility of ANME-2d between anaerobic methane oxidation and methanogenesis. Appl Microbiol Biotechnol 100:6481–6490. https://doi.org/10.1007/s00253-016-7475-y

Edgar RC, Haas BJ, Clemente JC et al (2011) UCHIME improves sensitivity and speed of chimera detection. Bioinformatics 27:2194–2200. https://doi.org/10.1093/bioinformatics/btr381

Egger M, Rasigraf O, Sapart CJ et al (2015) Iron-mediated anaerobic oxidation of methane in brackish coastal sediments. Environ Sci Technol 49:277–283. https://doi.org/10.1021/es503663z

Egger M, Riedinger N, Mogollón JM, Jørgensen BB (2018) Global diffusive fluxes of methane in marine sediments. Nat Geosci 11:421–425. https://doi.org/10.1038/s41561-018-0122-8

Eller G, Kanel L, Krüger M (2005) Cooccurrence of aerobic and anaerobic methane oxidation in the water column of Lake Plu see. Appl Environ Microbiol 71:8925–8928. https://doi.org/10.1128/AEM.71.12.8925-8928.2005

Ettwig KF, Butler MK, Le Paslier D et al (2010) Nitrite-driven anaerobic methane oxidation by oxygenic bacteria. Nature 464:543–548. https://doi.org/10.1038/nature08883

Ettwig KF, Zhu B, Speth D et al (2016) Archaea catalyze iron-dependent anaerobic oxidation of methane. Proc Natl Acad Sci 113:12792–12796. https://doi.org/10.1073/pnas.1609534113

Evans PN, Parks DH, Chadwick GL, Robbins SJ, Orphan VJ, Golding SD, Tyson GW (2015) Methane metabolism in the archaeal phylum Bathyarchaeota revealed by genome-centric metagenomics. Science 350:434–438. https://doi.org/10.1126/science.aac7745

Fenchel T, Bernard C, Esteban G et al (1995) Microbial diversity and activity in a Danish Fjord with anoxic deep water. Ophelia 43:45–100. https://doi.org/10.1080/00785326.1995.10430576

Gammal J, Norkko J, Pilditch CA, Norkko A (2017) Coastal hypoxia and the importance of benthic macrofauna communities for ecosystem functioning. Estuaries Coasts 40:457–468. https://doi.org/10.1007/s12237-016-0152-7

Garber AI, Nealson KH, Okamoto A, McAllister SM, Chan CS, Barco RA, Merino N (2020) FeGenie: a comprehensive tool for the identification of iron genes and iron gene neighborhoods in genome and metagenome assemblies. Front Microbiol 11:37. https://doi.org/10.3389/fmicb.2020.00037

Gantner S, Andersson AF, Alonso-Sáez L, Bertilsson S (2011) Novel primers for 16S rRNA-based archaeal community analyses in environmental samples. J Microbiol Methods 84:12–18. https://doi.org/10.1016/j.mimet.2010.10.001

Griffiths RI, Whiteley AS, O'Donnell AG, Bailey MJ (2000) Rapid method for coextraction of DNA and RNA from natural environments for analysis of ribosomal DNA- and rRNA-based microbial community composition. Appl Environ Microbiol 66:5488–5491. https://doi.org/10.1128/AEM.66.12.5488-5491.2000

Haroon MF, Hu S, Shi Y et al (2013) Anaerobic oxidation of methane coupled to nitrate reduction in a novel archaeal lineage. Nature 500:567–570. https://doi.org/10.1038/nature12375

Hoehler TM, Alperin MJ, Albert DB, Martens CS (1994) Field and laboratory studies of methane oxidation in an anoxic marine sediments: evidence for methanogen-sulphate reducer consortium. Glob Biochem Cycles 8:451–463

Holmkvist L, Ferdelman TG, Jørgensen BB (2011) A cryptic sulfur cycle driven by iron in the methane zone of marine sediment (Aarhus Bay, Denmark). Geochim Cosmochim Acta 75:3581–3599. https://doi.org/10.1016/j.gca.2011.03.033

Huse SM, Welch DM, Morrison HG, Sogin ML (2010) Ironing out the wrinkles in the rare biosphere through improved OTU clustering. Environ Microbiol 12:1889–1898. https://doi.org/10.1111/j.1462-2920.2010.02193.x

IPCC (2014) Climate change 2013—the physical science basis. Cambridge University Press, Cambridge

Iversen N, Jørgensen B (1985) Anaerobic methane oxidation rates at the sulphate-methane transition in marine sediments from Kattegat and Skagerrak (Denmark). Limnol Oceanogr 30:944–955

Jakobs G, Rehder G, Jost G et al (2013) Comparative studies of pelagic microbial methane oxidation within the redox zones of the Gotland Deep and Landsort Deep (central Baltic Sea). Biogeosciences 10:7863–7875. https://doi.org/10.5194/bg-10-7863-2013

Jilbert T, Asmala E, Schröder C et al (2018) Impacts of flocculation on the distribution and diagenesis of iron in boreal estuarine sediments. Biogeosciences 15:1243–1271. https://doi.org/10.5194/bg-15-1243-2018

Jilbert T, Slomp CP (2013) Iron and manganese shuttles control the formation of authigenic phosphorus minerals in the euxinic basins of the Baltic Sea. Geochim Cosmochim Acta 107:155–169. https://doi.org/10.1016/j.gca.2013.01.005

Jørgensen BB, Weber A, Zopfi J (2001) Sulfate reduction and anaerobic methane oxidation in Black Sea sediments. Deep Sea Res Part I 48:2097–2120. https://doi.org/10.1016/S0967-0637(01)00007-3

Kauppi L, Bernard G, Bastrop R et al (2018) Increasing densities of an invasive polychaete enhance bioturbation with variable effects on solute fluxes. Sci Rep 8:1–12. https://doi.org/10.1038/s41598-018-25989-2

Knittel K, Boetius A (2009) Anaerobic oxidation of methane: progress with an unknown process. Annu Rev Microbiol 63:311–334. https://doi.org/10.1146/annurev.micro.61.080706.093130

Kuever J, Rainey FA, Widdel F (2005) Order III. Desulfobacterales ord. nov. In: Brenner DJ, Krieg NR, Staley JT, Garrity GM (eds) Bergey's manual of systematic bacteriology, 2nd edn, vol. 2 (The Proteobacteria), part C (The Alpha-, Beta-, Delta-, and Epsilonproteobacteria). Springer, New York

Kuever J (2013) The Family Desulfarculaceae. In: Rosenberg E, DeLong EF, Lory S, Stackebrandt E, Thompson F (eds) The Prokaryotes. Springer, Berlin

Losekann T, Knittel K, Nadalig T et al (2007) Diversity and abundance of aerobic and anaerobic methane oxidizers at the Haakon Mosby Mud Volcano, Barents Sea. Appl Environ Microbiol 73:3348–3362. https://doi.org/10.1128/AEM.00016-07

Lovley DR, Phillips EJP (1988) Manganese inhibition of microbial iron reduction in anaerobic sediments. Geomicrobiol J 6:145–155. https://doi.org/10.1080/01490458809377834

Lovley D (2013) Dissimilatory Fe(III) and Mn(IV)-reducing prokaryotes. In: Rosenberg E, DeLong EF, Lory S, Stackebrandt E, Thompson F (eds) The Prokaryotes. Springer, Berlin

Magoč T, Salzberg SL (2011) FLASH: fast length adjustment of short reads to improve genome assemblies. Bioinformatics 27:2957–2963. https://doi.org/10.1093/bioinformatics/btr507

Maltby J, Sommer S, Dale AW, Treude T (2016) Microbial methanogenesis in the sulfate-reducing zone of surface sediments traversing the Peruvian margin. Biogeosciences 13:283–299. https://doi.org/10.5194/bg-13-283-2016

Martinez-Cruz K, Sepulveda-Jauregui A, Casper P et al (2018) Ubiquitous and significant anaerobic oxidation of methane in freshwater lake sediments. Water Res 144:332–340. https://doi.org/10.1016/j.watres.2018.07.053

McGlynn SE (2017) Energy metabolism during anaerobic methane oxidation in ANME archaea. Microbes Environ 32:5–13. https://doi.org/10.1264/jsme2.ME16166

McGlynn SE, Chadwick GL, Kempes CP, Orphan VJ (2015) Single cell activity reveals direct electron transfer in methanotrophic consortia. Nature 526:531–535. https://doi.org/10.1038/nature15512

Myllykangas J-P, Hietanen S, Jilbert T (2020) Legacy effects of eutrophication on modern methane dynamics in a boreal estuary. Estuaries Coasts 43:189–206. https://doi.org/10.1007/s12237-019-00677-0

Nazaries L, Murrell JC, Millard P, Baggs L, Singh BK (2013) Methane, microbes and models: fundamental understanding of the soil methane cycle for future predictions. Environ Microbiol 15:2395–2417. https://doi.org/10.1111/1462-2920.12149

Osudar R, Matoušů A, Alawi M et al (2015) Environmental factors affecting methane distribution and bacterial methane oxidation in the German Bight (North Sea). Estuar Coast Shelf Sci 160:10–21. https://doi.org/10.1016/j.ecss.2015.03.028

Rabus R, Hansen TA, Widdel F (2013) Dissimilatory sulfate- and sulfur-reducing prokaryotes. In: Rosenberg E, DeLong EF, Lory S, Stackebrandt E, Thompson F (eds) The Prokaryotes. Springer, Berlin

Raghoebarsing AA, Pol A, van de Pas-Schoonen KT et al (2006) A microbial consortium couples anaerobic methane oxidation to denitrification. Nature 440:918–921. https://doi.org/10.1038/nature04617

Rasigraf O, Helmond NAGM, Frank J, Lenstra WK, Egger M, Slomp CP, Jetten MSM (2019) Microbial community composition and functional potential in Bothnian Sea sediments is linked to Fe and S dynamics and the quality of organic matter. Limnol Oceanogr 65(S1):S113–S133. https://doi.org/10.1002/lno.11371

Reed DC, Gustafssson BG, Slomp CP (2016) Shelf-to-basin iron shuttling enhances vivianite formation in deep Baltic Sea sediments. Earth Planet Sci Lett 434:241–251. https://doi.org/10.1016/j.epsl.2015.11.033

Reed DC, Slomp CP, Gustafsson BG (2011) Sedimentary phosphorus dynamics and the evolution of bottom-water hypoxia: a coupled benthic-pelagic model of a coastal system. Limnol Oceanogr 56:1075–1092. https://doi.org/10.4319/lo.2011.56.3.1075

Rissanen AJ, Karvinen A, Nykänen H et al (2017) Effects of alternative electron acceptors on the activity and community structure of methane-producing and consuming microbes in the sediments of two shallow boreal lakes. FEMS Microbiol Ecol 93:1–16. https://doi.org/10.1093/femsec/fix078

Rissanen AJ, Peura S, Mpamah PA et al (2019) Vertical stratification of bacteria and archaea in sediments of a small boreal humic lake. FEMS Microbiol Lett 366:1–11. https://doi.org/10.1093/femsle/fnz044

Rooze J, Egger M, Tsandev I, Slomp CP (2016) Iron-dependent anaerobic oxidation of methane in coastal surface sediments: Potential controls and impact. Limnol Oceanogr 61:S267–S282. https://doi.org/10.1002/lno.10275

Roslev P, King GM (1994) Survival and recovery of methanotrophic bacteria starved under oxic and anoxic conditions. Appl Environ Microbiol 60:2602–2608

Rotaru A-E, Shrestha PM, Liu F, Shrestha M, Shrestha D, Embree M, Zengler K, Wardman C, Nevin KP, Lovley DR (2014) A new model for electron flow during anaerobic digestion: direct interspecies electron transfer to *Methanosaeta* for the reduction of carbon dioxide to methane. Energy Environ Sci 7:408–415. https://doi.org/10.1039/C3EE42189A

Rotaru A-E, Calabrese F, Stryhanyuk H, Musat F, Shrestha PM, Weber HS, Snoeyenbos-West OLO, Hall POJ, Richnow HH, Musat N, Thamdrup B (2018) Conductive particles enable syntrophic acetate oxidation between *Geobacter* and *Methanosarcina* from coastal sediments. mBio 9:e00226–e318. https://doi.org/10.1128/mBio.00226-18

Schloss PD, Westcott SL, Ryabin T et al (2009) Introducing mothur: open-source, platform-independent, community-supported software for describing and comparing microbial communities. Appl Environ Microbiol 75:7537–7541. https://doi.org/10.1128/AEM.01541-09

Schmale O, Schneider V, Deimling J, Gülzow W et al (2010) Distribution of methane in the water column of the Baltic Sea. Geophys Res Lett 37:1–5. https://doi.org/10.1029/2010GL043115

Schmieder R, Edwards R (2011) Quality control and preprocessing of metagenomic datasets. Bioinformatics 27:863–864. https://doi.org/10.1093/bioinformatics/btr026

Sivan O, Adler M, Pearson A et al (2011) Geochemical evidence for iron-mediated anaerobic oxidation of methane. Limnol Oceanogr 56:1536–1544. https://doi.org/10.4319/lo.2011.56.4.1536

Steinle L, Maltby J, Treude T et al (2017) Effects of low oxygen concentrations on aerobic methane oxidation in seasonally hypoxic coastal waters. Biogeosciences 14:1631–1645. https://doi.org/10.5194/bg-14-1631-2017

Takahashi S, Tomita J, Nishioka K et al (2014) Development of a prokaryotic universal primer for simultaneous analysis of Bacteria and Archaea using next-generation sequencing. PLoS ONE 9:e105592. https://doi.org/10.1371/journal.pone.0105592

Takai K, Horikoshi K (2000) Rapid detection and quantification of members of the archaeal community by quantitative PCR using fluorogenic probes. Appl Environ Microbiol 66:5066–5072. https://doi.org/10.1128/AEM.66.11.5066-5072.2000

Thang NM, Brüchert V, Formolo M et al (2013) The impact of sediment and carbon fluxes on the biogeochemistry of methane and sulfur in littoral Baltic Sea sediments (Himmerfjärden, Sweden). Estuaries Coasts 36:98–115. https://doi.org/10.1007/s12237-012-9557-0

Thauer RK (1998) Biochemistry of methanogensis: a tribute to Marjory Stephenson. Microbiology 144:2377–2407

Tiihonen R (2016) The distribution of iron and manganese in coastal sediments of the Gulf of Finland. University of Helsinki

Timmers PHA, Welte CU, Koehorst JJ et al (2017) Reverse methanogenesis and respiration in methanotrophic archaea. Archaea 2017:1–22. https://doi.org/10.1155/2017/1654237

Treude T, Krüger M, Boetius A, Jørgensen B (2005) Environmental control on anaerobic oxidation of methane in the gassy sediments of Eckernfoerde Bay(German Baltic). Limnol Oceanogr 50:1771–1786. https://doi.org/10.4319/lo.2005.50.6.1771

Valentine DL (2002) Biogeochemistry and microbial ecology of methane oxidation in anoxic environments: a review. Antonie Van Leeuwenhoek 81:271–282. https://doi.org/10.1023/A:1020587206351

Vaquer-Sunyer R, Duarte CM (2008) Thresholds of hypoxia for marine biodiversity. Proc Natl Acad Sci 105:15452–15457. https://doi.org/10.1073/pnas.0803833105

Wang Q, Garrity GM, Tiedje JM, Cole JR (2007) Naive Bayesian classifier for rapid assignment of rRNA sequences into the new bacterial taxonomy. Appl Environ Microbiol 73:5261–5267. https://doi.org/10.1128/AEM.00062-07

Weber HS, Habicht KS, Thamdrup B (2017) Anaerobic methanotrophic archaea of the ANME-2d cluster are active in a low-sulfate, iron-rich freshwater sediment. Front Microbiol 8:1–13. https://doi.org/10.3389/fmicb.2017.00619

Welte CU, Rasigraf O, Vaksmaa A et al (2016) Nitrate- and nitrite-dependent anaerobic oxidation of methane. Environ Microbiol Rep 8:941–955. https://doi.org/10.1111/1758-2229.12487

Xiao Q, Zhang M, Hu Z et al (2017) Spatial variations of methane emission in a large shallow eutrophic lake in subtropical climate. J Geophys Res Biogeosci 122:1597–1614. https://doi.org/10.1002/2017JG003805

Youssef N, Elshahed MS, McInerney MJ (2009) Microbial processes in oil fields: culprits, problems, and opportunities. Adv Appl Microbiol 66:141–251. https://doi.org/10.1016/S0065-2164(08)00806-X

Influence of electron acceptor availability and microbial community structure on sedimentary methane oxidation in a boreal estuary

Biogeochemistry, 10.1007/s10533-020-00660-z

Online supplement

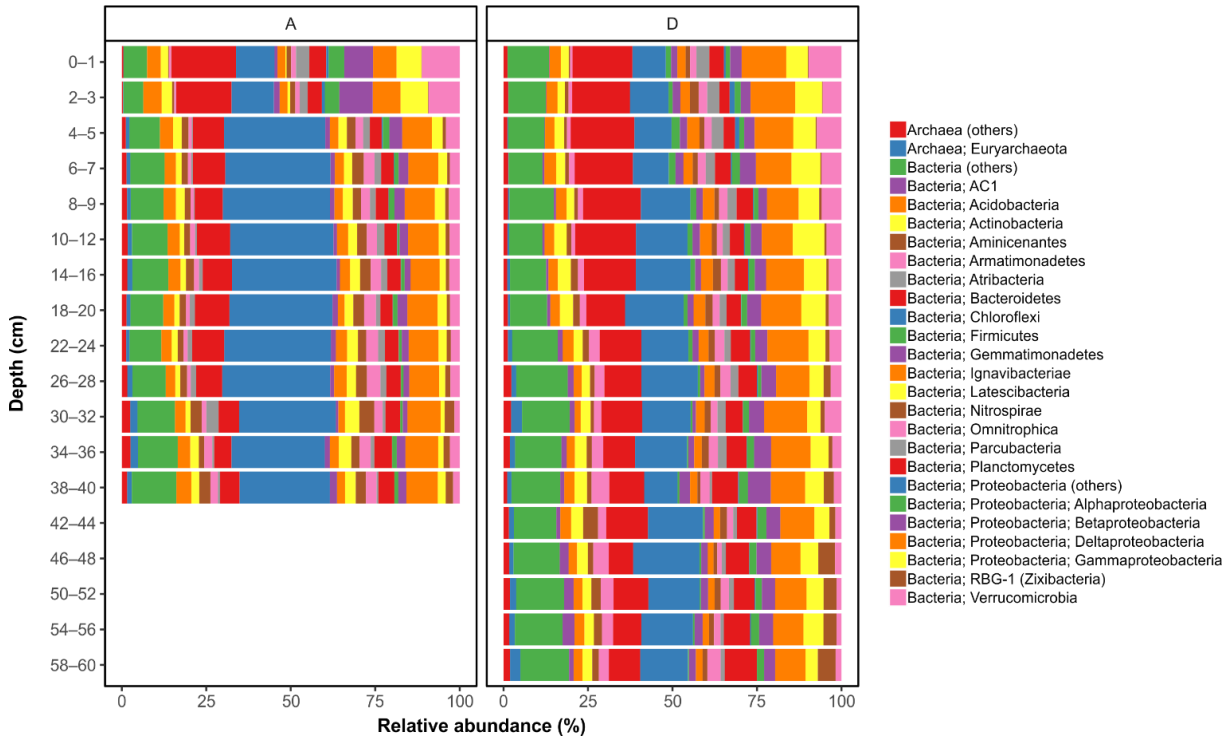

Fig. S1 Vertical distribution of dominant archaeal taxa (> 1 % relative abundance in at least one depth layer) based on archaeal 16S rRNA gene amplicon analysis (using primers targeting specifically archaea). Groups denoted "(others)" include less abundant taxa as well as taxa that could not be classified at higher taxonomic levels

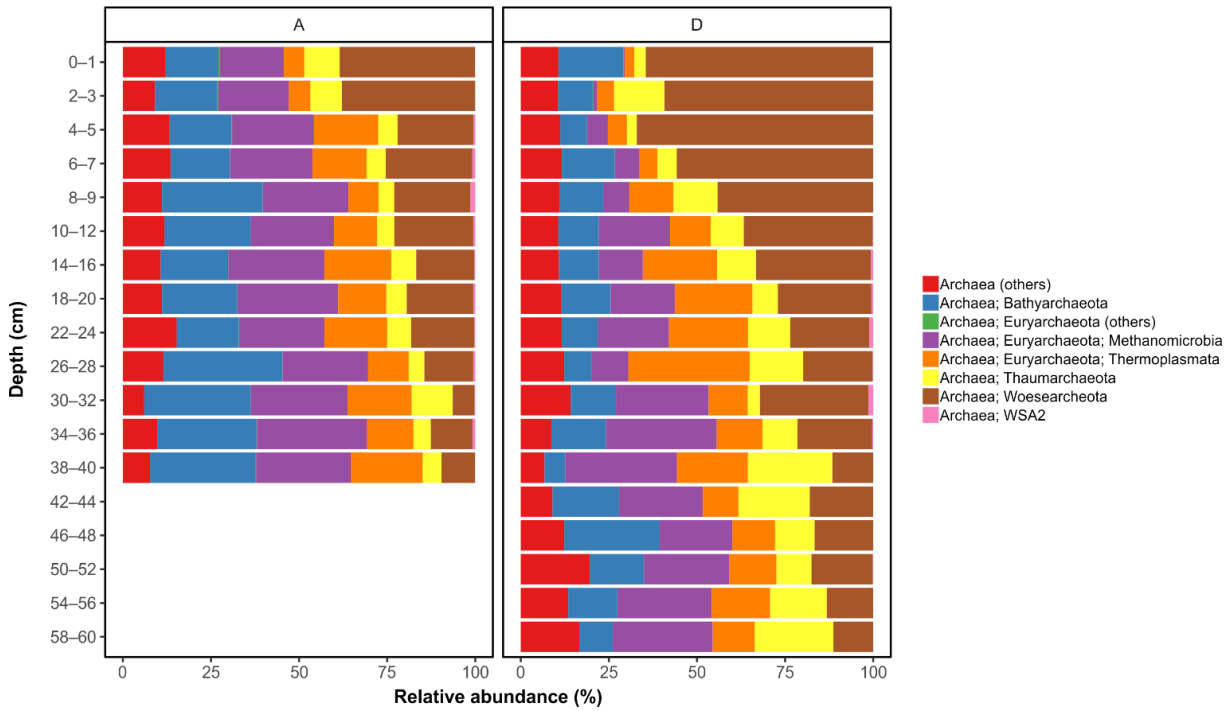

Fig. S2 Vertical distribution of dominant bacterial and archaeal taxa (> 2 % relative abundance in at least one depth layer) based on prokaryotic 16S rRNA gene amplicon analysis (using primers targeting bacteria and archaea simultaneously). Groups denoted "(others)" include less abundant taxa as well as taxa that could not be classified at higher taxonomic levels